UNIVERSIDADE TIRADENTES

PROGRAMA DE PÓS – GRADUAÇÃO EM ENGENHARIA DE PROCESSOS

DOUTORADO EM ENGENHARIA DE PROCESSOS

SÍNTESE E CARACTERIZAÇÃO DE ANODOS DE ÓXIDOS METÁLICOS MISTOS PARA DEGRADAÇÃO DE EFLUENTES CONTAMINADOS COM COMPOSTOS ORGÂNICOS.

Aluna: Marilia Moura de Salles Pupo

Orientadores: Prof. Giancarlo Richard Salazar Banda, Ph.D.

Profª. Katlin Ivon Barrios Eguiluz, Ph.D.

ARACAJU, SE - BRASIL

FEVEREIRO DE 2019

SÍNTESE E CARACTERIZAÇÃO DE ANODOS DE ÓXIDOS METÁLICOS MISTOS PARA DEGRADAÇÃO DE EFLUENTES CONTAMINADOS COM COMPOSTOS ORGÂNICOS.

Marilia Moura de Salles Pupo

DISSERTAÇÃO SUBMETIDA AO PROGRAMA DE PÓS-GRADUAÇÃO EM ENGENHARIA DE PROCESSOS DA UNIVERSIDADE TIRADENTES COMO PARTE DOS REQUISITOS NECESSÁRIOS PARA A OBTENÇÃO DO GRAU DE DOUTOR EM ENGENHARIA DE PROCESSOS.

Aprovado por:

_____
Giancarlo Richard Salazar Banda, Ph.D.

_____
Katlin Ivon Barrios Eguiluz, Ph.D.

_____
Elton Francheschini, Ph.D.

_____
Luiz Fernando Romanholo Ph.D.

_____
Daniel Moreira Fontes Lima Ph.D.

_____
Eliana Midori Sussuchi Ph.D.

ARACAJU, SE – BRASIL

FEVEREIRO DE 2019

SÍNTESE E CARACTERIZAÇÃO DE ÂNODOS DE ÓXIDOS METÁLICOS MISTOS PARA DEGRADAÇÃO DE EFLUENTES CONTAMINADOS COM COMPOSTOS ORGÂNICOS.

Marilia Moura de Salles Pupo

Por meio da analise das principais variáveis (pH, densidade de corrente e eletrólito) operacionais utilizadas para degradação eletroquímica de Cefalexina em reatores do tipo filtro prensa equipados com diamante dopado com boro (DDB) foi possível determinar condições ideais de operação (pH sem controle, Na_2SO_4 0.33 M e 10 mA cm^{-2}). Adicionalmente, testes de toxicidade em *E. coli* identificaram compostos β-lactamicos como intermediários responsáveis por aumento de toxicidade na degradação eletroquímica da Cefalexina. Posteriormente, estudos de síntese e caracterização de ânodos de mistura de óxidos metálicos analisando eletrodos de $(SnO_2)_{93}Sb_5M_{2(M=Ce, Bi, Ta, Gd)}$ com aplicação de metil imidazolium no preparo da solução precursora identificou a temperatura de calcinação de 550 ºC como ideal apresentando melhoras de até 5 vezes no tempo de vida de eletrodos de $Ti/(SnO_2)_{93}Sb_5Bi_2$. Além disso, taxas de remoção de até 34% de Diuron em 1 hora de tratamento em Na_2SO_4 0.33 M e aplicando 10 mA cm^{-2} confirmaram o potencial eletrocatalítico deste material. Por fim, estudos em reatores do tipo filtro prensa de fluxo perpendicular 3D equipados com eletrodos de $Ti/(SnO_2)_{93}Sb_5Bi_2$ em formato de malha metálica foram realizados e seu desempenho eletrocatalítico foi comparado com DDB usando agentes de contraste de raio x como molécula alvo. Mais adiante, para melhora das propriedades físicas e aumento no tempo de vida do eletrodo proposto, uma intercamada de nanotubos de TiO_2 foi obtida por meio de ataque químico. Os resultados obtidos neste estudo final mostram melhoras de até 4 vezes no tempo de vida do eletrodo mantendo sua capacidade eletrocatalítica intacta atingindo taxas de remoção dos compostos alvo (iohexol, iopromide e diatrizoato) de até 100% comparável a atividade do DDB em mesmas condições operacionais.

Abstract of Thesis presented to the Process Engineering Post-Graduate Program of Universidade Tiradentes as a partial fulfillment of the requirements for the qualification examination for the achievement of the degree as a Doctor of Science

SYNTHESIS AND CHARACTERIZATION OF METAL OXIDE MIXTURE ANODES FOR TREATMENT OF EFFLUENTS CONTAMINATED WITH ORGANIC COMPOUNDS:

Marilia Moura de Salles Pupo

By analyzing the main operational variables (pH, current density and electrolyte) used for electrochemical degradation of Cephalexin in filter-press reactor equipped with boron doped diamond (BDD) it was possible to determine the ideal operational conditions (pH with no control, Na_2SO_4 0.33 M and 10 mA cm^{-2}). Additionally, toxicity tests with *E. coli* identified compounds β-lactamic as the responsible for an increase in toxicity during the electrochemical degradation of Cephalexin. Afterwards, synthesis and characterization studies of mixed metal oxides analyzing $(SnO_2)_{93}Sb_5M_{2(M=Ce, Bi, Ta, Gd)}$ synthesis while using methyl imidazolium to prepare the precursor solution identified calcination temperature of 550 ºC as ideal presenting improvements of 5 folds on the service lifetime of $Ti/(SnO_2)_{93}Sb_5Bi_2$. Moreover, removal rates of 34% of Diuron in 1-hour treatment in Na_2SO_4 0.33 M and 10 mA cm^{-2} confirming the electrocatalytic potential of this material. Finally, studies in filter-press flow-through 3D reactors equipped with $Ti/(SnO_2)_{93}Sb_5Bi_2$ as metallic mesh were carried out comparing their activity with BDD using x-ray agents as the target compound. Moreover, to enhance the physical properties and increase the service lifetime of the anode proposed, a interlayer of TiO_2 nanotubes was obtained by means of chemical attack. The results obtained in this final study show a 4-fold increase in service lifetime of the electrode while maintaining its electrocatalytic capacity reaching removal rates of 100% of the target compounds (iohexol, iopromide and diatrizoate), comparable to the BDD outcomes in the same operational conditions.

Key-words: Electrolysis, contamination, effluent, anode, persistent contaminants.

SUMÁRIO

LISTA DE FIGURAS

LISTA DE TABELAS

Capítulo 1

1. INTRODUÇÃO

Processos industriais são tipicamente conhecidos por gerar uma grande carga de contaminantes que são lançados aos corpos d'água nos mais variados graus de degradação. De forma geral, estes contaminantes são misturas complexas de compostos orgânicos e inorgânicos muitas vezes tóxicos e de difícil mineralização (Särkkä *et al.*, 2015). Estes influem das formas mais variadas no meio ambiente resultando em prejuízos ao bioma e biota, por vezes gerando bioacumulação e atingindo o ser humano diretamente (Feng *et al.*, 2013; Puckowski *et al.*, 2016; Rivera-Utrilla *et al.*, 2013; Zhang *et al.*, 2013).

Considerando os avanços químicos das últimas décadas, os compostos aplicados na indústria tem se tornado cada vez mais complexos e, a depender de sua aplicação, ainda mais persistentes e de difícil degradação (Ranade e Bhandari, 2014). Neste sentido, atenção especial deve ser dada a compostos orgânicos da classe dos fármacos, pesticidas e corantes, que por conta de sua aplicação representam complexos de difícil degradação, em sua grande maioria resistentes a biodegradação e altamente solúveis em água (Ribeiro *et al.*, 2015; Sirés *et al.*, 2014; Vasudevan e Oturan, 2014; Wang e Lin, 2014).

Dentre as inovações tecnológicas propostas para tratar adequadamente estas classes de contaminantes, os processos de oxidação eletroquímica surgem como uma alternativa bastante viável, pois tais métodos são ambientalmente corretos, com uso limitado de aditivos químicos e alta capacidade de degradação de compostos orgânicos através dos radicais hidroxila gerados. Considerado uma das rotas de maior sustentabilidade ambiental, tratamentos eletroquímicos de diversos tipos de efluentes industriais são uma tendência crescente, com estudos buscando a redução de custos e otimização operacional sendo um campo de estudo de grande interesse comercial (Brillas e Martínez-Huitle, 2015; Feng *et al.*, 2013; Ganzenko *et al.*, 2014; Martínez-Huitle *et al.*, 2015; Oturan e Aaron, 2014; Särkkä *et al.*, 2015).

Adicionalmente, sendo o eletrodo parte essencial do processo de tratamento eletroquímico, a busca por materiais eletródicos que apresentem características tais como longa vida útil, elevada área superficial, ampla janela de potencial entre as reações de desprendimento de hidrogênio (RDH) e desprendimento de oxigênio (RDO), alta atividade catalítica, resistência à corrosão, além de facilidade de preparo tem sido objetivo de diversas pesquisas (Rao e Venkatarangaiah, 2014; Shao *et al.* 2014; Oturan e Aaron, 2014).

Tradicionalmente, os materiais suportados em placas de metal inerte, como, por exemplo, Ti, revestidos com óxidos metálicos, chamados de ânodos dimensionalmente estáveis (ADE), são os eletrodos com maior aplicabilidade industrial (Trasatti, 2000). Desde o seu surgimento, na década de 80, os ADE vem sendo estudados para diversas aplicações e com as mais variadas composições metálicas apresentando como maior entrave a estabilidade física do material e os custos relacionados com a manutenção do sistema (Berenguer *et al*., 2014; Carlesi *et al.*, 2011; Shao *et al.*, 2014).

No que concerne a avanços na síntese destes ADEs, estudos recentes desenvolvidos por De Mello *et al.* (2018) e Santos *et al.*, (2015) sugerem o uso de líquidos iônicos (LI) durante a síntese de solução precursora para fabricação de ADEs por meio de técnicas de decomposição térmica, reduzindo consideravelmente seu tempo de síntese. Os líquidos iônicos conferem inúmeras vantagens ao processo de síntese de eletrodo aumentando a viscosidade da solução precursora, levando a menor número de etapas de revestimento até a obtenção de uma camada uniforme (De Mello, 2017). Além disso eles também conferem uma certa maleabilidade à solução precursora até temperaturas mais altas, o que cria uma certa flexibilidade do revestimento levando a formação de rachaduras menores na camada final de revestimento melhorando sua estabilidade física e melhorando seu tempo de vida (Silva, 2018).

Todos esses fatores propõe um material eletrocatalítico que seja mais eficiente no tratamento de contaminantes orgânicos persistentes e que procurem de alguma forma melhorar as condições operacional do material final. Contudo, alguns fatores limitantes, tais como sua baixa estabilidade física e área superficial inviabilizam sua aplicação industrial. Neste sentido, estudos desenvolvendo materiais com maior estabilidade física e com maior área superficial ainda são requeridos.

Nos últimos anos, o desenvolvimento de novos materiais ganhou uma propulsão imensurável com a criação de novas conformidades físicas (Cesarino *et al.*, 2012; Pinheiro *et al*., 2016) capazes de aumentar a área superficial dos anodos utilizados em reações de degradação eletroquímica, fator limitante para sua aplicação industrial (Radjenovic e Sedlak, 2015). Neste enfoque, surgem diversas configurações físicas que buscam otimizar a eficiência catalítica dos reatores eletroquímicos (Eguiluz *et al.*, 2010; Moreira *et al.*, 2014, Pupo *et al*., 2014; Zhang *et al*., 2014).

Assim, o presente trabalho busca o desenvolvimento de rotas de síntese de eletrodos revestidos com óxidos metálicos otimizadas utilizando LI, analisando diversas composições e condições de síntese. Os óxidos metálicos escolhidos foram determinados conforme

levantamento bibliográfico buscando promover efeitos sinérgicos entre os mesmos. Adicionalmente, de forma a melhorar as propriedades físicas, modificação na superfície dos eletrodos por meio da inserção de camadas de nanotubos foi realizada como forma de garantir maior estabilidade física ao material.

Finalmente, estudos de otimização operacional para degradação eletroquímica compostos orgânicos foram realizados em reator filtro-prensa utilizando-se de um eletrodo comercial de diamante dopado com boro (DDB) para fins comparativos. Os estudos de degradação desenvolvidos nestes sistemas tiveram como moléculas alvos fármacos, herbicidas e agentes de contraste de raios x.

2. OBJETIVOS GERAIS

O presente trabalho busca o desenvolvimento de ânodos dimensionalmente estáveis com alta área superficial e estabilidade mecânica para aplicação em reações de degradação eletroquímica de compostos orgânicos variados (tais como, Diuron, Cefalexina e agentes de contraste de raio x), assim como o desenvolvimento de reatores eletroquímicos. Além disso, a analise comparativa do comportamento eletrocatalítico dos eletrodos obtidos considerando o eletrodo comercial DDB.

2.1 Objetivos Específicos

Degradação eletroquímica da Cefalexina em reatores do tipo filtro-prensa equipado com ânodo DDB analisando variáveis operacionais (pH, densidade de corrente e eletrólito), toxicidade da solução final para *E. coli* e determinando sua rota de degradação.

Desenvolvimento de ânodos mistura de óxidos metálicos com caracterização eletroquímica, física e eletrocatalítica dos eletrodos obtidos. Análise do percentual de remoção da molécula alvo Diuron estudando efeitos de temperatura de calcinação variados quando aplicando metil imidazolium como liquido iônico para síntese da solução precursora.

Melhora do tempo de vida operacional dos eletrodos de misturas de óxidos metálicos por meio da inserção de camada de nanotubos na superfície do substrato de suporte em uma estrutura de malha metálica. Estudos eletrocatalíticos aplicando o ânodo aprimorado em um reator do tipo filtro prensa 3D com análise com analise comparativa da capacidade eletrocatalítica do material considerando eletrodo comercial de DDB e agentes de contraste de raios x como molécula alvo.

3. REVISÃO BIBLIOGRÁFICA

3.1 Sistemas de Tratamento de Efluentes

Sistemas de Tratamento de Efluentes (STE) convencionais consistem da combinação de tratamentos físicos, químicos e biológicos. Sendo existentes quatro etapas de remoção: tratamento preliminar, primário, secundário, terciário e/ou tratamento avançado. O tratamento preliminar é usado para remoção de sólidos em suspensão e outros particulados encontrados no efluente bruto, visando reduzir os óleos, graxas, gorduras, areia e limo, feito mecanicamente por meio de filtração e grades. O tratamento primário é feito para remover os sólidos em suspensão e parte dos colóides, o qual é necessário para melhoria da operação e manutenção das subsequentes unidades de tratamento. O tratamento secundário é desenhado substancialmente para degradar conteúdo orgânico do esgoto, usualmente usando micro-organismos na fase de purificação; no tratamento terciário e/ou tratamento avançado do efluente aplica-se processos biológicos e físico-químicos. Na Figura 1, são mostradas as etapas existentes em uma estação de tratamento de esgoto exemplificando um sistema de tratamento de efluente convencional.

Contudo, os sistemas de tratamento convencionais não são projetados para remoção de micro poluentes, como anti-inflamatórios e outras drogas. É entendido que esses fármacos são provavelmente removidos por adsorção nos sólidos em suspensão ou através da associação com gorduras e óleos durante degradação aeróbica e anaeróbica, e degradação química (abiótica) por processos como hidrólises e fotodegradação *(Feng et al.*, 2013).
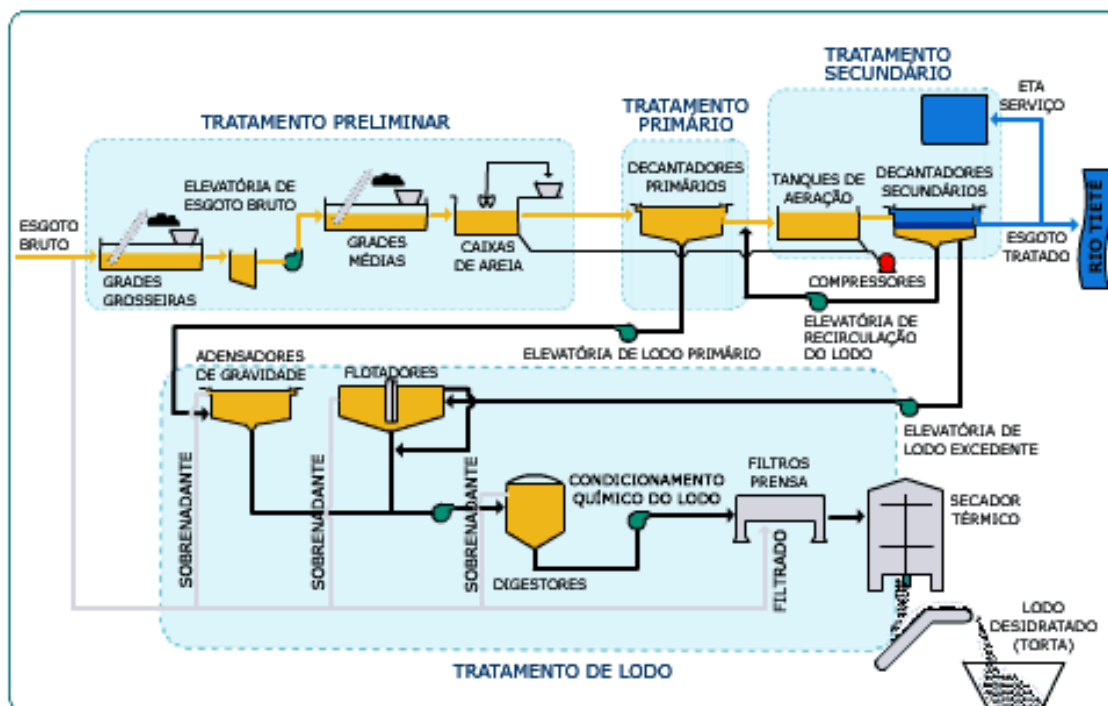
Figura 1: Etapas de Estação de Tratamento de Esgoto (adaptado de Novais, 2012).

O comportamento das drogas uma vez que atingem os sistemas de tratamento de efluentes pode ser dividido em três rotas (Matamoros, Rodríguez, e Albaigés, 2016; Michael *et al*., 2013) :

1) A droga ou metabolito parente da droga é biodegradável, isto é, ela é mineralizada por micro-organismos até dióxido de carbono e água.

2) A droga é menos persistente no STE, o que implica que, dependendo da lipofacilidade ou das ligações presentes, parte da substância pode sofrer degradação parcial. Se o lodo do sistema é reutilizado para fins agrícolas, a droga pode encontrar rotas de contaminação ambiental.

3) A droga é persistente, e ao mesmo tempo muito polar, sem capacidade de ligação com sólidos. Essas substâncias não serão degradadas no STE e atingirão o meio ambiente afetando os organismos aquáticos.

No que compete à Legislação Brasileira, temos que os efluentes hospitalares, contendo grande volume de fármacos, devem ser tratados através de Plantas de Estação de Tratamento antes de serem emitidos em corpos d'água ou em sistemas de disposição de efluentes, sempre que não houver sistema de tratamento direcional atendendo a área considerada (Dorion *et al*., 2012). Contudo, ela não é clara no que compete aos índices de

poluição e níveis de concentração permitidos na emissão ao meio ambiente deixando uma lacuna no que concerne aos níveis admissíveis.

Assim, dada a natureza dos compostos trabalhados, nota-se a conscientização ambiental em alguns ramos industriais dos quais é possível notar atenção direcionada a esta forma de contaminação. Por exemplo, em indústrias de produtos tóxicos ou medicamentos mutagênicos, o efluente é concentrado e incinerado a altas temperaturas, o que requer muita energia e gera dióxido de carbono como subproduto. Embora incineração possa completamente eliminar a toxicidade das substâncias, ele não é um método prático em um arranjo clínico o que abre espaço para o desenvolvimento de rotas menos agressivas como forma de tratar esse resíduo (Hirose *et al.*, 2005).

A escolha de métodos de tratamento de efluentes alternativos depende de uma série de fatores que envolvem desde o produto a ser degradado, à disponibilidade de espaço para instalação do sistema. Sirés *et al.* (2014) propõe uma escala baseada na concentração de demanda química de oxigênio (DQO), para determinar a aplicabilidade dos diversos tipos de sistemas usuais de tratamento, como pode ser visto na Figura 2.
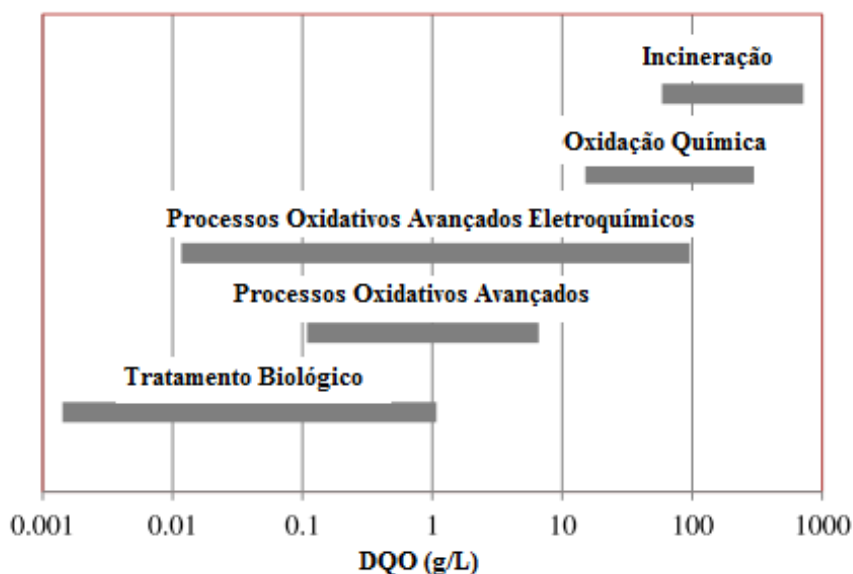
Figura 2: Aplicabilidade do tratamento de efluente baseado na carga orgânica (adaptado de Sirés *et al.,* 2014).

Desta forma, é possível notar que o método alternativo de tratamento de efluente que é capaz de tratar efetivamente a maior janela de DQO são os Processos Oxidativos Avançados Eletroquímicos (POAEs), o qual será foco no desenvolvimento do presente estudo.

3.2 Processos Oxidativos Avançados (POAs)

Processos Oxidativos Avançados (POAs), podem ser definidos como métodos de oxidação da fase aquosa baseados em espécies intermediárias altamente reativas levando a destruição do poluente alvo (Sirés *et al.*, 2014). Os POAs envolvem diversos processos com geração de radicais hidroxila (OH•) (Equação 1 e 2), os quais são muito reativos e não seletivos, e os mais comuns podem ser divididos em fotoquímicos (UV/O_3, UV/H_2O_2), fotocatalíticos (TiO$_2$/UV, foto-Fenton) ou oxidações químicas (O_3, O_3/H_2O_2, H_2O_2/Fe_2) (Pereira *et al.*, 2011). Além de tais processos existem também os POAs baseados na tecnologia eletroquímica, que são chamados de processos oxidativos avançados eletroquímicos (POAEs) como o eletro-Fenton (EF), fotoeletro-Fenton (FEF) e sonoeletroquímico (SE). (Palma-Goyes *et al.*, 2014) . Estes processos não apresentam as desvantagens dos POAs convencionais, que são: alto custo, a necessidade de adicionar reagentes químicos e complicações pelo uso da luz UV com vida útil relativamente baixa das lâmpadas e os altos coeficientes de absorção da água a ser tratada (Oturan e Aaron, 2014). O denominador comum de todos os POAs é a produção e uso da radical hidroxila, o qual é considerado um agente oxidante poderoso em fase aquosa (E = 2,8 V/HESS). As hidroxilas são capazes de atacar a maioria dos compostos orgânicos de forma a atingir uma mineralização total para CO_2, água e íons inorgânicos (Han *et al.*, 2014).

$$H_2O \rightarrow HO \bullet + H^+ + e^- \qquad \text{Equação 1}$$
$$HO^- \rightarrow HO \bullet + e^- \qquad \text{Equação 2}$$

Devido à sua alta reatividade, as hidroxilas possuem forte poder de se recombinar em:

$$2^\bullet OH \rightarrow H_2O_2 \qquad \text{Equação 3}$$

Considerando a habilidade dos POAs de atingirem a completa mineralização de poluentes para CO_2, água e compostos inorgânicos, ou ao menos sua oxidação parcial para compostos intermediários mais biodegradáveis e/ou menos danosos, eles permitem uma combinação com processos biológicos mais efetivos e menos custosos (Pereira *et al.*, 2011). Assim, um sistema de POA pode ser considerado como um processo terciário, posterior ao tratamento biológico (secundário) (Ikehata *et al.*, 2006).

3.2.1 Processos Oxidativos Avançados Eletroquímicos (POAEs)

Os POAEs diferentemente de outros processos de oxidação química, baseia-se no uso da energia elétrica para degradação dos contaminantes orgânicos. Os POAEs fornecem uma série de vantagens tanto do ponto de vista ambiental quanto econômico visto que estes se baseiam na utilização de um reagente limpo - o elétron, e somado com a possibilidade de degradação de até 99% do contaminante orgânico presente na água. Além disso, tais processos podem ser facilmente combinados com outros métodos convencionais permitindo um custo-benefício operacional ainda maior (Sirés *et al.*, 2014).

A eficiência e a flexibilidade dos POAEs têm sido provadas pela vasta gama de efluentes que podem ser tratados, os quais podem-se citar os corantes (Brillas e Martínez-Huitle, 2015), pesticidas (Cheng *et al.*, 2016) e os fármacos (Michael *et al.*, 2013).

Algumas características intrínsecas do efluente acabam por auxiliar nas reações de oxidação eletroquímicas. Por exemplo, a condutividade presente em grande parte dos efluentes reduz ou elimina a necessidade de adição de sal para compor o eletrólito. Sendo assim, favorecem as reações que ocorrem em meios altamente salinos reduzindo a demanda por energia. Adicionalmente efluentes contendo altas concentrações de cloro melhoram a degradação de compostos orgânicos devido à oxidação indireta melhorada pelos cloretos eletro-gerados. Tal oxidação indireta pode ocorrer tanto através dos radicais de cloro adsorvidos na superfície do catalisador quanto pelas espécies de cloreto reativas, como, por exemplo, o Cl_2, HOCl, ou OCl (Hurwitz *et al.*, 2014).

Além da quebra de compostos orgânicos, reações ocorrendo em meio ácido contendo cloreto favorecem a remoção de outros contaminantes, além de processos de desinfecção. Para processos eletroquímicos ocorrendo em meio ácido de cloretos é importante notar que três mecanismos de desinfecção de patógenos podem estar presentes (Hussain *et al.*, 2014):

a) desinfecção eletroquímica direta: oxidação dos microrganismos na superfície do catalisador por transferência de elétrons causando morte celular.

b) eletro cloração: o cloro na água é oxidado, gerando cloretos na superfície do absorvente.

c) efeitos de pH: oxidação anódica resultando na formação de íons de hidrogênio na superfície do ânodo diminuindo o pH local, destruindo a parede celular e causando a morte celular

Contudo, apesar das inúmeras vantagens apresentadas em sistemas aplicando o NaCl como eletrólito, o caráter fortemente reativo dos seus subprodutos contribui não apenas para a degradação do composto alvo, como também dos constituintes do sistema de tratamento. Assim, diversos estudos analisando os efeitos positivos e danosos dos cloretos são encontrados, chegando ao consenso que apesar de altamente reativo e positivo a termos de degradação do composto-alvo, seu uso deve ser feito de forma moderada e com cautela evitando prejuízos maiores nas tubulações, bombas e reatores envolvidos nos mais variados tipos de POAs aplicados (Brillas e Martínez-Huitle, 2015; Evdokimov, 2000; Fathollahi *et al.*, 2011; Hurwitz *et al.*, 2014; Moura *et al.*, 2014; Sales Solano *et al.*, 2013; Shao *et al.*, 2014)

Embora desinfecção por meio de reações eletroquímicas tenha sido vastamente usada, as principais dificuldades encontradas em sua implementação são o alto custo do sistema eletroquímico, e as altas voltagens necessárias associadas quando o efluente possui baixa condutividade (Hussain *et al.*, 2014) Um dos componentes mais representativos e de alto custo é o ânodo de trabalho, onde utiliza-se comumente o Diamante Dopado com Boro (DDB), devido à características operacionais atribuídas ao material e discutidas posteriormente.

Uma alternativa de baixo custo são os eletrodos baseados em filmes contendo óxido ou misturas de óxidos condutores, os chamados ânodos dimensionalmente estáveis (ADEs) e tem sido foco de pesquisas que avaliam seu desempenho no tratamento eletroquímico de efluentes (Rao e Venkatarangaiah, 2014). As vantagens deste tipo de ânodo são detalhadas mais adiante. Assim, considerando a aplicabilidade dos POAEs para degradação de compostos orgânicos e os altos custos associados com este procedimento, o presente trabalho busca a redução de custos operacionais focando no desenvolvimento de ADEs com baixo custo inicial e rápida síntese de forma a analisar a viabilidade de sua aplicação em degradações eletroquímicas.

3.3 Eletrodos de Trabalho

A eletrocatálise depende basicamente de dois fatores diferentes: os eletrônicos e geométricos. Os fatores eletrônicos envolvem as ligações da superfície com os intermediários e dependem da estrutura química da superfície, já os geométricos estão relacionados com a extensão da área superficial (Trasatti, 2000).

Assim, a escolha do material adequado que satisfaça os fatores acima citados para ser utilizado como ânodo de trabalho durante a degradação de cada composto tratado é de essencial importância para a obtenção de taxas de reação adequadas. Neste sentido, o conceito de ânodo inativo e ativo, onde o primeiro gera alta produção de radicais hidroxila e concentra suas rotas de degradação no seio da solução, enquanto o segundo apresenta reações superficiais de fissiosorção participando da degradação dos contaminantes de forma direta e no seio da solução, é de extrema importância (Shao *et al.*, 2014).

Com isso, surge uma gama de pesquisas focadas em desenvolver o material mais eletroativo e fisicamente estável possível para determinada reação.

3.3.1 *Diamante Dopado com Boro (DDB)*

Dentre os anodos mais conhecidos e aplicados industrialmente, o ânodo de DDB, merece destaque. Estes apareceram inicialmente em 1993, estudados por Tenne e colaboradores. Eles investigaram a redução do nitrato para amônia em um catodo de DDB. Carey e colaboradores patentearam o uso de eletrodos DDB como ânodos para oxidação de poluentes orgânicos em 1995 (Chen, Gao e Chen, 2005).

Os eletrodos de DDB apresentam boas propriedades que os distingue dos demais eletrodos, tais como: (1) uma ampla janela de potencial em eletrólitos aquosos e não aquosos; (2) estabilidade à corrosão em meios agressivos: a morfologia do diamante é estável em longos ciclos; (3) uma superfície inerte com propriedades de adsorção e forte tendência a resistir à desativação e (4) corrente capacitiva muito baixa (Panizza, Brillas e Comninellis, 2008).

O DDB é um material com boas propriedades eletroquímicas para tratamento de efluentes contaminados com compostos orgânicos, por que ele permite a quase completa mineralização dos compostos com altas eficiências de corrente. O uso de análise de carbono orgânico total (COT) é a melhor ferramenta para informar se houve realmente mineralização completa do composto (Aquino *et al.*, 2014).

Com baixas propriedades de adsorção em superfície, a maior parte dos radicais hidroxila adsorvidos se desprendem da superfície do DDB e se tornam radicais livres como segue na equação:

$$DDB + H_2O \rightarrow DDB\,(OH\,\cdot) + H^+ + e \rightarrow DDB + (OH\,\cdot) + H^+ + e \qquad \text{(Equação 4)}$$

Os radicais hidroxila consequentemente reagem com o composto orgânico e degradam completamente o poluente. Ademais, devido às fracas ligações de adsorção dos radicais hidroxila, o ânodo não participa da reação secundaria (produção de O_2). Assim, a decomposição de OH• é prolongada (Wei *et al.*, 2011).

Reações de degradação de compostos orgânicos, em especial os de foco central da presente pesquisa (tais como, corantes, fármacos e pesticidas), são vastamente vistos em literatura comprovando a sua eficiência para os sistemas propostos (Bogdanowicz *et al.*, 2013; Brillas, Thiam e Garcia-Segura, 2016; Silva *et al.*, 2013; Haidar *et al.*, 2013; Labiadh *et al.*, 2016; Panakoulias *et al.*, 2010; Souza *et al.,* 2014; Zhang *et al.*, 2016). Contudo, pesquisas focando na otimização do processo estudando a influência de variáveis como densidade de corrente (Guzman-Duque *et al.*, 2014), eletrólito de suporte (Zhang *et al.*, 2016), níveis de dopagem do ânodo (Bogdanowicz *et al.*, 2013), entre outros, são de crescente interesse. Assim, o presente estudo também analisará condições operacionais e sua influência na eficiência de degradação dos compostos orgânicos escolhidos.

3.3.2 *Ânodos Dimensionalmente Estáveis (ADEs)*

Os ADEs têm recebido bastante atenção devido às suas vantagens como alta atividade eletrocatalítica, baixo custo inicial e métodos de preparação simples. Um ADE é basicamente composto de um substrato metálico, uma camada protetora e o catalisador propriamente dito. Os ânodos utilizam frequentemente substratos de Ti por conta da estabilidade e uniformidade deste metal.

Os primeiros eletrodos suportados em placas de Ti foram sintetizados por Beer (1980) e chamados de ânodos dimensionalmente estáveis (ADE®) que apresentavam alto poder catalítico e forte estabilidade. Titânio é um metal barato que anodicamente gera uma camada de TiO_2 se auto protegendo contra corrosão (Rao e Venkatarangaiah, 2014). Em adição, temos uma camada de óxidos metálicos como, por exemplo, IrO_2 ou RuO_2 que são caros, ou o Sb_2O_5 que é tóxico ao meio ambiente (Shestakova *et al.*, 2014), ou ainda IrO_3 (Guzman-Duque *et al.*, 2014), TiO_2 (Moura *et al.*, 2016), SnO_2, PbO_2, dentre outros (Shao *et al.*, 2014). A Tabela 1 mostra um quadro histórico do desenvolvimento dos ADEs nos últimos 70 anos.

Tabela 1. Evolução do uso de ADE nos últimos 70 anos (adaptado de Rao e Venkatarangaiah 2014)

Ano	Material	Aspectos
Antes de 1950	Grafite/Chumbo/Ferro	Baixa eficiência e sofre corrosão
Anos 50	Ti/RuO$_2$ e Ti/RuO$_2$-TiO$_2$	Maior estabilidade, larga janela de potencial de operação, condutividade melhorada, barato e fácil fabricação
1965	Ti/Pt	Dimensionalmente estável, sofre corrosão lentamente, caro
1970	Ti/IrO$_2$-RuO$_2$-TiO$_2$	Alta atividade catalítica para geração de cloretos, maior tempo de vida útil, se dissolve em potenciais ânodicos mais altos
1970 – Atualidade	SnO$_2$ – RuO$_2$ – TiO$_2$, TaO$_2$ – IrO$_2$ e diversas misturas de óxidos metálico.	Adição de IrO$_2$ estabilizando o material e restringindo a dissolução de RuO$_2$ em pH básico, melhor custo benefício, alta atividade catalítica para geração de cloretos e oxigênio.

A dopagem de eletrodos tem sido um método comumente usados para melhorar a condutividade e estabilidade do eletrodo incorporando íons e átomos na estrutura matricial do mesmo (Dong *et al.*, 2014). A mistura de diferentes óxidos metálicos, gerando novos compostos estáveis, podem exibir significativas melhoras na atividade catalítica, o que se deve ao aumento dos sítios ativos ácidos ou básicos ou a troca no estado metálico dos íons (Wu, Huang e Lim, 2014).

Dentre as diferentes combinações metálicas propostas, um dos ânodos mais promissores é o dióxido de estanho dopado com antimônio, devido ao seu alto potencial de conversão do oxigênio, alta atividade de oxidação eletroquímica, baixo custo e baixa toxicidade (Shao *et al.*, 2014).

O dióxido de estanho isoladamente é um semicondutor do tipo n com um *band-gap* de cerca de 3.5 eV e exibe alta resistividade em temperatura ambiente, o que impossibilita seu uso de forma direta (Adams, Tian e Chen, 2009). Assim, a dopagem deste material tem sido vastamente estudada com diversos resultados ratificando o aumento em sua condutividade devido a dopagem com antimônio (Ahn *et al.*, 2016; Chaiyont *et al.*, 2013; Chen *et al.*, 2010; Correa-Lozano, Comninellis e Battisti, 1997; Feng *et al.*, 2008; Wang *et al.*, 2015; Xu, Li e Xu, 2015).

Tomando como referência a oxidação da água que ocorre em aproximadamente 1.2 V *vs.* NHE, temos que a diferença entre o ponto de oxidação da água e onde a reação realmente

ocorre é chamado de sobrepotencial de redução de oxigênio (Anglada, Urtiaga e Ortiz, 2009)..
Dados referentes a esse valor, considerando vários metais podem ser vistos na Tabela 2.

Tabela 2. Potencial de redução do oxigênio de diferentes ânodos, V *versus* NHE (adaptado de Anglada *et al.* 2009).

Ânodo	Potencial (V)	Condições
Pt	1.6	0.5 mol L^{-1} H_2SO_4
IrO_2	1.6	0.5 mol L^{-1} H_2SO_4
Grafite	1.7	0.5 mol L^{-1} H_2SO_4
PbO_2	1.9	1.0 mol L^{-1} H_2SO_4
SnO_2	1.9	0.5 mol L^{-1} H_2SO_4
TiO_2	2.2	1.0 mol L^{-1} H_2SO_4
Si/BDD	2.3	0.5 mol L^{-1} H_2SO_4
Ti/BDD	2.7	0.5 mol L^{-1} H_2SO_4

Estudos desenvolvidos por Kapałka *et al.*, (2008) sugerem que, quanto mais fraca a interação entre os radicais hidroxila e a superfície do eletrodo, menor a atividade eletroquímica de redução de oxigênio (ânodos de maior sobrevoltagem) e maior a reatividade química para oxidação de compostos orgânicos.

Em caso de o substrato do eletrodo ter uma sobrevoltagem de redução de oxigênio similar ao revestimento, a presença de orifícios no revestimento pode levar à reações de desprendimento de oxigênio na superfície do substrato. As bolhas geradas nesse processo tendem a causar desgaste mecânico e desprendimento do revestimento catalítico no eletrodo (Brungs, Haddadi-Asl e Skyllas-Kazacos, 1996).

É importante ainda notar que a quantidade de dopagem do material é outro fator limitante da qualidade do ADE obtido. Para o caso de SnO_2-Sb_2O_3, estima-se que pouco menos de 10% de massa dopada é adequada para o conteúdo do Sb. Uma vez que se aumenta além desse ponto a dopagem, nota-se que o material é menos homogêneo o que pode ser atribuído à diferenças de coeficiente de expansão térmica do material. Em baixos valores de dopagem, os radicais fissisorvidos são envolvidos na oxidação levando a combustão completa de orgânicos. A distribuição heterogênea de Sb reduz a atividade catalítica e expõe o metal de base levando a sua passivação (Rao e Venkatarangaiah, 2014).

Assim, embora os ADEs de Ti/SnO$_2$-Sb possuam propriedades interessantes, efeitos de passivação e desprendimento da camada de revestimento prejudicam a aplicação do material em potenciais variados ou por longos períodos de tempo (Del Río *et al.*, 2010)

Em busca de uma solução para esta problemática, a dopagem com um elemento ternário é uma alternativa a ser explorada. A partir destes uma série de materiais é sugerida em busca da formação de uma estrutura metálica uniforme, com alta atividade catalítica e fortemente aderida ao substrato de Ti (Feng *et al.*, 2010; Liu *et al.*, 2012; Shao *et al.,* 2014; Shestakova *et al.*, 2014; Sun *et al.*, 2015).

Para escolha dos óxidos metálicos a serem utilizados para dopagem foi levado em consideração o teorema de Hume – Rothery (Zhang *et al.*, 2008), onde:

a) Os óxidos metálicos dopados precisam apresentar similaridade de <15% em raio atômico.

b) Os óxidos metálicos devem apresentar eletronegatividade próximas.

c) Os óxidos metálicos devem apresentar fator de valência próximos.

SnO$_2$-SbBi

O Bi é conhecido por ter propriedades químicas similares ao Sb devido à sua proximidade na tabela periódica. De acordo com a Lei de Hume, onde é visto que óxidos metálicos com 15% de semelhança, em seus tamanhos de raios atômicos, podem facilmente formar uma solução sólida, como é o caso de Sn e Bi (Dong *et al.*, 2014; Zhang, Yang e Evans, 2008).

Outra vantagem do Bi é sua ampla energia de *band gap* (de 2 a 3.96 eV), alto índice refrativo, permissividade dielétrica além de fotocondutividade e fotoluminescência. Devido a tais características ele tem sido usado para diversas aplicações tais como: revestimento de sensores óticos, tecnologia sensitiva, vidros estruturais finos e eletro-redução (Xiaohong, Wei e Weidong, 2007).

A dopagem de Bi é sugerida como forma de melhorar as condições de revestimento do substrato de Ti, obtendo uma camada mais uniforme e altamente eletrocatalítica (Hor e Cava, 2009; Shmychkova *et al.*, 2013).

SnO₂-SbCe

Os compostos de cério têm um enorme potencial para aplicação em diversas áreas devido à suas propriedades, tais como, sua faixa de potencial redox, alta mobilidade de oxigênio na rede cristalina, alta afinidade por compostos contendo oxigênio, nitrogênio e enxofre. O cério é muito conhecido por sua capacidade de aumentar a adsorção de poluentes na superfície de catalisadores em processos heterogêneos, o que favorece o processo de degradação dos poluentes (Martins, Hewer e Freire, 2007).

Cério é conhecido como um dos elementos terra-rara mais ativo e tem sido bem estudado para aplicações eletrocatalíticas. A característica mais importante da dopagem com Ce é sua capacidade de armazenamento de oxigênio dado pelo processo redox Ce^{4+}/Ce^{3+}, combinada com a sua mobilidade em estrutura cristalina (Cui, Feng e Liu, 2009).

$$2Ce^{4+} + O_{lat}^{2-} \rightleftarrows Vo + 2Ce^{3+} + O_f \qquad \text{Equação 5}$$

Onde O^{2-}_{lat} é o oxigênio da matriz e O_f é o átomo de oxigênio livre.

Estudos de degradação eletroquímica com eletrodos apresentando dopagens de Cério são escassas em literaturas, onde grande enfoque das pesquisas é dado para degradação de fenóis (Cui *et al*., 2009; Sun *et al*., 2015).

SnO₂-SbTa

Estudos prévios demonstram que a adição de Ta (mesmo em frações molares pequenas) contribui para o aumento da área superficial do eletrodo, melhora da condutividade eletrônica e aumento na capacidade de acumulo de energia (*charge storage capacitance*), promovendo o enriquecimento da superfície do eletrodo (Ardizzone *et al.*, 2006).

Dopagens com Ta tem sido associadas com redução no tamanho de grãos superficiais dos ADEs o que favorece o aumento de sua área eletroquimicamente ativa e, portanto as taxas de degradação de compostos orgânicos (Ardizzone *et al*., 2006; Silva *et al.*, 2013; Salazar-Banda *et al.,* 2012).

SnO₂-SbGd

A adição de Gd tem mostrado a geração de ADEs mais compactos e uma melhora da condutividade dos mesmos. Estima-se que o Gd inserido no eletrodo, ocupe o *band-gap*

deixado pelo SnO_2 e contribui para o aumento da concentração de carreadores livres. Como resultado, a introdução de Gd leva a um processo de eletrólise direcionado para reações de oxidação no lugar de reações de redução (Feng e Li, 2003).

Dopagem com Gd também tem sido associado à formação de superfícies mais homogêneas o que favorece o recobrimento do substrato, evitando efeitos de corrosão ou oxidação do mesmo, além de gerar um material mais compacto e com maior área eletroquimicamente ativa (Feng *et al.,* 2008).

Ademais, apesar das vantagens apresentadas com adição de metais terras-rara (Cui *et al.*, 2009), estudos analisando a dopagem de Gd em matrizes de SnO_2-Sb são escassos e o desenvolvimento de maiores conhecimentos sobre o mesmo são de grande interesse.

Líquido Iônico (LI)

Líquidos iônicos (LIs) são líquidos que são compostos inteiramente por íons, mas são diferentes dos sais metálicos devido a seu baixo ponto de fusão: geralmente < 100 - 150 ºC. Contudo, eles são bons solventes para complexos metálicos de transição, mas pouco miscíveis com compostos orgânicos não polares, permitindo a formação de sistemas bifásicos e o uso no preparo de catalisadores homogêneos (Gordon, 2001).

Adicionalmente, é importante notar que os líquidos iônicos têm tipicamente alta viscosidade (Wasserscheid e Keim, 2000). Tal, viscosidade apresentada pelos líquidos iônicos em pressão ambiente evita a formação de oxigênio (pela penetração do ar atmosférico) na superfície do substrato de titânio durante a decomposição térmica, assim evitando a formação de TiO_2.

Em geral, é importante destacar alguns fatores a respeito do trabalho com líquidos iônicos, como segue (Wasserscheid e Keim, 2000):

1) A estabilidade térmica do líquido iônico é limitada pela força de suas ligações carbono-heteroátomo e hidrogênio-heteroátomo. Assim, alguns líquidos iônicos apresentam estado líquido numa variação superior à 400 ºC.

2) A densidade do material decresce a medida que a concentração do cátion orgânico aumenta. A formação de ligações de hidrogênio entre cátions de *imidazolium* e íons cloretos básicos pode levar a um aumento na viscosidade em até 10×. Já leves aumentos na temperatura ou adição de cosolventes orgânicos são capazes de reduzir sua viscosidade.

3) Muitos líquidos iônicos são completamente miscíveis com solventes orgânicos se suas constantes dielétricas estão acima do limite característico.

4) A acidez e propriedades de coordenação de um líquido iônico são controladas pela natureza dos seus ânions. A acidez latente dos líquidos iônicos surge quando bases fracas são adicionadas aos cloroaluminato neutros *buffered* (o qual consiste de um material no qual a neutralidade do meio é mantida por reações com excesso de cloretos metálicos alcalinos com adição de $AlCl_3$).

Precursores viscosos também auxiliam na formação uniforme de aglomerados no revestimento e acumulação do dopante na superfície do revestimento, ao passo que precursores alcoólicos levam à formação do tipo barro-rachado, tradução literal do inglês para *mud-crack* (Rao e Venkatarangaiah, 2014). O interesse em precursores com aglomerados mais uniformes está suportado na busca por um revestimento com maior taxa de recobrimento do substrato metálico utilizado protegendo o mesmo de reações de oxidação comumente vistas.

Estudos prévios desenvolvidos no nosso grupo de pesquisa por Santos *et al.* (2015), comprovam a eficácia do uso de líquidos iônicos no processo de síntese de catalisadores ADEs para degradação de pesticidas, o que reitera sua viabilidade para produção de um material com forte poder de degradação de compostos orgânicos.

3.4 Efluentes degradados

Uma vez visto que os POAEs são capazes de degradar efluentes com as mais variadas concentrações de DQO, o presente estudo foca na degradação de compostos orgânicos específicos (cefalexina, diuron e agentes de contraste de raios x). No entanto, nota-se que apesar da grande aplicabilidade atualmente, há uma dificuldade de biodegradação de tais compostos orgânicos marcadamente agravada por conta de suas características mutagênicas e citotóxicas.

Dentre a variedade de fármacos excretados no meio, um dos grupos mais representativos são os dos antibióticos, entendidos como agente que inibe ou limita o crescimento de microrganismos, tais como, bactérias, fungos ou protozoários. Atualmente, existem cerca de 250 tipos diferentes de compostos químicos na classe dos antibióticos utilizados na medicina e na veterinária (Kümmerer, 2009).
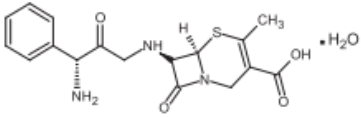
A grande maioria dos fármacos usados pelo homem não são totalmente degradados no corpo humano, alguns são excretados sem sequer sofrer alterações (Kümmerer, 2001). O que gera a crescente preocupação quanto à bioacumulação deste material no meio aquático e no solo. Adicionalmente, há provas de que os fármacos não são adequadamente degradados nos sistemas usuais de tratamento sanitário (Heberer, 2002).

Em 2011, a World Health Organization (WHO) publicou relatos de fármacos em água potável, o que trouxe à tona o risco associado para a saúde humana da exposição a contaminantes em nível traços dos fármacos na água, levantando suspeitas de que a ingestão contínua dos fármacos pode levar a riscos potenciais dos organismos em ambientes terrestres e aquáticos (Feng *et al.*, 2013).

3.4.1 Cefalexina

A cefalexina é um dos antibióticos mais prescritos no mundo sendo assim produzido em grandes quantidades. Ele tem uma ampla janela de atividade antibactericida e alta solubilidade em água. Já que a taxa de transformação da cefalexina é de apenas 10%, os demais 90% do composto é excretado sem modificação pela urina (Estrada, Li e Wang, 2012). As propriedades da cefalexina são mostradas na Tabela 3 abaixo.

Tabela 3. Propriedades da cefalexina (CLX).

Composto	Estrutura	Peso Molecular	Solubilidade
Cefalexina, CLX	$C_{16}H_{17}N_3O_4S \cdot H_2O$	365.40 u	1790 mg/L

Diversos estudos recentes têm focado na forte incidência da cefalexina nas plantas de tratamentos de esgoto doméstico mundialmente (Estrada *et al*., 2012; Locatelli, Sodré e Jardim, 2011; Lu *et al*., 2014). Estudos desenvolvidos por Gulkowska *et al.* (2008), determinando a concentração de antibióticos sendo inseridos em plantas de tratamento de efluentes, analisou 8 compostos, dos quais a cefalexina apresentava predominância percentual em quatro de cinco plantas de tratamento estudadas. As taxas de remoção para o antibiótico em

questão apresentavam valores que variavam de 9 a 89%, indicando que sua remoção por meio de tratamentos convencionais depende de inúmeros processos paralelos.

A baixa biodegradabilidade deste composto associado com os alarmantes níveis de prescrição do mesmo torna sua presença em efluentes um risco potencial para a saúde da população uma vez que os verdadeiros riscos da sua bioacumulação ou da sua persistência no meio ambiente ainda não são completamente entendidos. Estudos desenvolvidos por Li e Lin (2015) analisando um total de 74 fármacos comumente usados (dentre eles a cefalexina) presentes no Hospital de Veteranos de Zhudong e no Rio Toucian na Tailândia, atestaram que uma vez submetido à reações de fotodegradação, uma vez que o efluente é submetido ao meio ambiente, há formação de produtos mais tóxicos e resistentes à degradação. Estudos como estes enfatizam os fenômenos naturais como colaboradores em reações sinérgicas responsáveis por formação de subprodutos ainda mais danosos para a população humana.
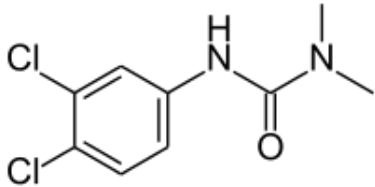
Assim, torna-se vital, para garantir a saúde e qualidade do meio ambiente, que os efluentes com fortes contribuições farmacológicas sejam tratados de forma controlada e individualizada evitando o desencadeamento de reações secundárias e sem controle que por vezes podem ser até mais prejudiciais à saúde ambiental.

3.4.2. Diuron

No que concerne o uso de compostos orgânicos complexos, além da produção e consumo crescente dos fármacos discutidos previamente, notamos uma crescente demanda por aditivos agrícolas que venham a garantir qualidade e volume produtivo do ramo. A crescente demanda por alimentos, somado as mudanças climáticas e as contínuas mutações sofridas pelas pragas levam à indústria química a um processo continuado de adaptação tecnológica, desenvolvendo compostos cada vez mais específicos e agressivos (Ribeiro *et al.*, 2015).

Dentre estes, o diuron é um herbicida comumente utilizado para erradicar pragas em áreas como beira de estrada, estacionamentos, rodoviárias, etc. Seu mecanismo de ação envolve o bloqueio de transporte de elétrons no processo de fotossíntese (Pipi, Neto e Andrade, 2013). Classificado como composto cancerígeno e genotóxico, o diuron e seus metabólicos têm sido associados com casos de má formação e problemas reprodutivos (Oturan *et al.*, 2008). A Tabela 4 informa as propriedades do herbicida Diuron®.

Tabela 4: Propriedades do Diuron®

Composto	Estrutura	Peso Molecular	Solubilidade
Diuron		233.09u	42 mg/L

Assim, rotas alternativas de degradação do Diuron tem sido enfoque de diversos estudos. Sistemas de degradação por métodos físico-químicos (Bouras *et al.*, 2007), Fenton, foto-Fenton, fotocatálise com TiO_2 (Katsumata *et al.*, 2009), e degradação biológica (Tixier *et al.*, 2000). Dentre as rotas alternativas propostas, as melhores taxas de mineralização têm sido vistas para sistemas de POAs testados em condições variadas (Oturan *et al.*, 2008; Pipi *et al.*, 2013; Polcaro *et al.*, 2004).

Assim, de modo a testar a efetividade do sistema de POAE proposto, o presente trabalho foca no desenvolvimento de reações de degradação eletroquímica dos citados compostos orgânicos de forma a testar a eficiência de tratamento para uma variada gama de compostos utilizando-se de BDD comercial e do ADE sintetizado por meio de metodologia inovadora proposta pelo grupo.

3.4.3. Agentes de Contraste de Raios X
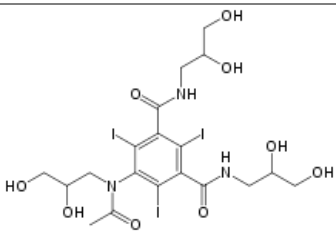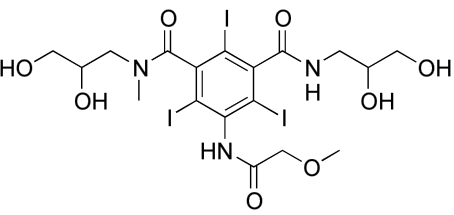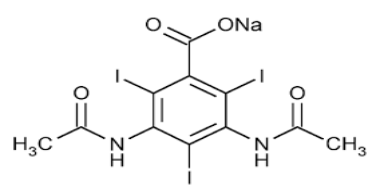
O problema ambiental causado pela emissão de agentes de contraste tem sido discutido ambientalmente a anos. Dentre todos os compostos usados, sabe-se que volumes de até 200 g pode ser excretada de uma única vez por pacientes em terapia. Estes compostos tem sido analisando buscando novas rotas de degradação capaz de efetivamente tratar os efluentes antes que estes atinjam o meio ambiente (Everslosh *et al.*, 2014).

Levando em conta o uso indiscriminado destes compostos e o fato de que as estacoes de tratamento não estão dimensionadas para receber e tratar este tipo de contaminante, muitas vezes estes compostos chegam ao meio sem modificação alguma (Del Moro *et al.*, 2015). Adicionalmente, devido a sua conformidade recalcitrante e sua alta estabilidade física estes compostos persistem no meio muitas vezes atingindo os lençóis freáticos e sendo posteriormente encontrados na água de consumo humano (Wu *et al.*, 2017).

De todas as espécies ioniazadas utilizadas, os compostos diatrizoato (DTR), iopromide (IPM) e iohexol (IOX) tem sido reportado por sua alta incidência e persistência no meio. Destes, o DTR foi submetido a tratamento por eletro-peroxona atingindo remoções de até 70% quando utilizando nanotubos de carbono em seu tratamento (Wu *et al.*, 2017). Já o IPM foi efetivamente removido completamente por tratamento eletroquímico em meio de cloreto de sódio, demonstrando o potencial de aplicação deste método de tratamento (Farhat *et al.* 2015).

Tabela 5: Propriedades de Aentes de Contraste de Raio X

Composto	Estrutura	Peso Molecular	Solubilidade
Iohexol		821.13u	0.796 mg/L
Iopromide		791.11u	0.0915 mg/mL
Diatrizoato		613.91u	350 mg/mL

4. ELECTROCHEMICAL MINERALIZATION OF CEPHALEXIN USING A CONDUCTIVE DIAMOND ANODE: A MECHANISTIC AND TOXICITY INVESTIGATION

Douglas A.C. Coledam[a], Marília M.S. Pupo[b], Bianca F. Silva[c], Adilson J. Silva[d], Katlin I.B. Eguiluz[b], Giancarlo R. Salazar-Banda[b], José M. Aquino[a,*]

* Corresponding Author. Phone: + 55 16 33066864

E-mail address: jmaquino@ufscar.br (José M. Aquino)

Abstract

The contamination of surface and ground water by antibiotics is of significant importance due to their potential chronic toxic effects to the aquatic and human lives. Thus, in this work, the electrochemical oxidation of cephalexin (CEX) was carried out in a one compartment filter-press flow cell using a boron-doped diamond (BDD) electrode as anode. During the electrolysis, the investigated variables were: supporting electrolyte (Na_2SO_4, NaCl, $NaNO_3$, and Na_2CO_3) at constant ionic strength (0.1M), pH (3, 7, 10, and without control), and current density (5, 10 and 20 mA cm^{-2}). The oxidation and mineralization of CEX was assessed by high performance liquid chromatography, coupled to mass spectrometry and total organic carbon. The oxidation process of CEX was dependent on the type of electrolyte and on pH of the solution due to the distinct oxidant species electrogenerated; however, the conversion of CEX and its hydroxylated intermediates to CO_2 depends only on their diffusion to the surface of the BDD. In the final stages of electrolysis, an accumulation of recalcitrant oxamic and oxalic carboxylic acids, was detected. Finally, the growth inhibition assay with *Escherichia coli* cells showed that the toxicity of CEX solution decreased along the electrochemical treatment due to the rupture of the β-lactam ring of the antibiotic.

Keywords: Boron-doped diamond; hydroxylation reactions; diffusion controlled process; *Escherichia coli*; toxicity assays.

4.1 Introduction

Surface and ground water contamination by synthetic organic compounds is one of the main concerns faced by the society in the 21st century (Zhang *et al*., 2013; Luo *et al*., 2014; Barbosa *et al*., 2016). Among the distinct classes of synthetic organic compound, such as dyes, plasticizers, personal care products, antibiotics are of significant concern due to their potential chronic toxic effects and resistance development by microorganisms (Homem and Santos, 2011; Van Doorslaer *et al.,* 2014). The main sources of environmental contamination by antibiotics are from human excretion after previous administration, veterinary applications or by inadequate disposal of expired drugs (Homem and Santos, 2011; Kong *et al*., 2016). Data gathered from the National Health Surveillance Agency (ANVISA) stated that, in Brazil, the consumption of antibiotics in 2005 was up to 390 tons of amoxicillin (AMX), 184 tons of ampicillin (AMP), 163 tons of cephalexin (CEX), 133 tons of sulfamethoxazole (SMX), 45 tons of tetracycline (TET), 38 tons of norfloxacin (NOR), 30 tons of ciprofloxacin (CIP), and 27 tons of trimethoprim (TMP). At total, these compounds are responsible for >80% of the antibiotics consumed in the country (Locatelli *et al*., 2011).

As the conventional wastewater treatment plants are inefficient to completely remove these synthetic compounds (Zhang *et al*., 2013; Van Doorslaer *et al.,* 2014; Derakhshan *et al*., 2016), they persist in the environment for long periods, leading to potential problems to the aquatic and human lives (Santos *et al.,* 2010; Orias and Perrodin, 2013; Puckowski *et al*., 2016). Moreover, synthetic compounds, such as antibiotics, are known for their persistence in the environment, being exposed to natural degradation processes such as hydrolysis, biodegradation and photodegradation (Li and Lin, 2015). Consequently, there is the necessity to treat effluents contaminated with synthetic compounds, as well as their transformation byproducts (Escher and Fenner, 2011), before disposal into the environment in order to avoid surface water contamination (Locatelli *et al*., 2011; Michael *et al.,* 2013) and production of even more toxic byproducts. There is a variety of methods to treat effluents contaminated with organic substances (Singh and Arora, 2011; Rivera-Utrilla *et al*., 2013; Ganzenko *et al*., 2014; Särkkä *et al.,* 2015; Derakhshan *et al*., 2016), whose choice depends on the physical-chemistry characteristics of effluents (Oller *et al*., 2011). Among these methods, the electrochemical oxidation (or simply electrooxidation) might be a reasonable option (Anglada *et al*., 2009; Panizza and Cerisola, 2009; Brillas and Martínez-Huitle, 2015). Further, combined approaches considering methods based on the Fenton reaction (Oturan *et al.,* 2008; Antonin *et al*., 2015; Cong *et al*., 2016; Pereira *et al*., 2016; Vasconcelos *et al*., 2016) or on photocatalysis (Sirés *et al.*, 2014; Aquino *et al.*, 2015; Kong *et al.,* 2016), due to its amenable operational conditions

(Radjenovic and Sedlak, 2015), are indicated treatments for effluents containing a significant range of dissolved organic compounds (Cañizares *et al*., 2009; Sirés *et al.,* 2014) and with adequate conductivity.

The efficiencies of organic compound removal and electrical energy consumed are strictly related to the choice of adequate electrode materials (Anglada *et al*., 2009; Quiroz *et al*., 2014; Sopaj *et a*l., 2015) and hydrodynamic conditions used during operation. Therefore, the electrode chosen is of crucial importance in order to guarantee the system feasibility. Among the anodes proposed, boron-doped diamond (BDD) is the most investigated and well succeeded electrode material to oxidize organic molecules in distinct water matrices, such as real (Sales *et al*., 2013; Aquino *et al*., 2014a; Garcia-Segura *et al.,* 2015a; Martín de Vidales *et al*., 2015) or simulated (Coledam *et al*., 2016) effluents, due to its ability to generate quasi-free hydroxyl radicals (HO•), high oxygen overvoltage, high resistance to corrosion in aggressive media, and resistance to deactivation (Sopaj *et al*., 2015). According to the literature (Guinea *et al.,* 2009; Garcia-Segura et al., 2015b; Coledam *et al*., 2016), the efficiency of BDD towards degradation of organic compounds might be also related to the levels of boron doping and the ratio of sp^2 to sp^3 carbon atoms.

As has been seen in previous studies (Lizhang *et al*., 2016), electrochemical degradation is closely related to the concentration of organic compounds, since according to their mass transfer coefficient, most experiments report exponential drops from the anode's surface (Kapalka *et al*., 2009). Therefore, the conversion of organic molecules to CO_2 (mineralization) is restricted by mass transfer (Tissot *et al*., 2012). This problem could be overcome adjusting the applied electrical current density and flow velocity during cell operation as well as using other cell geometries or turbulence promoters (Radjenovic and Sedlak, 2015). Additionally, the use of distinct electrolytes could lead to an improved oxidation (chemical oxidation) rate (Aquino *et al*., 2012), as oxidizing species such as active chlorine (mainly HOCl and OCl^-), persulfate, pyrophosphate and percarbonate could be produced when chloride, sulfate, phosphate and carbonate ions are used, respectively (Panizza and Cerisola, 2009; Sirés *et al*., 2014). However, it is unlikely that these oxidants promote complete mineralization due to their low oxidation potential.

Despite the extensive number of papers describing the application of electrochemical methods to treat contaminated effluents and synthetic solutions with a variety of organic compounds, literature on the impact of those treated effluents and solutions towards their toxicity, is still very limited (Hurwitz *et al*., 2014; Karci, 2014; Li and Lin, 2015). This

might be due to the difficulty in finding a specific and sensitive (Guerra, 2001; Oturan *et al.*, 2008) testing organism with respect to the target pollutant.

Thus, the aim of the present work is to investigate the electrooxidation of cephalexin (CEX), which is an antibiotic representative of the penicillin class containing a β-lactam ring, using distinct supporting electrolytes and a BDD as anode. The performance of the system will be compared through the decays of the CEX concentration (assessed by high performance liquid chromatography - HPLC) and total organic carbon (TOC), as well as the generated intermediate compounds (aromatic and short chain) by mass spectrometry analyses. The toxicity evolution of the electrolyzed solution will be followed through growth inhibition assays using the *Escherichia coli* (*E. coli*) bacterium. In addition, the experimental data of the CEX electrooxidation, using a flow cell, will be compared to a theoretical model based on a system purely controlled by mass-transport.

4.2 Experimental

4.2.1. *Chemicals*

All chemicals, including CEX (monohydrate 99.9% Vita Nova), Na_2SO_4 (a.r., Qhemis), NaCl (a.r., Qhemis), $NaNO_3$ (a.r., Synth), Na_2CO_3 (a.r., Synth), KH_2PO_4 (a.r., Sigma Aldrich), H_3PO_4 (85%, Mallinckrodt), $Na_2S_2O_8$ (a.r., Sigma Aldrich), carboxylic acids (a.r., Sigma Aldrich), formic acid (HPLC grade, JT Baker), tryptone (a.r., Himedia), yeast extract (a.r., Himedia), and methanol (HPLC grade, JT Baker) were used as received. Deionized water (Millipore Milli-Q system, resistivity $\geq$18.2 MΩ cm) was used for the preparation of all solutions.

4.2.2. *BDD electrode*

BDD films with 100 ppm of boron (sp^3 to sp^2 C ratio equal to 215) were synthesized through hot filament chemical vapor deposition technique on a monocrystalline Si p-doped substrate and were purchased from NeoCoat SA (Switzerland). The values in parenthesis refer to the ratio of the C atoms measured through Raman spectroscopy and were provided by the manufacturer.

4.2.3. *Electrochemical degradation experiments*

The electrochemical experiments were carried out in a one-compartment filter-press flow cell containing a BDD and an AISI 304 stainless steel plate, as anode and cathode, respectively. The exposed area of the anode was 3.54 cm × 6.71 cm. More information regarding the setup of the assembled system can be found elsewhere (Coledam *et al.*, 2016). The investigated variables and their ranges in the electrooxidation process were: supporting electrolyte at 0.1 M of ionic strength (i.e. 33 mM Na_2SO_4, 100 mM NaCl, 100 mM $NaNO_3$ and 33 mM Na_2CO_3), pH (3, 7, 10, and without specific control), and applied electric current density (5, 10, and 20 mA cm^{-2}). The solution pH was continuously monitored and kept constant in the desired value by additions of concentrated H_2SO_4 or NaOH solutions; the condition of "without specific control" means that no acidic or alkaline solutions were added to adjust the pH. The initial CEX concentration, as well as, flow rate (flow velocity), electrolysis time, solution temperature, and electrolyzed solution volume were fixed at 100 mg L^{-1}, 420 L h^{-1} (0.7 m s^{-1}), 360 min, 25 ºC, and 1000 mL, respectively. Before any degradation electrolysis and in order to eliminate any adsorbed organic compound, the BDD anode was electrochemically pre-treated in a 0.5 M H_2SO_4 solution by applying 20 mA cm^{-2} for 15 min.

4.2.4. *Analyses*

Concentration of CEX was monitored by high performance liquid chromatography (HPLC) using a core shell C-18 reversed phase as the stationary phase (150 mm × 4.6 mm, 5 μm particle size from Phenomenex®) and a mixture of 10 mM KH_2PO_4 at pH 3 (eluent A) and methanol (eluent B) in a gradient elution mode as the mobile phase and flow rate of 1 mL.min^{-1}. The gradient elution protocol started with 10% of eluent B, increasing to up to 90% after 12 min. Then, the composition of the mobile phase returned to 10% of eluent B after being kept at 90% for 2 min. The sample injection volume was 25 μL.

The intermediate compounds analyses were carried out with samples collected every 1 h until 8 h of electrolysis. The extracted samples of 2 mL were first frozen and then dried in a lyophilization system (CHRIST alpha 2-4 LD Plus) for 24 h. After this period, the samples were resuspended in 1 mL of methanol and filtered using a 0.22 μm cartridge. The intermediates formed during the CEX degradation were determined in a HPLC 1200 Agilent Technologies coupled to a mass spectrometer 3200 QTRAP (LC-MS/MS, Linear Ion Trap

Quadrupole), AB SCIEX Instruments operating in a positive mode and TurboIonSpray ionization. *Lightsight*® 2.3 (Nominal Mass Metabolite ID Software, AB SCIEX) software was used to investigate all possibilities of metabolites. The software application was performed through the all ionization and fragmentation parameters optimized for the initial compound. The parameters were obtained using a direct infusion of 10 µL min^{-1} of a solution containing CEX compound (1 mg L^{-1}) in H_2O:MeOH (1:1, *V/V*, with 0.1% of formic acid). The parameters conditions were: curtain gas at 20 psi, ion spray at 5200 V, gas 1 and gas 2 at 50 psi, temperature of 600°C, declustering potential of 41 V, entrance potential of 8 V and with interface heater ON. Optimized selected reaction monitoring (SRM) and full scan experiments were automatically performed by *LightSight*® to investigate different kinds of possible reactions, such as oxidation, hydroxylation, reduction, C-C bond cleavage and others. During the LC-MS/MS analyses, the phosphate buffer used in the mobile phase was changed to water containing 0.1% of formic acid. The injection volume was 20 µL and the samples collected at 0, 1, 2 and 3 h were diluted to one third before injection.

Short chain carboxylic acids were also determined by the electrolysis processes for the distinct types of salts used as supporting electrolyte, by HPLC. A Rezek ROA-H^{TM} column from Phenomenex® was used as the stationary phase and a 2.5 mM H_2SO_4 solution as the mobile phase at 0.5 mL min^{-1}. The carboxylic acids were identified through comparison of retention times with previously analyzed standards and by UV detection at 210 nm. The injection volume and column temperature were maintained at 25 µL and 23 ºC, respectively.

The toxicity test with *E. coli* was carried out with electrolyzed samples extracted each 1.5 h and at the beginning of the electrochemical experiment. Tryptone, yeast extract, and NaCl (Lennox LB broth) were added to each sample to a final concentration of 10, 5, and 5 g L^{-1}, respectively, and these solutions were filter-sterilized. An overnight culture of *E. coli* K12 MG1655 was used to inoculate 15 mL tubes containing 3 mL of samples, with 9×10^5 cfu mL^{-1} (cfu, colony forming units). Three tubes containing only LB medium were also inoculated to be used as negative controls. All tubes (in triplicate for each analyzed electrolysis time) were incubated at 37 ºC for 24 h at 200 rpm. After this period, *E. coli* growth was analyzed by measuring the absorbance of solutions at 600 nm, and the toxicity of samples was assessed through the inhibition index (*I*), calculated according to Silambarasan and Vangnai (2016):

$$I= (A_0-A.A_0)\times100 \qquad\qquad\qquad (1)$$

where A_0 and A are the absorbance values in the absence (control samples) and presence (samples from all the investigated electrolysis time) of CEX, respectively. The minimum inhibitory concentration (MIC) of CEX was determined by the micro-dilution method. Successive dilutions (dilution factor of 2) of a filter-sterilized LB medium containing 100 mg L^{-1} CEX were applied to a 96-well microplate and test wells were inoculated with 2 × 10^5 cfu mL^{-1} of an overnight culture of *E. coli* K12 MG1655. After incubation at 37 °C for 24 h, bacterial growth was analyzed by adding 50 µL of a 0.2 mg mL^{-1} p-iodonitrotetrazolium chloride solution to each well and further incubation at 37 °C for 30 min. Bacterial growth was visualized by a color change (from colorless to reddish pink), whereas clear wells indicated growth inhibition. The assay was repeated twice with three replicates each. The minimum CEX concentration where the growth of *E. coli* was confirmed to be inhibited (no color change) was 12.5 mg L^{-1}. This MIC value is in agreement with the one reported by Giacomino *et al*. (2012), whose value was equal to 16 mg L^{-1}.

The extent of mineralization (i.e. conversion to CO_2 and H_2O) was monitored by total organic carbon (TOC) measurements every 1 h after sampling and dilution of 5 mL of the electrolyzed solution using a GE Sievers Innovox analyzer. The TOC determination was carried out after mixing the electrolyzed sample with H_3PO_4 (6 M) and $Na_2S_2O_8$ (30% m/m) solutions. The oxidation was accomplished after the temperature and pressure corresponding to the supercritical point of water was reached. The TOC content was given by subtraction of the measured values of inorganic and total carbon, in terms of generated CO_2 and after comparison with a previously determined calibration curve, using a nondispersive infrared detector.

The mineralization current efficiency (*MCE*) was calculated according to the work of Brillas *et al.* (2009):

$$MCE = \frac{\Delta(TOC)_t n F V}{4.32 \times 10^7 m I t} \times 100 \tag{2}$$

where $\Delta(TOC)_t$ is the measured TOC removal (mg carbon L^{-1}) after a certain time, t (h), n is the number of exchanged electrons considering that the total electrical applied charge was consumed in the mineralization process (see eq. 3), F the Faraday constant (96,485 C mol^{-1}), 4.32 X 10^7 is a conversion factor (3600 s h^{-1} X 12000 mg mol^{-1} carbon), V the electrolyzed solution volume (L), m the number of carbon atoms of the CEX molecule, and I the applied electrical current (A).

$$C_{16}H_{17}N_3O_4S + 41H_2O \rightarrow 16CO_2 + 99H^+ + 3NO_3^- + SO_4^{-2} + 94e^- \tag{3}$$

The extent of total electrochemical combustion (φ) (Miwa *et al.,* 2006) was calculated through the ratio between the percentages of CEX and TOC samples taken at each 1 h of electrolysis in optimized conditions:

$$\varphi = \%[TOC]removed\%[CEX]removed \tag{4}$$

The φ value gives an indication of the extent to which the CEX molecules are being converted to CO_2 or to other intermediate compounds. So, this parameter can assume values between 0 and 1, which means no combustion or total combustion with respect to the initial compound, respectively.

The energy consumption per unit mass of TOC (w) for the electrochemical mineralization process was calculated according to Brillas *et al.* (2009):

$$w = (UIt\Delta[TOC]V) \tag{5}$$

where U is the cell voltage (V), I the applied electrical current (A), t the reaction time (h), $\Delta[TOC]$ the concentration variation of TOC (mg L^{-1}) after a certain reaction time, and V the electrolyzed solution volume (L).

4.3. Results and Discussion

4.3.1. *Effect of operational variables*

Fig. 1 shows the relative concentration decay of CEX ($100[CEX]_{rel}$; $[CEX]_{rel} = [CEX]_t/[CEX]_0$ where $[CEX]_t$ and $[CEX]_0$ are the CEX concentration at time t and at the beginning of the electrolysis) and TOC ($100[TOC]_{rel}$; $[TOC]_{rel} = [TOC]_t/[TOC]_0$ where $[TOC]_t$ and $[TOC]_0$ are the TOC concentration at time t and at the beginning of the electrolysis) as a function of electrolysis time for distinct salts used as supporting electrolyte at constant ionic strength (0.1 M). A theoretical line based on a process purely controlled by mass transfer, whose main parameter is the mass transfer coefficient (k_m), was also included to show the important contribution of indirect processes (chemical oxidation) on the CEX oxidation and mineralization performances. The k_m value (3.09×10^{-5} m s^{-1}) was calculated after determination of the thickness of the stagnant layer (2.32×10^{-5} m), by a simple electrochemical

assay based on the $Fe(CN)_6^{4-}/Fe(CN)_6^{3-}$ redox pair (Cañizares *et al.,* 2006), and of the diffusion coefficient of the CEX (7.17×10^{-10} m^2 s^{-1}) using a diaphragm cell. Thus, the theoretical first order kinetic constant and exponential decay can be calculated according to previous reports (Coledam *et al.,* 2014; Coledam *et al.,* 2016).
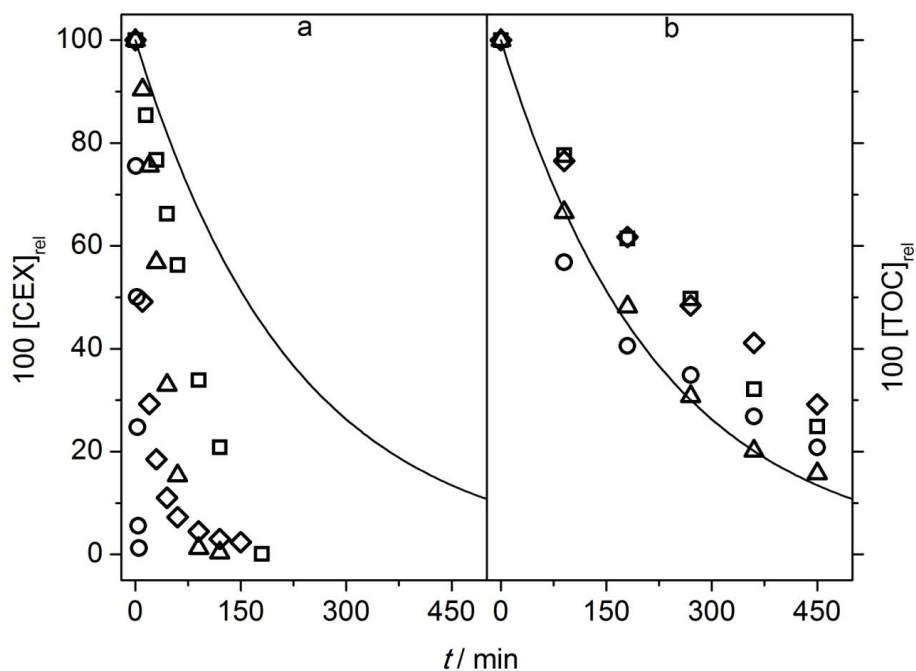
Figure 1*: Relative concentration decay of a) CEX (100 [CEX]$_{rel}$) and b) TOC (100[TOC]$_{rel}$) as a function of electrolysis time using distinct salts as supporting electrolyte at a constant ionic strength (0.1 M): (▩) Na$_2$SO$_4$, (○) NaCl, (△) NaNO$_3$, (◇) Na$_2$CO$_3$. (——) theoretical line based on a purely mass transport controlled process. Conditions of the electrolysis: 25 °C and using 20 mA cm^{-2}.

It is interesting to note that the oxidation process, which is related to small modifications on the initial CEX molecule, is a faster kinetic process than the one based on mass transfer probably due to the contribution of oxidant species produced during the electrolysis. Thus, all salts used led to higher removal rates than the theoretical line, i.e. the oxidation is not limited to the surface of the anode. Similar results are commonly seen for electrochemical degradation on BDD, as was reported recently by Lizhang *et al.* (2016), while

studying the kinetics of phenol electrochemical oxidation highlighting the importance of bulk reactions during total mineralization

Moreover, the use of Cl^- ions led to the highest rate of oxidation (only a few minutes to complete oxidation) within the tested salts, as a consequence of the generation of active chlorine (mainly HOCl and OCl^-), which may react through addition, oxidation or substitution reactions (Deborde and von Gunten, 2008) in a non-selective way. When carbonate, sulfate, and nitrate based electrolytes were used, the pseudo-first order kinetic constants gradually increased in that order, but their values remained lower than the one using Cl^- ions (see the pseudo-first order kinetic constants of Table SM-1, in the electronic supplementary material section).

On the other hand, the TOC decay was similar for all tested electrolytes. The TOC removal is related to a much more severe oxidation route, i.e. the molecule has to undergo many oxidation steps before a significant CO_2 conversion (Aquino *et al.,* 2014b). Similar results were reported in previous studies (Hurwitz *et al*., 2014), considering that BDD is a non-active electrode and that their mineralization reaction routes are strongly associated to the generation of hydroxyl radicals, a close TOC decay for various electrolytes used was expected.

Moreover, as the electrogenerated oxidants (chemical oxidation) are incapable to mineralize CEX molecules, these molecules need to diffuse towards the anode surface to be oxidized and mineralized by HO•. This explains why the experimental points and theoretical line are close for the TOC removal in comparison to the data regarding the oxidation removal. The conversion of CEX and its intermediates to CO_2 is dependent on the HO• produced on the anode surface and, as expected, the extent of total electrochemical combustion (φ), which remained around 0.77, was similar for all the investigated electrolytes after 7 h (see Fig. SM-1, in the electronic supplementary material section). The remaining experiments were carried out using a sulfate medium (33 mM Na_2SO_4) to avoid the possible electrogeneration of toxic organic (Garcia-Segura *et al*., 2015a) and inorganic (Bergmann *et al*., 2009; Lin *et al*., 2016) compounds, and also to avoid fouling of the BDD anode by nitrate substituted intermediates (Murugananthan *et al*., 2011).

Fig. 2 shows the 100[CEX]$_{rel}$ and 100[TOC]$_{rel}$ as a function of electrolysis time for distinct values of investigated pH in sulfate medium. Once again, different profiles can be observed for the oxidation and mineralization processes. During the CEX oxidation, all the experimental data exhibited higher rates than the theoretical one due to the contribution of the

electrogenerated oxidants (chemical oxidation process) such as H_2O_2 and $S_2O_8^{2-}$, as discussed above and also showed experimentally in other works (Coledam *et al.*, 2016). In addition, the oxidation process was dependent on the pH value: neutral to acidic solutions and the ones with no control (variation range: from 6.5 to 3.0) led to the highest oxidation rates (see Table SM-2, in the electronic supplementary material section), which slightly diminished when alkaline solutions were used. This behavior might be due to the distinct pK_a values of the CEX molecule (5.2 and 7.3 (Giacomino *et al.,* 2012)), which is in the ionic form at pH 10 and could have influenced the interaction with electrogenerated oxidants or even their oxidation power. For the mineralization process, the experimental data exhibited a lower rate than the theoretical one and no pH dependence is observed. Clearly, that process seems to not depend on the ionic character of the CEX molecule, as the conversion to CO_2 occurs on the surface of the anode (reaction cage) by HO•.
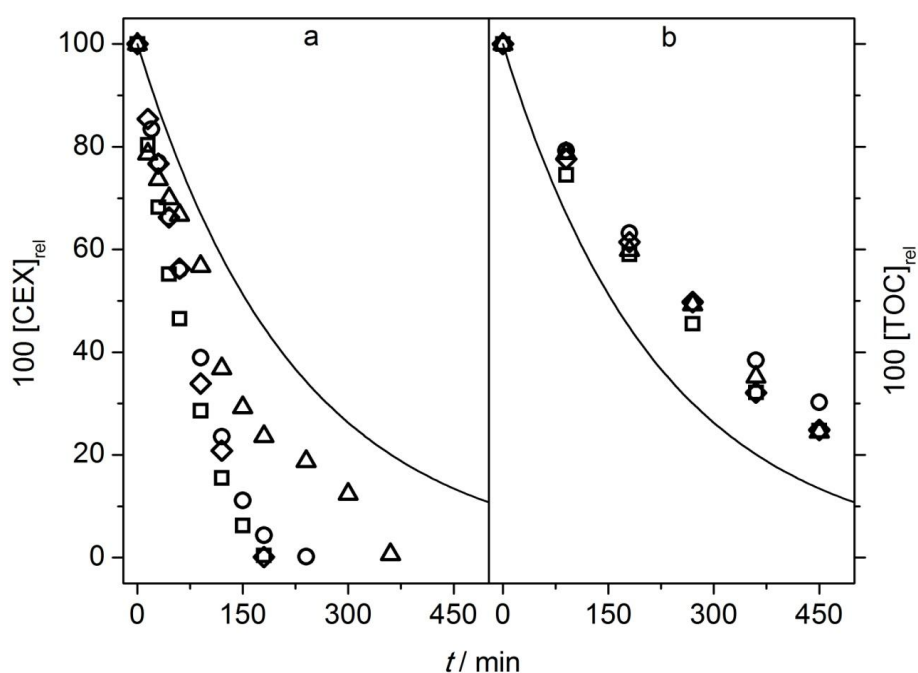
Figure 2: Relative concentration decay of a) CEX (100 $[CEX]_{rel}$) and b) TOC (100$[TOC]_{rel}$) as a function of electrolysis time at distinct pH values: (■) 3, (○) 7, (△) 10, and (◇) no control. Conditions of the electrolysis: 25 ºC and using 20 mA cm^{-2} in the presence of Na_2SO_4 0.033 M.

As discussed above, the conversion to CO_2 is limited by the diffusion of the CEX molecule and its intermediates to the anode surface to react with HO•, which might occur

through several steps due to the complexity of the organic compound. As discussed in the work of Farhat *et al.* (2015), the mineralization of CEX could also be mediated by sulfate radicals ($SO_4^{\bullet-}$) in acidic solutions, which are produced from oxidation of sulfate ions or by their reaction with HO•.

Fig. 3 shows the $100[CEX]_{rel}$ and $100[TOC]_{rel}$ as a function of the applied electrical charge per unit volume of electrolyzed solution (Q_{ap}) for distinct values of applied electrical current density values investigated and without pH control. Once again, the oxidation process required a lower Q_{ap} than the mineralization process, as the conversion to CO_2 only occurs on the surface of the BDD anode. It is interesting to observe that the rate of CEX oxidation significantly increased from 5 to 10 mA cm^{-2}, and the theoretical line (considering the oxidation process at 5 mA cm^{-2}) was very close to the experimental points at 5 mA cm^{-2}. That behavior might be due to the limiting current density (j_{lim}) value, which is equal to 8 mA cm^{-2}.

Thus, when current densities higher than j_{lim} are used, the excess electrical energy is consumed by the side reaction of O_2 evolution, as well as, production of oxidants. This last point explains why there is a significant disagreement between the theoretical and experimental points at 20 mA cm^{-2}. Previous reports (Carlesi Jara and Fino, 2010) highlight that the current density is mainly influenced by the initial contaminant concentration and mass transport limitation inside the electrochemical reactor, which is in accordance with our findings.
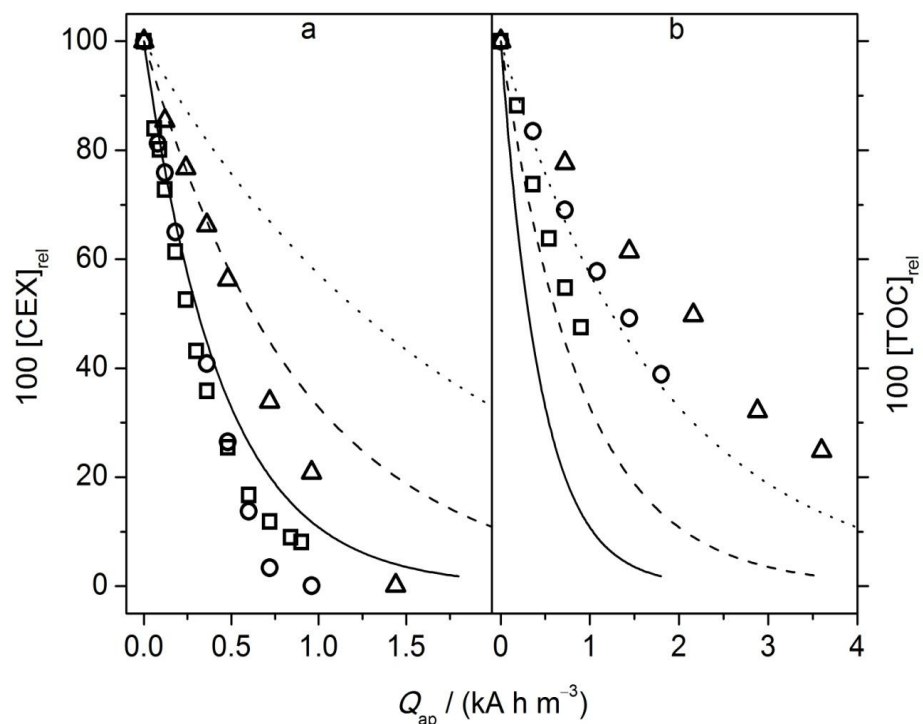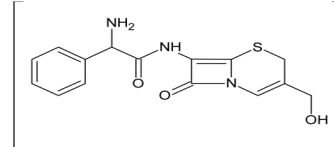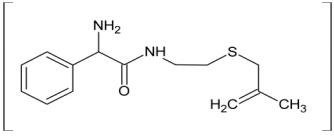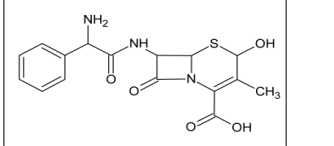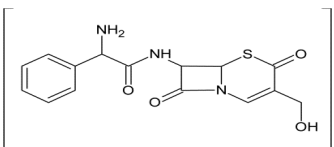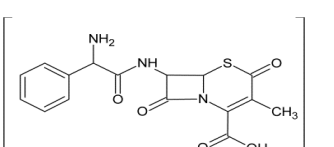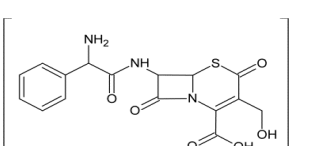
Figure 3: Relative concentration decay of a) CEX (100 [CEX]$_{rel}$) and b) TOC (100[TOC]$_{rel}$) as a function of electrical applied charge per unit volume of electrolyzed solution (Q_{ap}) using distinct current density values: (▢) 5, (○) 10, and (△) 20 mA cm^{-2}. Theoretical lines based on a purely mass transport controlled process using (——) 10, (– – –) 20, and (• • •) 30 mA cm^{-2}. Conditions of the electrolysis: no pH control at 25 °C and in the presence of Na$_2$SO$_4$ 0.033 M.
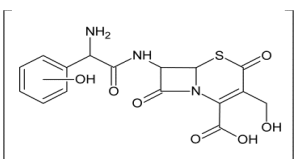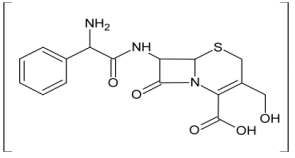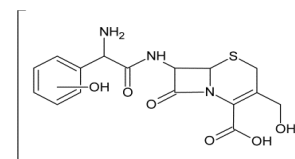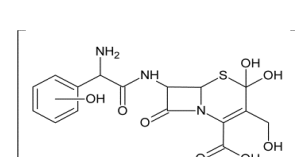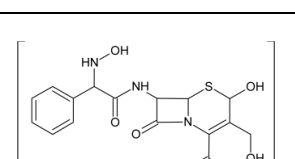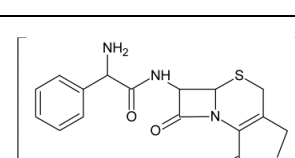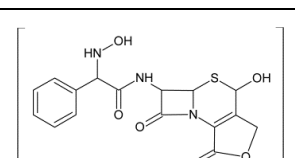
In the case of TOC removal, all the experimental values remained above the theoretical line due to the several oxidation steps that the CEX molecule, and its intermediates, need to overcome before conversion to CO_2. Moreover, the oxidation promoted by the electrogenerated oxidants is incapable to result in significant mineralization, which could explain the higher Q_{ap} required for the mineralization process. Table SM-3, in the electronic supplementary material section, shows the obtained pseudo-first order kinetic constants for the oxidation and mineralization processes. As expected, the k values increase with the applied current density values. The obtained *MCE* and w values as a function of TOC removal can be seen in Fig. SM-2, in the electronic supplementary material section. As the system is under mass transfer control, the use of high electrical current densities led to low values of *MCE* and a consequent increase of the side reaction of O_2 evolution. Moreover, increasingly high w values were attained at high current densities.

4.3.2. *Intermediate compounds and toxicity assays*

Table 1 shows some of the main detected intermediate compounds by LC-MS/MS analyses that were generated during electrooxidation of CEX using a BDD anode (for the proposed fragmentation route of the main detected intermediates and the IUPAC names of the proposed chemical structures, see Figs. SM-3 to SM-15 and Table SM-4, respectively, in the electronic supplementary material section). Other *m/z* relations were detected, but their concentration was very low to perform MS/MS analysis.

Table 1: LC-MS/MS data for the intermediate compounds detected during electrochemical oxidation of CEX using a BDD anode.

	Molar mass / g mol^{-1}	Retention time / min	Molecular ion (M+H)$^+$ / Da	Main fragment ions / Da	Proposed chemical structures
1	317	7.19	318	301, 269, 216, and 106	
2	264	9.12	265	216, 158, 145, and 106	
3	363 (a)	1.88	364	346, 156, 106	
4	333	6.54	334	317, 285, 167, 144, and 132	
5	361	8.77	362	257, 212, 177, and 133	
6	377 (a)	5.51	378	361, 329, 233, 218, 186, 158, 106	

7	393	5.82	394	346, 329, and 106	
8	363 (b)	3.09	364	346, 329, 206, 156, and 106	
9	379	7.59	380	363, 362, 331, and 106	
10	411	10.75	412	377, 346, 152, and 106	
11	395	8.90	396	346, 329, 297, and 106	
12	345	6.70	346	329, 285, 211, 156, and 106	
13	377 (b)	7.39	378	329, 300, 274, 156, and 106	

An initial possible degradation pathway is also proposed in Fig. 4. It is interesting to observe that all detected intermediates result from hydroxylation (see compounds **3**, **10**, **11**, and **13**) and oxidation (see compounds **1**, **4**, and **5**) reactions in the cephem group (formed by the β-Lactam containing thiazine ring) or in the substituent methyl group (see compounds **1**, **6**, **7**, **8**, **9**, **10 11**, **12**, and **13**). These reactions are common when advanced oxidation processes are used to oxidize and mineralize organic compounds (Klauson *et al*., 2010; Coledam *et al*., 2016).
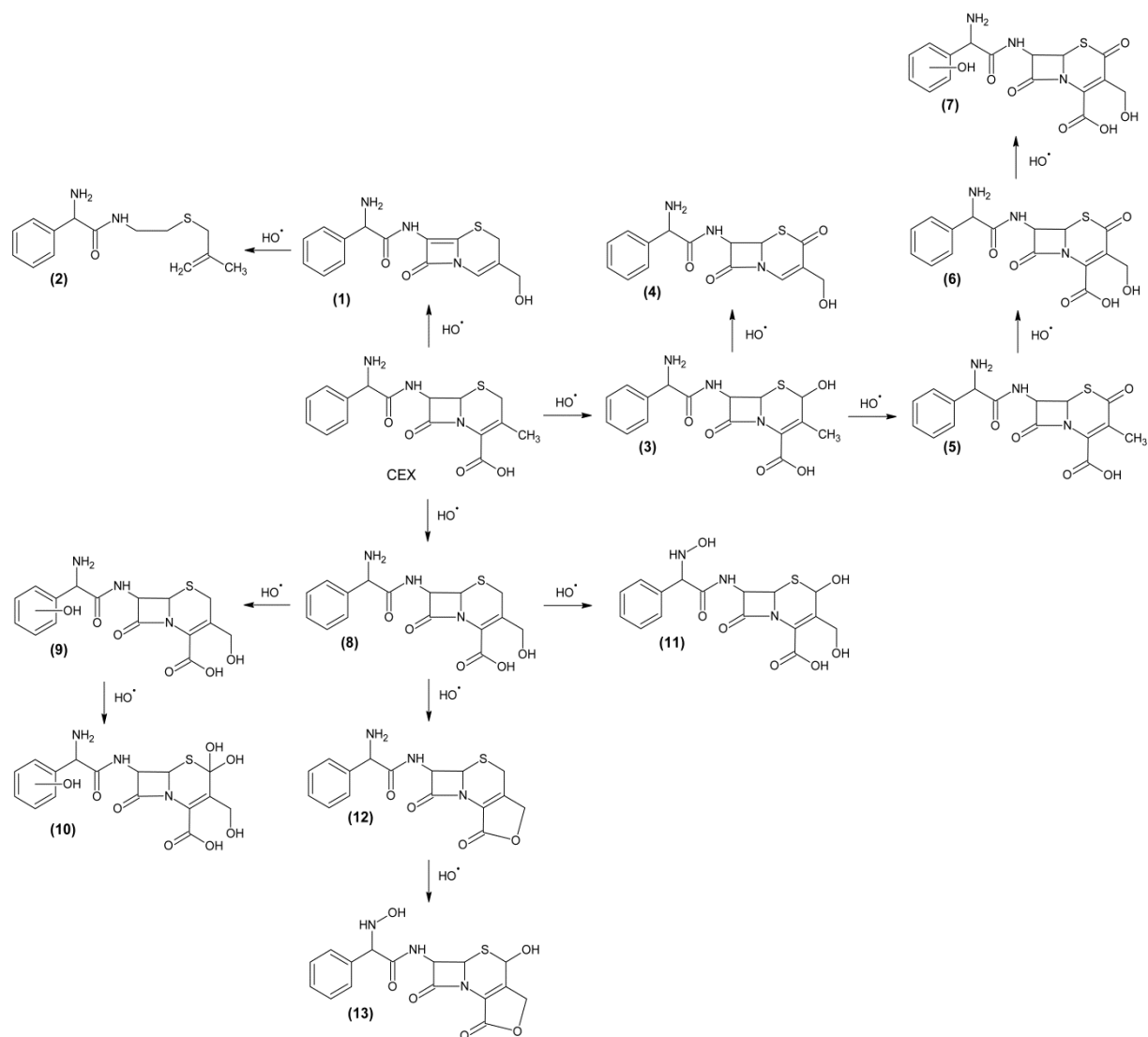
Figure 4: Proposed degradation pathway of CEX under electrochemical oxidation using a BDD anode. Conditions of the electrolysis: 25 ºC, no pH control, and using 10 mA cm^{-2} in the presence of Na$_2$SO$_4$ 0.033 M.

On the other hand, the breakage of the cephem group, which is the active part of the CEX molecule and it is responsible for its antibacterial properties, occurred during the electrooxidation process, as shown by compound number **2**, which was detected after 4 h of electrolysis. The benzene and amino groups were also hydroxylated (see compounds **7**, **9**, **10**, **11** and **13**) during the electrochemical process; however, no intermediate resulting from the benzene ring opening was detected. This behavior might be due to the low applied electrical current density, which is close to the limiting one. Consequently, it is expected that a high conversion of CEX molecules to its intermediates before significant conversion to carboxylic

acids and CO_2, would be seen. The majority of the identified intermediates reported in this work is mainly due to hydroxylation reactions in the six-member β-lactam ring. That behavior seems to be different from the one reported by Song *et al.* (2008), where hydroxylation in the aromatic ring of other β-lactam antibiotics (four-member β-lactam ring compounds: Penicillin G, Penicillin V, and Amoxicilin) was predominantly when using radiolysis as an advanced oxidation process. As also reported by Rickman and Mezyk (2010), during investigation of the oxidation of four- and six-member β-lactam ring antibiotics through sulfate or hydroxyl radicals using advanced oxidation and reduction processes, the presence of sulfate radicals can promote oxidation reactions in the six-member β-lactam ring rather than on the aromatic substituent.

That behavior was also observed by Dodd *et al.* (2010) during treatment of CEX by an ozonation process (no oxidation reaction in the aromatic substituent). Thus, this might explain the observed high number of byproducts in this work with the six-member β-lactam ring oxidized when using the electrochemical technology in the presence sulfate ions. The concentration evolution of short chain compounds (carboxylic acids in this study) resulting from consecutive oxidation steps of the CEX compound, as a function of the electrolysis time, can be seen in Fig 5. Oxamic, oxalic, malic and propionic acids presented the highest concentration during the electrochemical treatment of CEX, even after 7 h electrolysis, and only small amounts of pyruvic, succinic and fumaric acids were detected. Clearly, there is a tendency of accumulation of recalcitrant oxamic and oxalic carboxylic acids (Garcia-Segura and Brillas, 2011) during the final stages of electrochemical oxidation of CEX. Further, it is well known and typically seen in electrolysis reaction, that oxalic acid is the last carboxylic acid that is directly transformed into CO_2 (Han *et al.,* 2014).
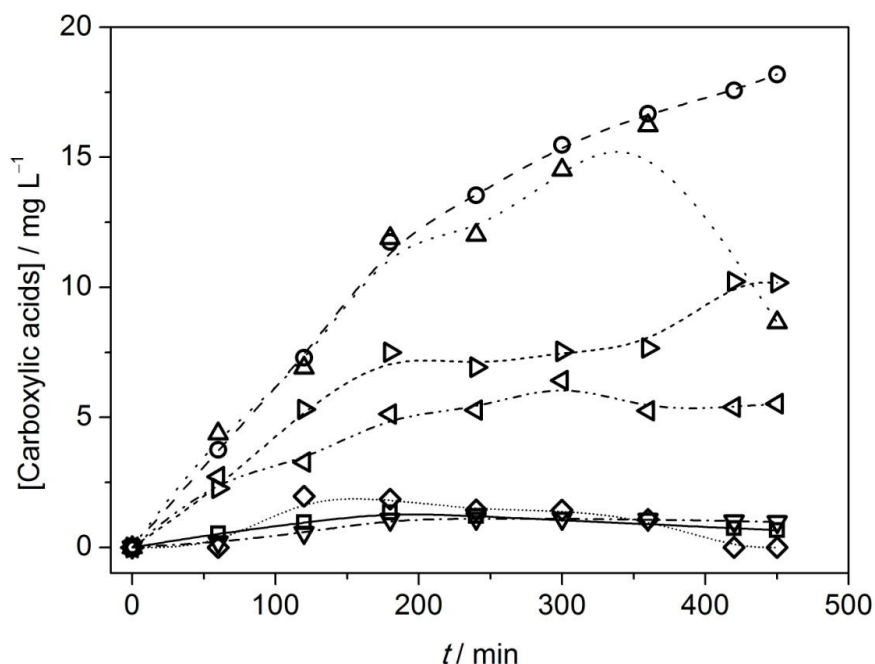
Figure 5: Concentration evolution of the main detected carboxylic acids as a function of electrolysis time: (∇) fumaric, ($\triangle$) malic, ($\circ$) oxamic, ($\triangleright$) oxalic, ($\triangleleft$) propionic, (▨) pyruvic, and ($\diamond$) succinic acids. Conditions of the electrolysis: 25 °C, no pH control, and using 10 mA cm^{-2} in the presence of Na$_2$SO$_4$ 0.033 M.

Finally, Fig. 6 shows the evolution of the inhibition index (I) of *E. coli* and the CEX concentration as a function of the electrolysis time. During the initial 3 h of electrolysis, the growth of *E. coli* was completely inhibited even after diminishment of the CEX concentration below the MIC (see dashed line in Fig. 6), which occurred at 3 h of electrolysis. This might indicate that the byproducts of the CEX molecule, particularly those after successive hydroxylation reactions shown in the degradation pathway of Fig. 4, continues to inhibit the growth of *E. coli*, as the cephem group was not broken. Then, after 4 h of electrolysis, no significant growth inhibition towards the growth of *E. coli* was observed, probably due to the rupture of the β-Lactam ring of the CEX intermediates (without complete TOC abatement), as shown by compound **2** in Fig. 4. On the other hand, Dimitrakopoulou *et al*. (2012) showed that the antibacterial activity of amoxicillin (another antibiotic representative of the penicillin group) towards *E. coli* was only dependent on the removal of the parent compound and not on its degradation byproducts, during a photocatalytic treatment using TiO$_2$ and UV-A radiation.

That behavior might be due to the rapid rupture of the β-lactam ring of the amoxicillin compound whose intermediates were not detected. In addition, the accumulation of oxamic and oxalic acids detected during treatment of CEX did not seem to inhibit the growth of *E. coli* cells.
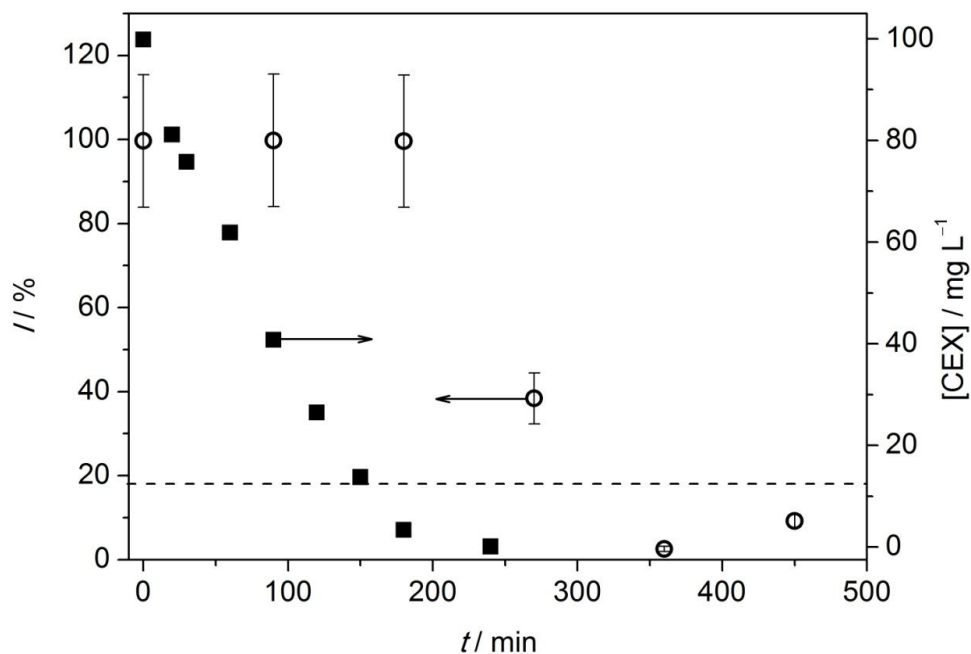
Figure 6: Inhibition index (I) and absolute concentration evolution of CEX ([CEX]) as a function of the electrolysis time: (○) I, (■) [CEX], and (– – –) the obtained experimental value of the minimum inhibitory concentration (MIC - see text). Conditions of the electrolysis: 25 ºC, no pH control, and using 10 mA cm^{-2} in the presence of Na_2SO_4 0.033 M.

4.4. Conclusions

The CEX molecule and its hydroxylated intermediate compounds were completely eliminated during electrolysis using a BDD as anode. The oxidation rate of CEX using distinct salts as supporting electrolyte exhibited distinct rates due to the different types and amounts of electrogenerated oxidants; however, none of them were capable to mineralize CEX and its intermediates, which only occurred on the surface of BDD through a diffusion process. Neutral to acidic solutions led to the best removal rates of CEX; however, no significant difference was observed towards the conversion to CO_2 as the system is under mass transfer limitations.

Consequently, the use of high values of electrical current density is not indicated since a high energy consumption and low mineralization current efficiencies are attained. The main detected CEX intermediates were due to hydroxylation reactions in the cephem group, which remained as toxic as the parent compound. The inhibition growth of *E. coli* was limited when the cephem group, particularly the β-lactam ring, was broken. The presence and accumulation of recalcitrant oxamic and oxalic carboxylic acids did not lead to any significant inhibition towards growth of *E. coli*.

Acknowledgments

References

Anglada, A., Urtiaga, A., Ortiz, I., 2009. Contributions of electrochemical oxidation to waste-water treatment: fundamentals and review of applications. J. Chem. Technol. Biotechnol. 84, 1747-1755.

Antonin, V.S., Santos, M.C., Garcia-Segura, S., Brillas, E., 2015. Electrochemical incineration of the antibiotic ciprofloxacin in sulfate medium and synthetic urine matrix. Water Research 83, 31-41.

Aquino, J.M., Parra, K.N., Miwa, D.W., Motheo, A.J., 2015. Removal of phthalic acid from aqueous solution using a photo-assisted electrochemical method. J. Environ. Chem. Eng. 3, 429-435.

Aquino, J.M., Rocha-Filho, R.C., Ruotolo, L.A.M., Bocchi, N., Biaggio, S.R., 2014a. Electrochemical degradation of a real textile wastewater using b-PbO$_2$ and DSA® anodes. Chem. Eng. J. 251, 138-145.

Aquino, J.M., Rocha-Filho, R.C., Sáez, C., Cañizares, P., Rodrigo, M.A., 2014b. High efficiencies in the electrochemical oxidation of an anthraquinonic dye with conductive-diamond anodes. Environ. Sci. Pollut. Res. 21, 8442-8450.

Aquino, J.M., Rodrigo, M.A., Rocha-Filho, R.C., Sáez, C., Cañizares, P., 2012. Influence of the supporting electrolyte on the electrolyses of dyes with conductive-diamond anodes. Chem. Eng. J. 184, 221-227.

Barbosa, M.O., Moreira, N.F.F., Ribeiro, A.R., Pereira, M.F.R., Silva, A.M.T., 2016. Occurrence and removal of organic micropollutants: An overview of the watch list of EU Decision 2015/495. Water Research 94, 257-279.

Bergmann, M.E.H., Rollin, J., Iourtchouk, T., 2009. The occurrence of perchlorate during drinking water electrolysis using BDD anodes. Electrochim. Acta 54, 2102-2107.

Brillas, E., Martínez-Huitle, C.A., 2015. Decontamination of wastewaters containing synthetic organic dyes by electrochemical methods. An updated review. Appl. Catal., B: Environ. 166-167, 603-643.

Brillas, E., Sirés, I., Oturan, M.A., 2009. Electro-Fenton process and related electrochemical technologies based on Fenton's reaction chemistry. Chem. Rev. 109, 6570-6631.

Cañizares, P., García-Gómez, J., de Marcos, I.F., Rodrigo, M.A., Lobato, J., 2006. Measurement of mass-transfer coefficients by an electrochemical technique. J. Chem. Educ. 83, 1204-1207.

Cañizares, P., Paz, R., Sáez, C., Rodrigo, M.A., 2009. Costs of the electrochemical oxidation of wastewaters: a comparison with ozonation and Fenton oxidation processes. J. Environ. Manage. 90, 410-420.

Carlesi Jara, C., Fino, D., 2010. Cost optimization of the current density for electroxidation wastewater processes. Chem. Eng. J. 160, 497-502.

Coledam, D.A.C., Aquino, J.M., Rocha-Filho, R.C., Bocchi, N., Biaggio, S.R., 2014. Influence of chloride-mediated oxidation on the electrochemical degradation of the Direct Black 22 dye using boron-doped diamond and β-PbO_2 anodes. Quim. Nova 37, 1312-1317.

Coledam, D.A.C., Aquino, J.M., Silva, B.F., Silva, A.J., Rocha-Filho, R.C., 2016. Electrochemical mineralization of norfloxacin using distinct boron-doped diamond anodes in a filter-press reactor, with investigations of toxicity and oxidation by-products. Electrochim. Acta 213, 856-864.

Cong, V.H., Sakakibara, Y., Komori, M., Kishimoto, N., Watanabe, T., Mishima, I., Ihara, I., Tanaka, T., Yoshida, Y., Ozaki, H., 2016. Recent developments in electrochemical technology for water and wastewater treatments. J. Water Environ. Technol. 14, 25-36.

Deborde, M., von Gunten, U., 2008. Reactions of chlorine with inorganic and organic compounds during water treatment-Kinetics and mechanisms: A critical review. Wat. Res. 42, 13-51.

Derakhshan, Z., Mokhtari, M., Babaie, F., Ahmadi, R.M., 2016. Removal methods of antibiotic compounds from aqueous environments – a review. J. Environ. Health Sustainable Dev. 1, 51-74.

Dimitrakopoulou, D., Rethemiotaki, I., Frontistis, Z., Xekoukoulotakis, N.P., Venieri, D., Mantzavinos, D., 2012. Degradation, mineralization and antibiotic inactivation of amoxicillin by UV-A/TiO2 photocatalysis. J. Environ. Manage. 98, 168-174.

Dodd, M.C., Rentsch, D., Singer, H.P., Kohler, H.-P.E., von Gunten, U., 2010. Transformation of beta-lactam antibacterial agents during aqueous ozonation: reaction pathways and quantitative bioassay of biologically-active oxidation products. Environ. Sci. Technol. 44, 5940-5948.

Escher, B.I., Fenner, K., 2011. Recent advances in environmental risk assessment of transformation products. Environ. Sci. Technol. 45, 3835-3847.

Farhat, A., Keller, J., Tait, S., Radjenovic, J., 2015. Removal of persistent organic contaminants by electrochemically activated sulfate. Environ. Sci. Technol. 49, 14326-14333.

Ganzenko, O., Huguenot, D., van Hullebusch, E.D., Esposito, G., Oturan, M.A., 2014. Electrochemical advanced oxidation and biological processes for wastewater treatment: a review of the combined approaches. Environ. Sci. Pollut. Res. 21, 8493-8524.

Garcia-Segura, S., Brillas, E., 2011. Mineralization of the recalcitrant oxalic and oxamic acids by electrochemical advanced oxidation processes using a boron-doped diamond anode. Water Res. 45, 2975-2984.

Garcia-Segura, S., Keller, J., Brillas, E., Radjenovic, J., 2015a. Removal of organic contaminants from secondary effluent by anodic oxidation with a boron-doped diamond anode as tertiary treatment. J. Hazard. Mater. 283, 551-557.

Garcia-Segura, S., Vieira dos Santos, E., Martínez-Huitle, C.A., 2015b. Role of sp3/sp2 ratio on the electrocatalytic properties of boron-doped diamond electrodes: A mini review. Electrochem. Commun. 59, 52-55.

Giacomino, N., Cerra, M., Gumiy, D., Stiefel, S., Notaro, U., Baroni, E., Formentini, E., 2012. Pharmacokinetic-pharmacodynamic modeling of antibacterial activity of cephalexin on *E. coli* in presence of canine serum. Revue Méd. Vét. 163, 431-440.

Guerra, R., 2001. Ecotoxicological and chemical evaluation of phenolic compounds in industrial effluents. Chemosphere 44, 1737-1747.

Guinea, E., Centellas, F., Brillas, E., Cañizares, P., Sáez, C., Rodrigo, M.A., 2009. Electrocatalytic properties of diamond in the oxidation of a persistant pollutant. Appl. Catal. B: Environ. 89, 645-650.

Han, W., Zhong, C., Liang, L., Sun, Y., Guan, Y., Wang, L., Sun, X., Li, J., 2014. Electrochemical degradation of triazole fungicides in aqueous solution using TiO_2-NTs/SnO_2-Sb/PbO_2 anode: Experimental and DFT studies. Electrochim. Acta 130, 179-186.

Homem, V., Santos, L., 2011. Degradation and removal methods of antibiotics from aqueous matrices – A review. J. Environ. Manage. 92, 2304-2347.

Hurwitz, G., Pornwongthong, P., Mahendra, S., Hoek, E.M.V., 2014. Degradation of phenol by synergistic chlorine-enhanced photo-assisted electrochemical oxidation. Chem. Eng. J. 240, 235-243.

Kapalka, A., Fóti, G., Comninellis, C., 2009. The importance of electrode material in environmental electrochemistry: Formation and reactivity of free hydroxyl radicals on boron-doped diamond electrodes. Electrochim. Acta 54, 2018-2023.

Karci, A., 2014. Degradation of chlorophenols and alkylphenol ethoxylates, two representative textile chemicals, in water by advanced oxidation processes: The state of the art on transformation products and toxicity. Chemosphere 99, 1-18.

Klauson, D., Babkina, J., Stepanova, K., Krichevskaya, M., Preis, S., 2010. Aqueous photocatalytic oxidation of amoxicillin. Catalysis Today 151, 39-45.

Kong, X., Jiang, J., Ma, J., Yang, Y., Liu, W., Liu, Y., 2016. Degradation of atrazine by UV/chlorine: Efficiency, influencing factors, and products. Water Res. 90, 15-23.

Li, S.-W., Lin, A.Y.-C., 2015. Increased acute toxicity to fish caused by pharmaceuticals in hospital effluents in a pharmaceutical mixture and after solar irradiation. Chemosphere 139, 190-196.

Lin, Z., Yao, W., Wang, Y., Yu, G., Deng, S., Huang, J., Wang, B., 2016. Perchlorate formation during the electro-peroxone treatment of chloride-containing water: Effects of operational parameters and control strategies. Water Res. 88, 691-702.

Lizhang, W., Shengxiang, Y., Bo, W., Peng, L., Zhe'nan, L., Yuemin, Z., 2016. The influence of anode materials on the kinetics toward electrochemical oxidation of phenol. Electrochim. Acta 206, 270-277.

Locatelli, M.A.F., Sodré, F.F., Jardim, W.F., 2011. Determination of antibiotics in brazilian surface waters using liquid chromatography–electrospray tandem mass spectrometry. Arch. Environ. Contam. Toxicol. 60, 385-393.

Luo, Y., Guo, W., Ngo, H.H., Nghiem, L.D., Hai, F.I., Zhang, J., Liang, S., Wang, X.C., 2014. A review on the occurrence of micropollutants in the aquatic environment and their fate and removal during wastewater treatment. Sci. Total Environ. 473–474, 619-641.

Martín de Vidales, M.J., Millán, M., Sáez, C., Pérez, J.F., Rodrigo, M.A., Cañizares, P., 2015. Conductive diamond electrochemical oxidation of caffeine-intensified biologically treated urban wastewater. Chemosphere 136, 281-288.

Michael, I., Rizzo, L., McArdell, C.S., Manaia, C.M., Merlin, C., Schwartz, T., Dagot, C., Fatta-Kassinos, D., 2013. Urban wastewater treatment plants as hotspots for the release of antibiotics in the environment: A review. Water Res. 47, 957-995.

Miwa, D.W., Malpass, G.R.P., Machado, S.A.S., Motheo, A.J., 2006. Electrochemical degradation of carbaryl on oxide electrodes. Water Res. 40, 3281-3289.

Murugananthan, M., Latha, S.S., Bhaskar Raju, G., Yoshihara, S., 2011. Role of electrolyte on anodic mineralization of atenolol at boron doped diamond and Pt electrodes. Sep. Purif. Technol. 79, 56-62.

Oller, I., Malato, S., Sánchez-Pérez, J.A., 2011. Combination of advanced oxidation processes and biological treatments for wastewater decontamination - a review. Sci. Total Environ. 409, 4141-4166.

Orias, F., Perrodin, Y., 2013. Characterisation of the ecotoxicity of hospital effluents: a review. Sci. Total Environ. 454–455, 250-276.

Oturan, N., Trajkovska, S., Oturan, M.A., Couderchet, M., Aaron, J.-J., 2008. Study of the toxicity of diuron and its metabolites formed in aqueous medium during application of the electrochemical advanced oxidation process "electro-Fenton". Chemosphere 73, 1550-1556.

Panizza, M., Cerisola, G., 2009. Direct and mediated anodic oxidation of organic pollutants. Chem. Rev. 109, 6541-6569.

Pereira, G.F., El-Ghenymy, A., Thiam, A., Carlesi, C., Eguiluz, K.I.B., Salazar-Banda, G.R., Brillas, E., 2016. Effective removal of Orange-G azo dye from water by electro-Fenton and photoelectro-Fenton processes using a boron-doped diamond anode. Sep. Purif. Technol. 160, 145-151.

Puckowski, A., Mioduszewska, K., Łukaszewicz, P., Borecka, M., Caban, M., Maszkowska, J., Stepnowski, P., 2016. Bioaccumulation and analytics of pharmaceutical residues in the environment: A review. J. Pharm. Biomed. Anal., http://dx.doi.org/10.1016/j.jpba.2016.1002.1049.

Quiroz, M.A., Sánchez-Salas, J.L., Reyna, S., Bandala, E.R., Peralta-Hernández, J.M., Martínez-Huitle, C.A., 2014. Degradation of 1-hydroxy-2,4-dinitrobenzene from aqueous solutions by electrochemical oxidation: Role of anodic material. J. Hazard. Mater. 268, 6-13.

Radjenovic, J., Sedlak, D.L., 2015. Challenges and opportunities for electrochemical processes as next-generation technologies for the treatment of contaminated water. Environ. Sci. Technol. 49, 11292-11302.

Rickman, K.A., Mezyk, S.P., 2010. Kinetics and mechanisms of sulfate radical oxidation of beta-lactam antibiotics in water. Chemosphere 81, 359-365.

Rivera-Utrilla, J., Sánchez-Polo, M., Ferro-García, M.Á., Prados-Joya, G., Ocampo-Pérez, R., 2013. Pharmaceuticals as emerging contaminants and their removal from water. A review. Chemosphere 93, 1268-1287.

Sales, A.M.S., de Araújo, C.K.C., de Melo, J.V., Peralta-Hernandez, J.M., da Silva, D.R., Martínez-Huitle, C.A., 2013. Decontamination of real textile industrial effluent by strong oxidant species electrogenerated on diamond electrode: Viability and disadvantages of this electrochemical technology. Appl. Catal., B: Environ. 130–131, 112-120.

Santos, L.H.M.L.M., Araújo, A.N., Fachini, A., Pena, A., Delerue-Matos, C., Montenegro, M.C.B.S.M., 2010. Ecotoxicological aspects related to the presence of pharmaceuticals in the aquatic environment. J. Hazard. Mater. 175, 45-95.

Särkkä, H., Bhatnagar, A., Sillanpää, M., 2015. Recent developments of electro-oxidation in water treatment — A review. J. Electroanal. Chem. 754, 46-56.

Silambarasan, S., Vangnai, A.S., 2016. Biodegradation of 4-nitroaniline by plant-growth promoting Acinetobacter sp. AVLB2 and toxicological analysis of its biodegradation metabolites. J. Hazard. Mater. 302, 426-436.

Singh, K., Arora, S., 2011. Removal of synthetic textile dyes from wastewaters: A critical review on present treatment technologies. Crit. Rev. Environ. Sci. Technol. 41, 807-878.

Sirés, I., Brillas, E., Oturan, M.A., Rodrigo, M.A., Panizza, M., 2014. Electrochemical advanced oxidation processes: today and tomorrow. A review. Environ. Sci. Pollut. Res. 21, 8336-8367.

Song, W., Chen, W., Cooper, W.J., Greaves, J., Miller, G.E., 2008. Free-radical destruction of beta-lactam antibiotics in aqueous solution. J. Phys. Chem. A 112, 7411-7417.

Sopaj, F., Rodrigo, M.A., Oturan, N., Podvorica, F.I., Pinson, J., Oturan, M.A., 2015. Influence of the anode materials on the electrochemical oxidation efficiency. Application to oxidative degradation of the pharmaceutical amoxicillin. Chem. Eng. J. 262, 286-294.

Tissot, G.B., Anglada, A., Dimitriou-Christidis, P., Rossi, L., Arey, J.S., Comninellis, C., 2012. Kinetic experiments of electrochemical oxidation of iohexol on BDD electrodes for wastewater treatment. Electrochem. Commun. 23, 48-51.

Van Doorslaer, X., Dewulf, J., Van Langenhove, H., Demeestere, K., 2014. Fluoroquinolone antibiotics: An emerging class of environmental micropollutants. Sci. Total Environ. 500–501, 250-269.

Vasconcelos, V.M., Ponce-de-León, C., Nava, J.L., Lanza, M.R.V., 2016. Electrochemical degradation of RB-5 dye by anodic oxidation, electro-Fenton and by combining anodic oxidation–electro-Fenton in a filter-press flow cell. J. Electroanal. Chem. 765, 179-187.

Zhang, J., Chang, V.W.C., Giannis, A., Wang, J.-Y., 2013. Removal of cytostatic drugs from aquatic environment: A review. Sci. Total Environ. 445–446, 281-298.

5. SYNTHESIS AND CHARACTERIZATION OF TERNARY METALLIC OXIDE ELECTRODES CONTAINING $(SNO_2)_{93}SB_5M_2$ (M = CE, TA, BI, GD) USING AN IONIC LIQUID AS THE PRECURSOR SOLVENT

Marilia Moura de Salles Pupo[a,b], Leticia Mirella da Silva[a], Géssica de Oliveira Santiago Santos[a,b], Katlin Ivon Barrios Eguiluz[a,b], Giancarlo Richard Salazar-Banda[a,b,*]

[a] Laboratório de Eletroquímica e Nanotecnologia, LEN, Instituto de Tecnologia e Pesquisa, Aracaju, SE, Brazil

[b] Programa de Pós-graduação em Engenharia de Processos, Universidade Tiradentes, Aracaju, SE, Brazil

*Corresponding author: gianrsb@gmail.com (Giancarlo Richard Salazar-Banda)

Abstract

The present study synthetized mixed metal oxide (MMO) anodes composed of $(SnO_2)_{93}Sb_5M_2$ (M=Ce,Ta,Bi,Gd) through thermal decomposition calcinated at 500, 550, and 600°C. The anodes were characterized by linear and cyclic voltammetry, electrochemical impedance spectroscopy, service lifetime tests, and morphology factors. Furthermore, physical characterizations included X-ray diffractometry and scanning electron microscopy to obtain information on their crystallographic structure and surface morphology, respectively. Finally, electrocatalytic activity was tested by electrolysis for 1 h in solutions containing 10 ppm of Diuron® using various electrolytes (Na_2SO_4, Na_2CO_3, $NaNO_3$, NaCl). The highest superficial area, oxygen evolution onset potential, longest service lifetime, and considerable Diuron degradation rates in all electrolytes were obtained for $(SnO_2)_{93}Sb_5Ce_2$ (32%). However, it is important to highlight the outstanding service lifetime presented by $(SnO_2)_{93}Sb_5Bi_2$ (46.32 h), overcoming the results for $(SnO_2)_{93}Sb_5Ce_2$ by over 50-fold. This behavior is associated with the peculiar nanoflower star-like surface organization seen in the scanning electronic microscopy (SEM) images.

5.1 Introduction

Due to the increase in agricultural demands, the use of chemical products such as herbicides, pesticides, and insecticides has become common. Naturally, the excess of these products are washed into waterbodies and further inserted into various food chains, affecting human and environmental health. One of the most frequently applied herbicides is Diuron, used for controlling plagues, which acts in photosynthesis by blocking electron transport (Pipi, Neto, & De Andrade, 2013). Further, Diuron has been classified as a genotoxic and cancerous compound, also associated with reproductive problems (Oturan, Trajkovska, Oturan, Couderchet, & Aaron, 2008). Thus, the development of alternative treatments that can degrade compounds such as Diuron have been the focus of several studies, among which, electrochemical treatments have been of growing interest (Luo et al., 2014; Särkkä, Bhatnagar, & Sillanpää, 2015).

One of the main restrictions in electrochemical systems is the electrodes used to promote electro-oxidation. In this sense, dimensionally stable anodes (DSAs) have received considerable attention due to their electrocatalytic advantages, such as long service lifetime and high electroactive area. In addition, they present low cost and easy synthesis. Similarly, mixed metal oxide (MMO) electrodes are basically composed of a metallic substrate, normally Ti due to its stability and uniformity, and a metal oxide as a coating layer, such as RuO_2, IrO_3, TiO_2, SnO_2, PbO_2, and Ta_2O_5 (Li, Shao, Xu, Lv, & Yan, 2016; Pupo et al., 2013; Shao, Li, Xu, & Yan, 2014; Xu & Song, 2015).

Additionally, considering the thermal treatments applied in the synthesis of MMO electrodes, they present a *"mud-cracked"* structure that creates high porosity and increases the superficial area of the electrode, enhancing its catalytic activity. The increase in catalytic activity eases the reduction of current density, which reduces the anodic potential of the electrode (Brillas, Martínez-Huitle, Brillas, & Martínez-Huitle, 2015).

From the metallic oxides used in MMOs, SnO_2 is one of the most commonly used (Ding, Feng, & Lu, 2010; Duan, Wen, Chen, Zhou, & Duan, 2014; Li et al., 2016; Ni, Kirk, & Thorpe, 2015; Shao, et al., 2014; Sun, Zhang, Wei, Ma, & Hu, 2015; Wang, Hu, Hu, & Zhou, 2015; Xu & Song, 2015; Zhang, Xu, He, & Zhang, 2014). In its pure form, SnO_2 is a *n*-type semiconductor with a very wide band gap (3.87–4.30 eV), with its electric conductivity due to a modest level of non-stoichiometric impurities. For electrochemical processes, it has been observed that doping PbO_2 or SnO_2 with rare earth metals modifies the crystallinity of the oxide layer, enhancing its complete mineralization capacity for organic compounds (Shestakova, Bonete, Gómez, Sillanpää, & Tang, 2014).

SnO$_2$ particles have oxygen vacancies that form during the calcination process, which can be represented by Equation 1 as follows:

$$SnO_2 \rightarrow Sn_{Sn}^{x} + O_O^{x} + \frac{1}{2}O_2(g) + V_O^{''} + 2e^{''} \tag{1}$$
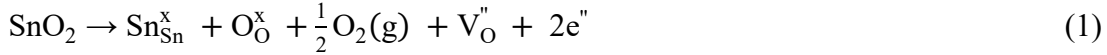
$V_O^{''}$ represents the oxygen vacancies with two positive charges and Sn_{Sn}^{x} and O_o^{x} are elements in their position with no charge. Oxygen vacancies and electron generation contributes to SnO$_2$ conductivity. Therefore, the presence of oxygen during the calcination process reduces Sn conductivity due to the decrease in the free electrons present and the oxygen vacancies. Thus, the addition of Sb^{3+} to SnO$_2$ increases the oxygen vacancies and causes an increase in the material conductivity (Rodrigues & Olivi, 2003).

However, despite the advantages presented by the use of Sb–SnO$_2$, this anode is susceptible to deactivation during electrochemical oxidation in acidic solutions due to passivation/corrosion of the oxide layer (Gonçalves, Santos, Franco, & Silva, 2014). To enhance the stability of the anode, many studies have been developed, exploring various synthesis methods (Duan et al., 2014; Li et al., 2016; Xu & Song, 2015) and doping with various metals, such as IrO$_2$ (Chaiyont et al., 2013), CeO$_2$ (Sun et al., 2015), PbO$_2$ (Lin, Niu, Ding, & Zhang, 2012), and other rare earths elements (Cui, Feng, & Liu, 2009).

As for materials considered to be doping metals, the present study focused on Sb–SnO$_2$ MMO type electrodes, synthesized using the thermal decomposition method and doped with the following four metal oxides: cerium (Ce), gadolinium (Gd), bismuth (Bi), and tantalum (Ta). The main advantages of doping with these materials are better described below.

Gd doping is well known for generating more compact MMOs, enhancing its conductivity (Cui et al., 2009; Feng, Cui, Logan, & Liu, 2008). It is estimated that Gd doping occupies the SnO$_2$ band gap and contributes to the increase in free carriers. As a result, Gd doping leads to electrolysis focused on oxidation reactions instead of reduction reactions (Feng & Li, 2003). Further, studies developed by Feng *et al.* (2008) showed that when doping Sb–SnO$_2$ with Gd by thermal decomposition methods, the concentration of Gd used is of fundamental importance. Since the atomic radius of Gd^{+3} (94 pm) is larger than that of Sn^{+4} (71 pm), it is difficult to observe the addition of Gd atoms to the crystalline matrix of SnO$_2$. Therefore, excess Gd can lead to superficial deposition or even the formation of larger particles of SnO$_2$, which also leads to the reduction of the superficial electrochemical active area.

In a previous study seeking to increase the superficial active area of MMOs (Shestakova et al., 2014), synthesized Ti/SnO$_2$ electrodes were doped with tantalum by a thermal decomposition method at 550℃. Even at small molar fractions, the doping contributes

to an increase in electronic conductivity and enhances the charge storage capacitance of the MMOs, thus promoting improvement of MMO surface properties.

On the other hand, Bi presents chemical properties similar to Sb due to its proximity in the periodic table. According to the Hume–Rothery Law, compounds like Bi and Sb are capable of forming a solid solution due to the following: (*i*) their atomic radii differ by less than 15%, (*ii*) the crystalline structure of the solute and solvent are similar; (*iii*) complete solubility is reached since the solvent and solute have the same valence, and (*iv*) the solute and solvent present the same electronegativity (Zhang, Yang, & Evans, 2008).

When Bi is used for doping in adequate concentrations it is known to increase the stability of the electrodes. This can be explained by the following: (*i*) the solid solution formed by the intermediary and superficial layer can enhance the stability by causing deformation of the crystalline structure, incorporating impurities, which can make migration of O^{2-} difficult and (*ii*) Bi_2O_3 acts as a physical barrier for the onset and development of matrix corrosion, which can effectively block the oxygen atom from penetrating the surface of Ti, therefore, limiting TiO_2 formation (Dong et al., 2014).

Additionally, Bi doping is advantageous since it presents a high refractive index, dielectric permissiveness, photoconductivity, and photoluminescence. Due to such features, it has been frequently applied in optical sensor coverage, sensitive technology, and electroreduction (Xiaohong, Wei, & Weidong, 2007).

Cerium IV oxides are strong oxidant agents with high standard reduction potentials (E^o) around 1.6 V for Ce^{4+}/Ce^{3+} reactions (Equation 2). The Ce^{4+} ion can reduce several organic compounds, ferric salts, hydrogen peroxide, organic acids, and other inorganic compounds (Martins, Hewer, & Freire, 2007).

$$2Ce^{4+} + O_{lat}^{2-} \leftrightarrows Vo + 2Ce^{3+} + O_t \qquad (2)$$
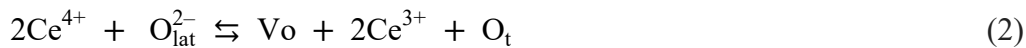
Ce is known as one of the most active rare earth elements, and catalysts based on Ce have been intensely studied due to multiple positive effects in catalytic performance (Arenas, Ponce de León, & Walsh, 2016; Duan, Chen, Wen, & Duan, 2015; Liu, Liu, Ma, & Li, 2012; Piro, Robinson, Walsh, & Schelter, 2014; Santos, Silva, Eguiluz, & Salazar-Banda, 2015; Zhang, Liu, Zeng, Lin, & Liu, 2011). The most important property of catalysts based on Ce is related to their buffer capacity due to large oxygen storage by means of Ce^{4+}/Ce^{3} redox reactions and crystalline structure mobility (Cui et al., 2009).

For the MMOs proposed, a thermal decomposition method using an ionic liquid (IL) as the solvent was applied (Carlesi-Jara et al., 2011). ILs are liquids composed entirely of ions, but they differ from metallic salts due to their low fusion temperature, normally around <100–150°C. They are normally less corrosive than their equivalents and are incompatible with several organic compounds, such as alcohol and acetone. However, they are good solvents for transition metals complexes, but less miscible with non-polar organic compounds, allowing the formation of biphasic systems and the use of homogenous catalysts (Gordon, 2001). Additionally, it is important to note that ILs have low viscosities (Gordon, 2001; Wasserscheid & Keim, 2000).

Therefore, considering the relevance of MMOs in electrochemical systems and their operational advantages from the use of IL in the synthesis process, the present work proposes the synthesis and characterization of ternary oxide electrodes obtained by thermal decomposition using an IL as the metal precursor solvent. The electrodes obtained were of the form $(SnO_2)_{93}Sb_5M_2$, where M=Ce, Bi, Ta, or Gd. The obtained anodes were electrochemically analyzed by means of cyclic and linear voltammetry, electrochemical impedance spectroscopy, and service lifetime tests. The morphology factor (φ) was also determined by means of cyclic voltammetry. Physical characterization was carried out by scanning electronic microscopy (SEM) and X-ray diffraction (XRD). Additionally, electrolysis of Diuron® at 10 ppm (as a model molecule) in various electrolytes (NaCl, Na_2SO_4, $NaCO_3$, $NaNO_3$) was tested to determine the most electrochemically active and stable type of MMO electrode obtained.

5.2 Materials and Methods

Titanium plates (1 cm × 1 cm) with a 2 cm^2 active area were used as the metallic support for MMO deposition. Initially, the plates were polished with sanders of 320, followed by 220, and rinsed with ultrapure water (by Gehaka MS 2000 system). To ensure the removal of superficial impurities, the plates were submitted to thermal treatment in HCl (20%) for 15 min at 110°C, followed by 10 min thermal treatment in $COOH_2$ (10%) at 90°C. Finally, the supports were rinsed with ultrapure water. The electrodes were then weighed to determine their initial weights.

$SnCl_2$ (98%, Sigma-Aldrich), $SbCl_3$ (99%, Sigma-Aldrich), $TaCl_5$ (99%, Sigma-Aldrich), $GdCl_3$ (99%, Sigma-Aldrich), $BiCl_3$ (98%, Sigma-Aldrich), and $CeCl_3•7H_2O$ (98%, Sigma-Aldrich) were used without further purification. The precursor salts were weighed to correspond to molar ratios of SnO_2:Sb:M (93:5:2, respectively) and then dissolved in 1 mL of

the ionic liquid (*Methylimidazolium hydrogensulfate)* by mechanical agitation for 10 min, followed by microtip ultrasound agitation for 5 min in an Eco-Sonics QR300 Ultrasound Equipment. The solution was then deposited on the titanium plate and submitted to thermal decomposition treatments with heating rates of 10°C min^{-1} up to 500, 550, or 600°C and kept at this specific temperature for 10 min in an EDG 3P-S oven. The electrode was then weighed and brushed repeatedly until its final deposited mass reached 1.2 g cm^{-2}. The determination of this mass is described by Equation 3.

$$m = \frac{(m_{initial} - m_{after\ treatment}) x 1000}{\text{Electrode total area}} \qquad (3)$$

In the equation, *m* corresponds to the actual weight deposited, $m_{initial}$ is the initial weight of the substrate, $m_{after\ treatment}$ is the weight after thermal decomposition, and Electrode total area, considering the actual area 1×1 cm, and the remaining support structure.

Proper pre-treatment is key for strong oxide coverage on the substrate surface (Rao & Venkatarangaiah, 2014). When the final mass was obtained, the supports were submitted to a final calcination temperature at 550, 550, and 600°C for 1 h with heating rates of 10°C min^{-1}. A slow cooling methodology was adopted according to the literature (Rufino & Silva, 2011) with a temperature decrease of 2°C min^{-1}. This method ensures the formation of smaller and better dispersed grains, thus increasing electrode stability.

Cyclic voltammetry (CV) experiments were carried out to analyze the voltammetric profiles obtained for each electrode, establishing the oxidation and reduction potential and analyzing the electrochemically active area of the electrode. CV measurements were carried out in a three-electrode glass cell composed of a platinum counter electrode, a Ag/AgCl reference electrode, and a 2 cm^2 working electrode that consisted of the titanium substrate with the metal oxide layers deposited as described. All measurements were taken in 0.33 M Na$_2$SO$_4$, applying potentials from 0.2 to 2.0 V at 100 mV s^{-1}. Linear voltammetry (LV) was also carried out to precisely determine the oxygen evolution reaction onset potential of the electrodes proposed, which were analyzed between 1.0 and 3.5 V in 0.33 M Na$_2$SO$_4$ at 10 mV s^{-1} (**Figure S1**, Supplementary Material).

Electrochemical impedance spectroscopy (EIS) was carried out to analyze the ion transfer capacity of the obtained electrodes. Measurements were taken in a range of 0.1–10^3 Hz at an applied potential encompassing the region of the oxygen evolution reaction (OER) with 10 points per decades and a 5 mV amplitude sine wave. The applied potential chosen was

directly related to the OER onset of each electrode studied, determined by analyzing the linear voltammetry.

The morphology factor (φ) was determined by a methodology previously reported (Da Silva, De Faria, & Boodts, 2001). Therefore, the contribution of the internal sites of the electrode for the overall capacitance was determined by the following:

$$\varphi_{morph} = \frac{C_{d,i}}{C_d} \qquad (4)$$

The variables $C_{d,i}$ and C_d are the "internal" and "total" differential capacitance of the electrodes, respectively. The value obtained for φ can vary from 0 to 1, where 0 represents small or irrelevant internal sites and 1 indicates an electrode with a large internal area (Malpass, Neves, & Motheo, 2006).

Finally, service lifetime tests were carried out by applying 10 mA cm^{-1} as the current density in a 0.33 M Na$_2$SO$_4$ solution. The electrodes were considered deactivated when they reached a limiting potential of 10 V. All electrochemical experiments were carried out with a Metrohm Autolab Potenciostat/Galvanostat 302N.

XRD patterns were obtained with a Rigaku Rint 2000/PC diffratometer operating with Co Kα radiation (λ=1.788965) generated at 40 kV and 40 mA. All scans were carried out at 2° min^{-1} for 2θ values between 20° and 80°. SEM measurements were carried out with a JSM 6510 CV from JEOL by applying a voltage of 15 kV to investigate the morphology of the coating surfaces.

Electrochemical degradation of 10 ppm Diuron was attempted by applying a current density of 2.5 mA cm^{-2} using a three-electrode electrochemical glass cell composed of a working electrode (synthesized MMO), platinum counter electrode, and Ag/AgCl reference electrode. Diuron degradation was analyzed in four different electrolytes (NaCl, NaNO$_3$, NaCO$_3$, and Na$_2$SO$_4$), testing the electrocatalytic activity for all anodes obtained.

Highest degradation outcomes observed by ultra-pressure liquid chromatography (UPLC) were obtained for all electrodes calcined at 550℃ using NaCl as the electrolyte. However, due to the high activity of chlorides when working in this specific electrolyte, the electrodes had shorter service lifetimes associated with the intense oxidation activity that is typically seen under these conditions.

5.3 Results

Cyclic voltammetry is an electrochemical technique used to generate oxides and, therefore, used to study their mechanisms and kinetics (Woldemedhin, Raabe, & Hassel, 2012). In **Figure 1**, cyclic voltammograms taken between potential limits of 0.02 and 2.00 V *vs* Ag/AgCl for electrodes prepared at different calcination temperatures (500, 550, and 600°C), are presented. In **Figure 1a**, it is possible to note a very close OER onset around 1.8 V for all electrodes, except for the $(SnO_2)_{93}Sb_5Ta_2$ anode.

Similar results were previously found in other reports and associated with the large gap formed by Ta_2O_5 and SnO_2 behaving as *n* semiconductors, where no reaction occurs until high overpotentials are reached (Shestakova et al., 2014). This finding is also in accordance with the Nyquist plots seen in **Figure 2a** where $(SnO_2)_{93}Sb_5Ta_2$ presented a smaller arc, indicating a higher electron transfer rate, which will be discussed below.

In **Figure 1b**, the repeated OER onset close to 1.8 V is seen, except for $(SnO_2)_{93}Sb_5Bi_2$, where the onset is over 2.0 V. Furthermore, a pronounced redox reaction peak appears for $(SnO_2)_{93}Sb_5Ce_2$, as described by Equation 2. It is important to note that the reduction and oxidation peaks are near the oxidation around 1.1 V and the reduction around 0.65 V and it is widely known that the difference between the reduction and oxidation peaks indicates the reversibility of the redox process, therefore, the closer the peaks, the more reversible the system (Del Río, Fernández, Molina, Bonastre, & Cases, 2010). Moreover, the presence of the redox reaction seen in this particular electrode considerably increases its electrochemically active surface area (ECSA).

In **Figure 1c**, an overall reduction in the electrochemically active area is seen for all electrodes, except for $(SnO_2)_{93}Sb_5Gd_2$. The tendency for lower OER potentials for $(SnO_2)_{93}Sb_5Ta_2$ and $(SnO_2)_{93}Sb_5Gd_2$, which are 1.77 V and 1.25 V, respectively, is clearly seen. Further, a reduction in the redox peak for Ce^{4+}/Ce^{3+} is also seen for $(SnO_2)_{93}Sb_5Ce_2$, which can be attributed to a less arranged surface of the electrode.
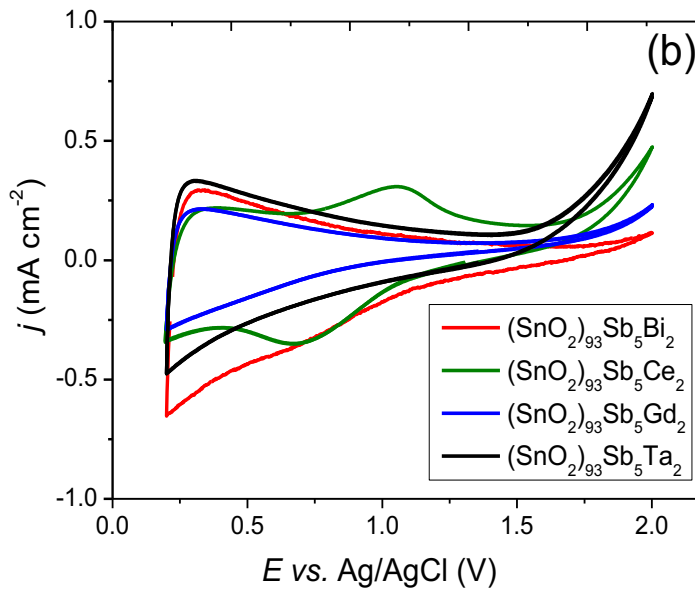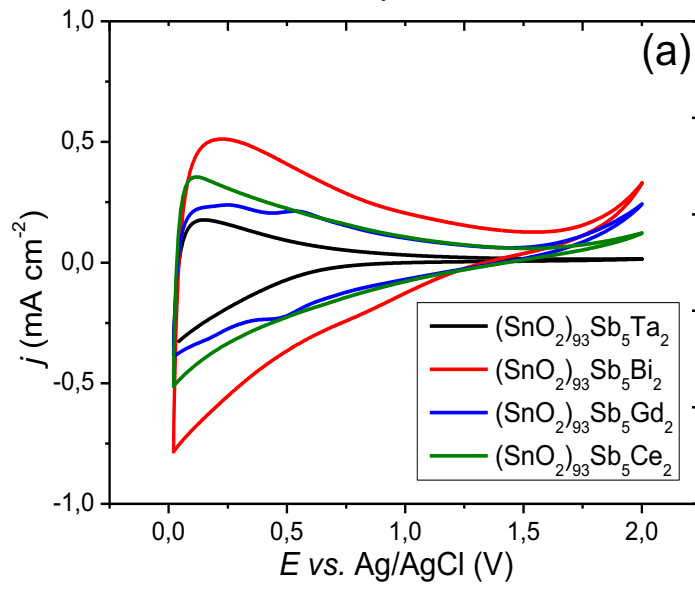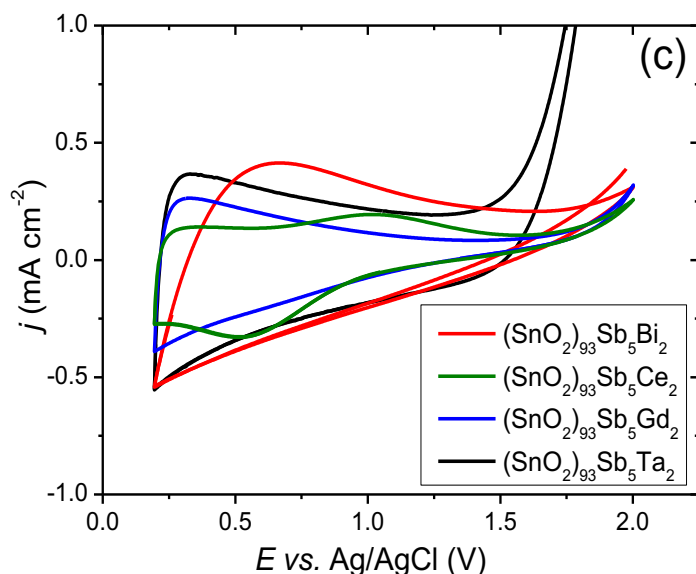
Figure 1. Cyclic voltammograms taken between limiting potentials of 0.02–2.00 V at 100 mV s^{-1} for $(SnO_2)_{93}Sb_5M_{2(M=Ta, Bi, Gd, or Ce)}$ electrodes synthetized with calcination temperatures of (a) 500, (b) 550, and (c) and 600°C in 0.33 M Na$_2$SO$_4$.

The total voltammetric charge density (q^*), calculated by integration of the voltammetric profiles, is a measurement of the ECSA. For the ECSA, the $(SnO_2)_{93}Sb_5Bi_2$ electrode presented the highest area, followed by $(SnO_2)_{93}Sb_5Ce_2$. The smallest area was seen for $(SnO_2)_{93}Sb_5Ta_2$, followed by $(SnO_2)_{93}Sb_5Gd_2$. Although the area for $(SnO_2)_{93}Sb_5Ta_2$ was smaller than for the remaining electrodes, it is worth noting that the OER of this electrode was higher than the others, implying that the same electrode presents a higher ability for electron transfer in a wider range of voltages. **Table 1** shows the dependence of q^* on the composition at different calcination temperatures.

Table 1 Total voltammetric charge densities of all electrodes obtained in the present study, varying the doping metal and calcination temperatures.

Composition	q^* (mC cm^{-2})		
	500 °C	550 °C	600 °C
$(SnO_2)_{93}Sb_5Ta_2$	2.00	4.72	10.02
$(SnO_2)_{93}Sb_5Bi_2$	8.47	5.72	9.42
$(SnO_2)_{93}Sb_5Gd_2$	4.37	2.54	3.69
$(SnO_2)_{93}Sb_5Ce_2$	5.12	5.57	6.15

EIS is usually measured by applying a sinusoidal potential with low AC amplitude to the system and measuring its current response, which is a sinusoidal wave in the same frequency, but with reversed phase. Frequency rates varied from 100 kHz to several μHz have been used to study the system endurance and deactivation mechanisms (Wu, Huang, & Lim, 2014).

As seen in previous reports (Wang et al., 2015), in MMO synthesis, a smaller arc indicates a lower opposition to electrode charge transfer, which suggest a more active surface. Therefore, it is possible to have a better understanding of superficially active areas of the electrode based on the analysis of the Nyquist diagram, where it is possible to analyze the charge transfer resistance. Thus, from **Figure 2**, it is possible to conclude that electrodes synthesized with calcination temperatures of 550℃ are all more conductive than their equivalents with the remaining calcination temperatures analyzed. This particular reduction in charge transfer resistance can be associated with a better fixation of the precursor solution to the titanium substrate.

Considering the low amount of ternary doping on the Sb–SnO$_2$ matrix, all electrodes presented a well-developed semi-circle when analyzed according to their calcination temperatures. Additionally, **Figure 2a–c** shows the EIS for electrodes calcined at 500, 550, and 600℃, respectively. The smallest arc was found for (SnO$_2$)$_{93}$Sb$_5$Ta$_2$ at 500 and 600℃, corroborating the previous discussion of its behavior as a *n* semiconductor, requiring high voltages for reactions to occur.
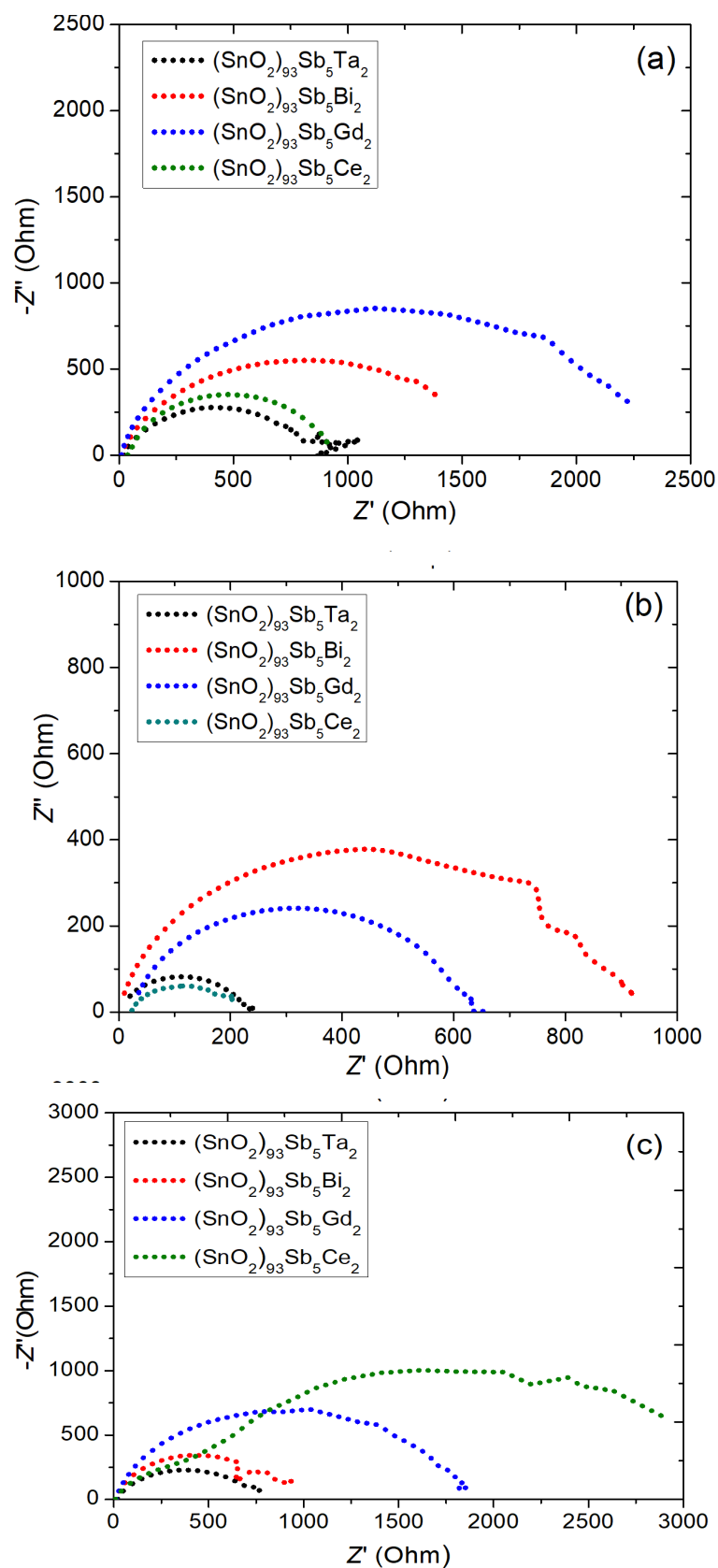
Figure 2. Typical Nyquist plots for $(SnO_2)_{93}Sb_5M_{2(M=Ce, Bi, Ta, Gd)}$ calcined at (a) 500, (b) 550, and (c) 600°C in 0.33 M Na_2SO_4 (0.1–10^5 Hz) at the oxygen evolution reaction onset potential.

For determination of the morphology factor, according to the methodology previously described (Da Silva et al., 2001), several cyclic voltammetry tests were carried out for electrodes synthesized at 550℃ to further investigate the morphology factor of these materials. When considering electrolysis and the use of MMO as catalysts, a high superficial area combined with high porosity is of crucial importance when increasing the electrochemically active area.

Considering the analysis of altering cyclic voltammetry potentials from initially low values up to values estimated for OER, the voltammogram obtained is directly related to the active superficial sites and, therefore, the morphology of the electrode. Due to difficulty accessing the inner regions of the oxide film when applying rapid scan rates, only the outer layer sites are considered responsive. On the other hand, as the scan rate is reduced, the less accessible sites are active and the internal charge of the electrode can be properly estimated from the total charge obtained with slow scan rates minus the outer charge obtained for rapid scan rates (Song et al., 2010).

While carrying out cyclic voltammetry at slow scan rates (10–50 mV s^{-1}) and rapid scan rates (100–500 mV s^{-1}) it is possible to estimate the total (C_d), external ($C_{d,e}$), and internal capacitance ($C_{d,i}$) and morphology factor (φ) of the electrodes obtained **(Table 2)**. As can be seen, the highest morphology factor is associated with $(SnO_2)_{93}Sb_3Gd_2$ and $(SnO_2)_{93}Sb_3Bi_2$, which indicates a higher contribution of the internal area for the materials obtained (Malpass et al., 2006). These findings will be further discussed with physical characterizations.

Table 2 Values of total capacitance (C_d), external capacitance ($C_{d,e}$), internal capacitance ($C_{d,i}$) and morphology factor (φ) for electrodes synthetized with calcination temperature of 550 ℃. Analyses were carried out in 0.033 M Na_2SO_4.

Composition	C_d (mF cm^{-2})	$C_{d,i}$ (mF cm^{-2})	$C_{d,e}$ (mF cm^{-2})	Morphology Factor (φ)	q^* (mC cm^{-2})
$(SnO_2)_{93}Sb_5Ta_2$	2.98	0.1	2.88	0.03	4.72
$(SnO_2)_{93}Sb_5Bi_2$	0.68	0. 19	0.49	0.27	5.72
$(SnO_2)_{93}Sb_5Gd_2$	0.183	0.13	0.049	0.71	2.54
$(SnO_2)_{93}Sb_5Ce_2$	4.23	0.44	3.79	0.10	5.57

While analyzing MMO behavior, an increase in coating layers indicated an increase in the stability of the electrodes, which is associated with endurance during the layer detachment

process, typically seen with OER conditions. In the present study, obtaining an optimal reduced amount of coating was one of the main goals of applying an IL as an alternative route for adequate coverage of the Ti support and a decrease in synthesis time. Mechanical stress and differences in thermal expansion between the substrate and the oxide metal layer were the main reasons for the service lifetime reduction (Shao, Yan, Li, Yang, & Xu, 2014).

The process of mechanical stress occurs from electrolyte contamination by cracks formed on the surface of the MMO. The Ti substrate is, therefore, exposed and the formation of TiO_2 (isolator) will spread on the surface of the substrate and over the coating layer. The formation of micro-bubbles on the cracks, which do not spread effectively, will generate mechanical stress, which will lead to layer detachment (Shao et al., 2014).

Additionally, loss in the service lifetime is given by means of electrode poisoning, where the electrochemically active surface is impregnated with organic compounds that were not able to further degrade and are somewhat adsorbed on the surface, which would result in more electrochemically resistive behavior of the electrode, therefore, reaching higher potentials more rapidly (Fathollahi, Javanbakht, Norouzi, & Reza, 2011).

Thus, service lifetime tests were carried out under the same operational conditions for all electrodes synthetized, seeking to analyze the influence of the different calcination temperatures and doping effects on the service lifetime of the electrodes. For such analysis, a current density of 10 mA cm^{-2} was applied to the electrodes in 0.33 M Na_2SO_4 electrolyte **(Figure 3)**.

From **Figure 3** showing electrodes calcined at 500℃, it is possible to note that both $(SnO_2)_{93}Sb_5Ce_2$ and $(SnO_2)_{93}Sb_5Bi_2$ present very short service lifetime outcomes, reaching the upper limit of 10 V with around 1.5 h of reaction. Considering their higher electrochemically active areas presented in **Figure 1a**, it is possible to presume that the electrodes experienced intense electrolysis reactions between the surface of the electrodes and the dissociation ions (SO_x) that are typically formed. Additionally, when considering the charge transfer resistance in EIS analysis presented in **Figure 2a**, the electrode average behavior also supports the possibility of a highly porous surface with cracks and intrusions, which would facilitate the infiltration of organic compounds and further layer detachment by the mechanism previously described. For $(SnO_2)_{93}Sb_5Ta_2$, the small electrochemically active area for 500℃ **(Figure 1a)** associated with the smallest charge transfer resistance in EIS analysis **(Figure 2a)** indicates a slightly active area, which would generate mild degradation reactions, avoiding the mechanical stress on the surface of the Ti support. Therefore, the predominating deactivation mechanism for this electrode is expected to be chemical poisoning by ion fixation on the surface of the

electrode, which would explain its longer service lifetime (Berenguer, Sieben, Quijada, & Morallón, 2014).

Finally, when analyzing the EIS for $(SnO_2)_{93}Sb_5Gd_2$ **(Figure 2a)** and considering its electrochemically active area presents values very similar to those for $(SnO_2)_{93}Sb_5Ta_2$, it could be inferred that the electrode with Gd-doping did not support the low reactive area theory and, therefore, the slower poisoning effect. While further analyzing the results, it is possible to note that all EIS readings were carried out by applying 1.8 V as the OER potential, which would be expected to properly report outcomes for all the electrodes obtained considering the small amount of doping of the Sb–SnO_2 matrix. However, it is important to note that according to the cyclic voltammetry presented in **Figure 1a** and the linear voltammetry carried out during analysis (not shown), the OER potential of $(SnO_2)_{93}Sb_5Gd_2$ was slightly dislocated to lower potentials and, therefore, more adequately reported at 1.4 V.

The $(SnO_2)_{93}Sb_5Gd_2$ and $(SnO_2)_{93}Sb_5Ta_2$ anodes in **Figure 3b** displayed the smallest service lifetimes of around 7 and 1.5 h, respectively. Considering the varying expansion rates of these metals and the Ti support, the increase in calcination temperature could induce the formation of a denser and more compact surface with few very deep cracks, which would ease electrolyte infiltration and further layer detachment. Additionally, physical characterization was carried out to clarify these findings. When considering $(SnO_2)_{93}Sb_5Bi_2$, a considerably longer service lifetime was seen, reaching up to 46 h of activity. As for $(SnO_2)_{93}Sb_5Ce_2$, the service lifetime presented barely reached 5 h. Analyzing the previous findings reported in **Figure 1b** and **Figure 2b**, it is expected that the surfaces of both electrodes were coated with very densely packed layers. Therefore, the formation of smaller grain sizes is expected to justify the significantly higher service lifetimes of both electrodes and the higher electrochemically active surface. Additional SEM and XRD analyses were carried out.

Figure 3 presents the service lifetime results for electrodes calcined at 600°C and a significant decrease in service lifetime is seen. While analyzing previous results shown in **Figure 1c**, it was observed that when submitted to calcination temperatures of 600°C the electrodes presented consistent electrochemically active surface areas, which would not justify the low service lifetime outcomes. However, while analyzing **Figure 2c**, the EIS results for these electrodes all presented higher charge transfer resistances, showing a very strong tendency of these electrodes for electrochemical fixation of contaminants on their surfaces and, therefore, faster deactivation rates. For example, when comparing service lifetime outcomes for $(SnO_2)_{93}Sb_5Bi_2$ calcined at 550 and 600°C, a 10-fold reduction was seen, which is in accordance with the decreased charge transfer resistance seen in the EIS analysis for $(SnO_2)_{93}Sb_5Bi_2$ calcined at 600°C

Thus, electrochemical characterization successfully presented variations in electrochemical behavior of all electrodes according to metal doping and calcination temperatures. From the electrochemical outcomes presented, a higher service lifetime for electrodes calcined at 550°C was estimated, which was further investigated by physical characterizations and electrolysis reactions.
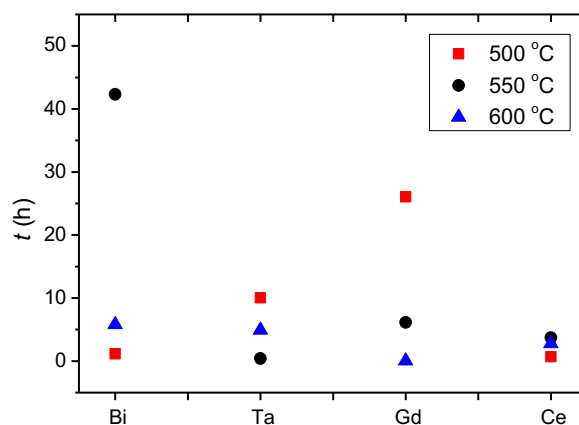
Figure 3. Accelerated Service Lifetime tests for electrodes calcined at 500, 550, and 600°C carried out in 0.33 M Na_2SO_4 applying a current density of 10 mA cm^{-2} considering an upper limiting potential of 10 V.

According to the SEM analysis of the electrodes calcined at 500°C (seen in **Figure 4**), most electrodes presented the *"mud-cracked"* behavior typically associated with thermal decomposition methods, except for $(SnO_2)_{93}Sb_5Bi_2$ **(Figure 4b)**, which presented a very compact layer. The doping of Gd into the SnO_2–Sb matrix led to the formation of smaller grains and to a more uniformly covered surface, as previously discussed. As pointed out in previous reports (Feng et al., 2008), while analyzing the optimal amount of Gd-doping in the SnO_2–Sb matrix, up to 2% mol of Gd/Sn led to the formation of a smoother surface which favors resistance to corrosion and helps prolong the service lifetime of the electrode, as was confirmed and seen in **Figure 3a**.

From **Figure 4a**, the formation of very small gains and the presence of several small cracks are observed, which is commonly seen for MMO of SnO_2–Sb doped with Ta (Ardizzone et al., 2006; Shestakova et al., 2014). As the most obvious feature, Ta led to a reduction in grain size, which is associated with distortion effects caused by the similarity in atomic radius of Ta^{4+} (73 pm) and SnO^+ (71 pm), thus, there is a strong tendency for Ta to be introduced into the reticular structure of the electrode. This reduction in grain size on the surface of the electrode is of great interest since it increases the electrochemically active area.

As seen in previous reports (Shmychkova, Luk'yanenko, Velichenko, Meda, & Amadelli, 2013), doping with Bi leads to the formation of agglomerates in the form of rods with dimensions smaller than 2 μm. **Figure 4b** shows that Bi doping led to the formation of grains, which would explain the higher superficial area seen in **Figure 3**. However, coating procedure was not uniform, and therefore it was possible to easily reach the substrate, which further explains the short service lifetime seen for the same material **(Figure 3)**.

Studies developed by Duan *et al.* (2015) analyzing the doping effect of Ce on Ti/SnO$_2$–Sb by thermal decomposition and electrodeposition also found that Ce-doping favors the reduction of particle size, forming a more compact surface. **Figure 4d** clearly shows smaller particles for these electrodes, presenting very well-defined agglomerations, leading to substrate exposure and smaller service lifetimes (as seen in **Figure 3**).
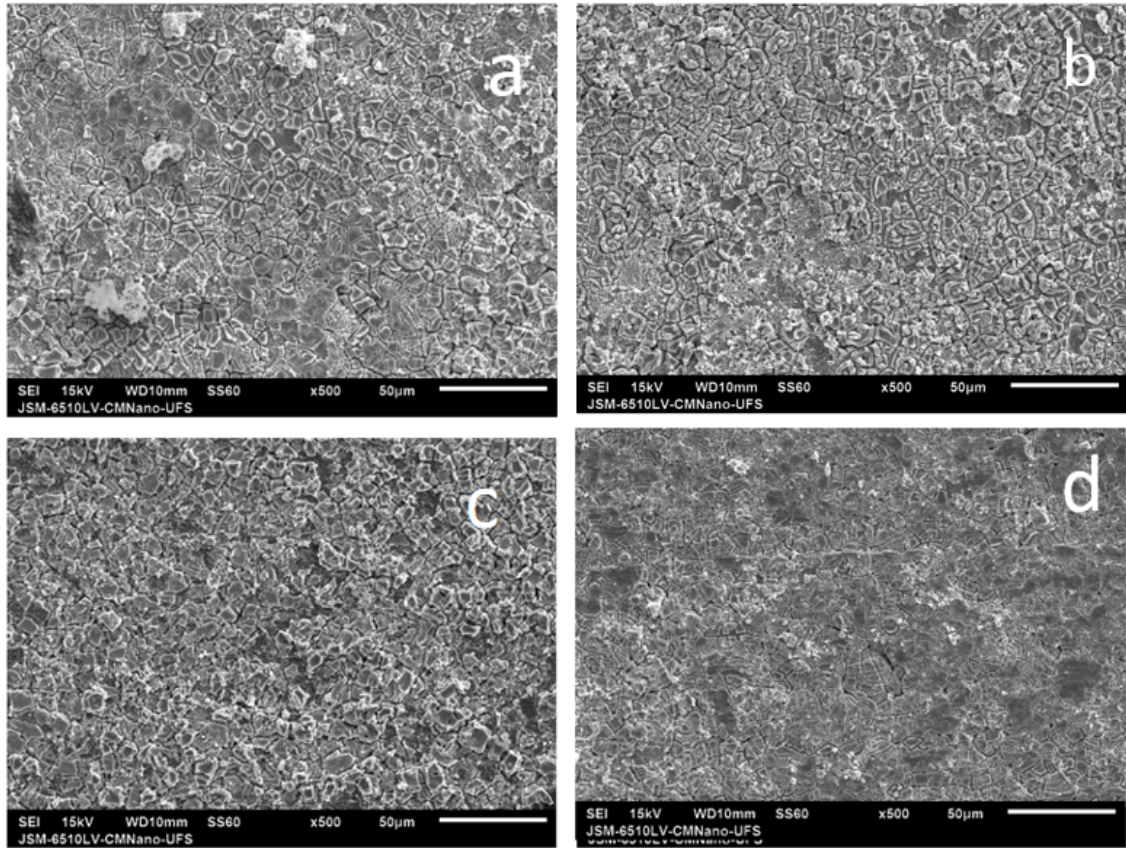
Figure 4. SEM images of (a) (SnO$_2$)$_{93}$Sb$_5$Ta$_2$, (b) (SnO$_2$)$_{93}$Sb$_5$Bi$_2$, (c) (SnO$_2$)$_{93}$Sb$_5$Gd$_2$, and (d) (SnO$_2$)$_{93}$Sb$_5$Ce$_2$ obtained by thermal decomposition with a calcination temperature of 500°C and 500× magnification.

As previously discussed, most electrodes presented similar superficial formations with the increase in final calcination temperature to up to 550°C, except for $(SnO_2)_{93}Sb_5Ta_2$ **(Figure 5a)** and $(SnO_2)_{93}Sb_5Ce_2$ **(Figure 5d)**, where well-coated structures were seen, similar to previous results where close packed agglomerates were seen for $(SnO_2)_{93}Sb_5Bi_2$ **(Figure 5b)** and where a slightly more homogenous crack formation was seen for $(SnO_2)_{93}Sb_5Gd_2$ **(Figure 5c)**.
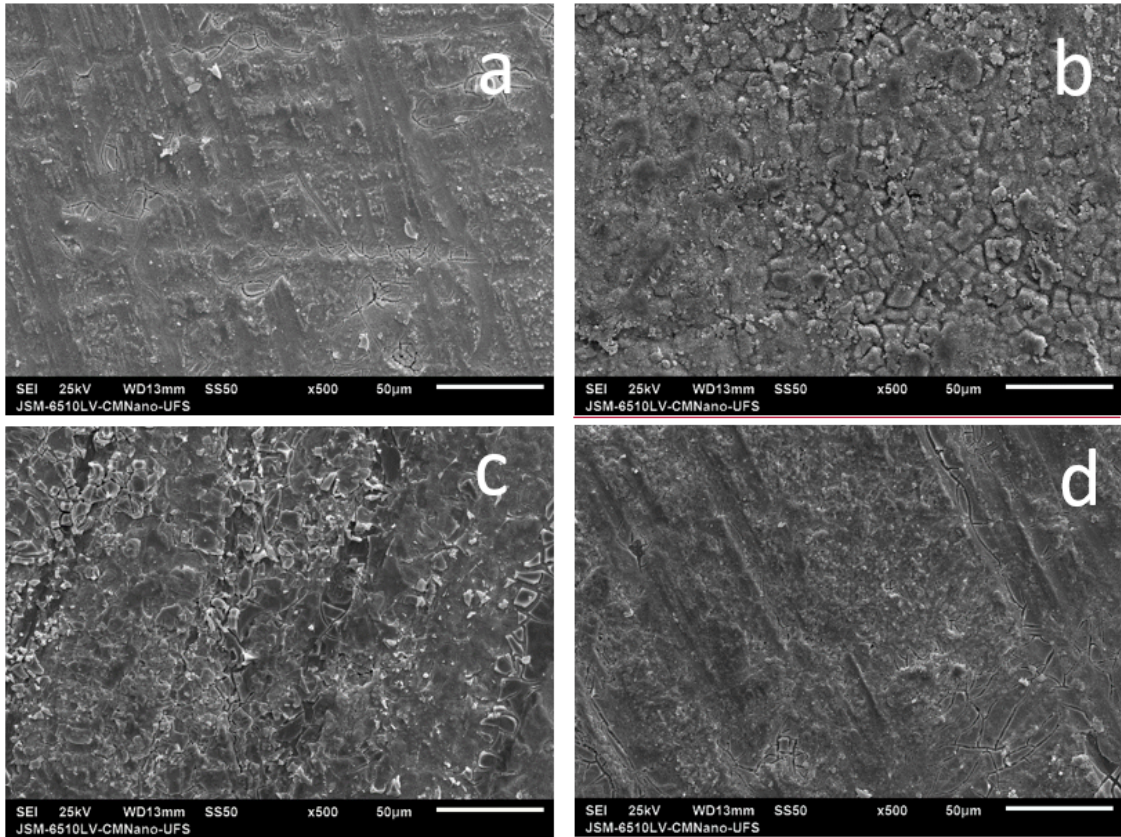
Figure 5. SEM images of (a) $(SnO_2)_{93}Sb_5Ta_2$, (b) $(SnO_2)_{93}Sb_5Bi_2$, (c) $(SnO_2)_{93}Sb_5Gd_2$, and (d) $(SnO_2)_{93}Sb_5Ce_2$ obtained by thermal decomposition with a calcination temperature of 550°C and 500× magnification.

Considering the electrode synthesis is based on several coating steps, for $(SnO_2)_{93}Sb_5Ta_2$, $(SnO_2)_{93}Sb_5Gd_2$, and $(SnO_2)_{93}Sb_5Ce_2$, a more homogenous surface was obtained, which is associated with the sequential filling of the *"mud-cracked"* structures noted at 500°C. It is believed that the higher temperature promoted the initial formation of a large gap that was sequentially filled during further coating. As for $(SnO_2)_{93}Sb_5Bi_2$, the evidence of gaps is still easily noted. However, the coating layer appeared to increase in width and form star-like structures.

As found by Shmychkova *et al.* (2013), Bi doping considerably modifies the electrode surface, increasing roughness, which is highly recommended for catalytic activities since it tends to increase superficial area. Similar results were found in the literature (Petrović et al., 2015; Song et al., 2010) where compact coatings were formed when doping anodes with Bi, promoting longer service lifetimes due to substrate protection from mechanical stress (due to the formation of bubbles) or even Ti substrate oxidation. Further SEM analyses were carried out on this substrate to investigate the specific superficial formation for the electrode obtained and to support the results found in the present research. SEM images with zooms of $\times 2000$ and $\times 5000$ for $Sn_{93}Sb_5Bi_2$ with a final calcination temperature of 550℃ will be discussed below.

Figure 6 presents the SEM images obtained with 500× amplification for all electrodes with a final calcination temperature of 600℃. The presence of a "*mud-cracked*" structure is prevalent in these images, which corroborates our presumption that the progressive coating positively contributes to surface homogenization. However, it seems that the further increase in calcination temperature reinforces the stretching effects, which increases the formation of "*mud-cracked*" structures. As presented in **Table 1**, the increase in the formation of "*mud-cracked*" structured was clearly responsible for the superficial area increase, especially for $(SnO_2)_{93}Sb_5Gd_2$. However, further service lifetime tests showed that the increase in superficial area was not always associated with a more durable electrode. $Sn_{93}Sb_5Gd_2$ presented a 2-fold increase in superficial area when the calcination temperature increased from 500 to 600℃, but it also presented a decrease in service lifetime from 25 h (500℃) to nearly 1 h (600℃).
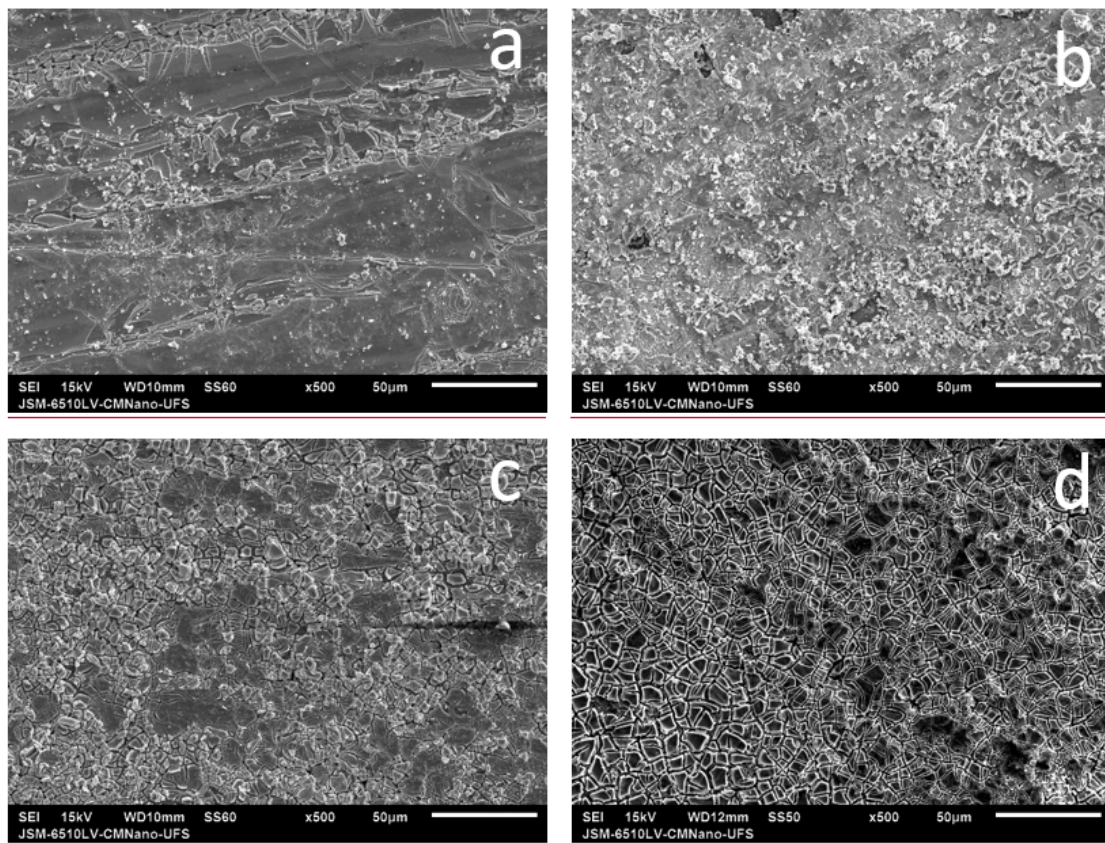
Figure 6. SEM images of (a) $(SnO_2)_{93}Sb_5Ta_2$, (b) $(SnO_2)_{93}Sb_5Bi_2$, (c) $(SnO_2)_{93}Sb_5Gd_2$, and (d) $(SnO_2)_{93}Sb_5Ce_2$ obtained by thermal decomposition with a calcination temperature of 600°C and 500× magnification.

XRD provides information on the structural surface of the electrode to examine its crystalline phase. In ternary electrodes, the metallic oxide mixture can influence XRD in the following ways: (i) the formation of additional diffraction peaks as a result of the formation of a new crystalline phase and (ii) peak width and intensity differences due to the expansion of the metal oxides by the incorporation of other elements (Wu et al., 2014).

Tin oxide is a semiconductor with non-cubic structure and a stable *d* orbital. According to the Pourbaix diagram, tin oxide is stable in water considering its anodic dissolution in pH that can vary from pH 2–12. By adding antimony, oxygen vacancies in the structures are created, leading to cation repulsion and an increase in the cell unit because of the higher ionic radios of Sb^{+3} in comparison to Sn^{+4} (Jara et al., 2011).

As expected for electrodes synthetized by thermal decomposition methods, all XRD analyses presented an intense peak associated with typical "*mud-cracked*" formations of Ti where partial exposure of the substrate used is expected (Shao, et al., 2014). However, to ensure longer service lifetimes, proper layer deposition and total coverage of the substrate is crucial

for preventing its oxidation and further electrode passivation (Ding et al., 2010). Therefore, all electrodes obtained for the three calcination temperatures were analyzed to determine the influence of expansion rates and final calcination temperature on layer deposition and crystallinity.

For electrodes calcined at 500°C **(Figure 7a)**, the most intense main peak for Ti was seen for $(SnO_2)_{93}Sb_5Ta_2$, which indicates that the substrate was more exposed for this material. Considering variations in expansion rates of the oxide metals applied in this material and the substrate used, the formation of intense cracking and further agglomeration of the particles obtained contributes to the formation of larger grains deposited on the surface of the material and corroborates with the smallest electrochemically active area seen in **Figure 1a**. Furthermore, the presence of cracks on the surface of the electrode is, as previously explained, a source of electrode poisoning, where smaller molecules obtained from prior cleavage reactions are strongly adsorbed on the electrode surface, infiltrating the cracks. Progressively, the molecules will deposit on the electrochemically active surface slowly, leading to electrode deactivation (Jara et al., 2011). For $(SnO_2)_{93}Sb_5Ta_2$, the slow deactivation process seen by this mechanism explains the longer service lifetime seen in **Figure 3** for the same electrode.

Still considering the increased service lifetime observed for the electrodes calcined at 500°C, it would be expected that the same behavior seen for $(SnO_2)_{93}Sb_5Ta_2$ would apply for $(SnO_2)_{93}Sb_5Gd_2$. However, from the XRD peaks, the latter electrodes presented a more uniform layer deposition and proper protection of the Ti substrate, presenting a smaller presence of deep cracks. In addition, from the results obtained for **Figure 1a**, it is possible to note a slightly higher electrochemically active area for this electrode, which would suggest the formation of smaller grains.

As for $(SnO_2)_{93}Sb_5Ce_2$ and $(SnO_2)_{93}Sb_5Bi_2$, the results obtained in **Figure 7a** are very similar, with the presence of broader SnO_2 peaks for the $(SnO_2)_{93}Sb_5Bi_2$ electrode. Previous studies developed by Shmychkova *et al.* (Shmychkova et al., 2013) found that doping MMO with Bi leads to Bi incorporation, reducing the crystal size with diameters smaller than 2 µm and segregation of Bi to the surface of the material. Thus, matrix incorporation of Bi would lead to less defined peaks, as found in the present research.

As expected, all Ti peaks for electrodes calcined at 550°C were smaller, which is in agreement with data estimated by cyclic voltammetry and SEM, indicating improved recovering of the Ti substrate. The results presented in **Figure 7b** also present smaller peaks associated with the formation of Sb_2O_5 at around 42°, which are associated with the formation of a more compact superficial matrix. This homogeneity obtained with this specific calcination

temperature can be associated with the higher accelerated service lifetime associated with all electrodes obtained at this temperature.

For electrodes calcined at 600°C **(Figure 7c)**, slightly smaller Ti peaks are clearly seen, which would indicate higher layer coverage of the substrate, providing a more stable material. Also, at this temperature, the XRD pattern for $(SnO_2)_{93}Sb_5Bi_2$ showed an additional diffraction peak at 54.58°, corresponding to (220) reflection attributed to monoclinic α–Bi_2O_3 (Petrović et al., 2015). However, the increase in calcination temperature clearly led to an increase in crystallinity, highlighted by the narrower peaks related to the oxides deposited, as seen in all XRD results.
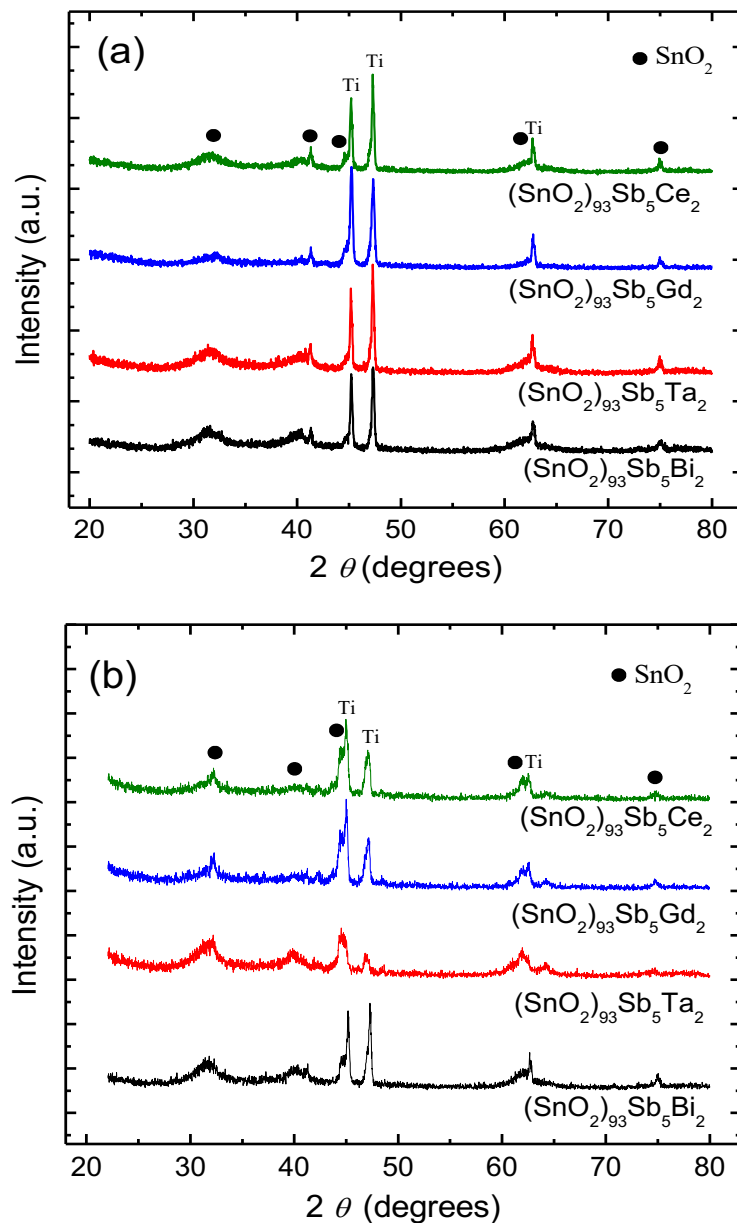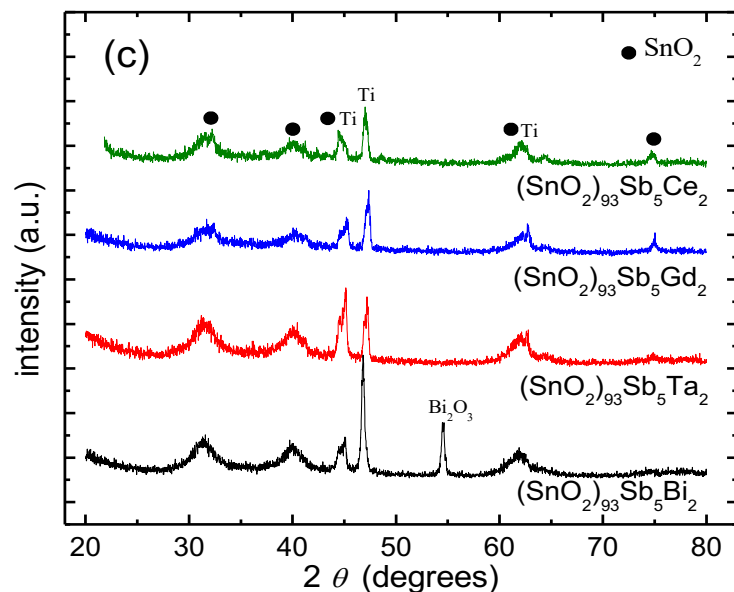
Figure 7. XRD patterns obtained for all SnO₂–Sb electrodes with different doping metals calcined at (a) 500, (b) 550, and (c) 600°C.

From the physical analysis, it was concluded that electrode superficial organization is strongly influenced by the metallic composition (Cui et al., 2009) and by its heating rate (Zhu, Wang, Chen, Kobayashi, & Maeda, 2013). The various expansion rates seen for both the Ti support and the oxide metal coatings determine the depth and amount of "*mud-cracked*" formation and can influence the electrochemical behavior of the material.

Physical characterization showed that the innovative methodology using ionic liquids as solvents in the precursor solution was able to produce well-recovered electrodes with variations in electrochemical behavior according to metal doping and calcination temperature. For applications in electro-oxidation reactions, the electrocatalytic activity of these materials will be further investigated for the electro-oxidation of Diuron®.

As the goal of the present work was the development of MMO for electrochemical oxidation of pesticides, in particular Diuron, further electrolysis reactions were carried out to determine the most electrocatalytically active material obtained.

Best degradation outcomes observed by UPLC were found for all electrodes obtained at a calcination temperature of 550°C, while the best results were seen for degradation with NaCl as electrolyte medium. However, due to the formation of toxic organochlorides typically seen in this medium (Solano et al., 2013), the remaining electrolysis reaction was carried out using Na₂SO₄ as the electrolyte.

Figure 8 shows the degradation results for all electrodes applied under Na_2SO_4. Considering the methodology applied in UPLC analysis, it is possible to point out that the best degradation was seen for $(SnO_2)_{93}Sb_5Ce_2$, followed by $(SnO_2)_{93}Sb_5Bi_2$. It is also worth mentioning that although Diuron removal was around 30%, the electrolysis time was very short. It was estimated that an increase in time would lead to an increase in Diuron removal. Further, additional investigations of the electrodes obtained with calcination temperatures of 500 and 600°C and applying the same metal doping were performed **(Figure S2)**. It is important to highlight that electrodes calcined at 500°C were unable to carry through the electrolysis experiment, reaching the operational limit of 10 V of the equipment within less than 30 min of the experiment. In addition, the electrodes calcined at 600°C, in both cases of metal doping with cerium and bismuth, presented lower outcomes for the electrochemical degradation of Diuron.
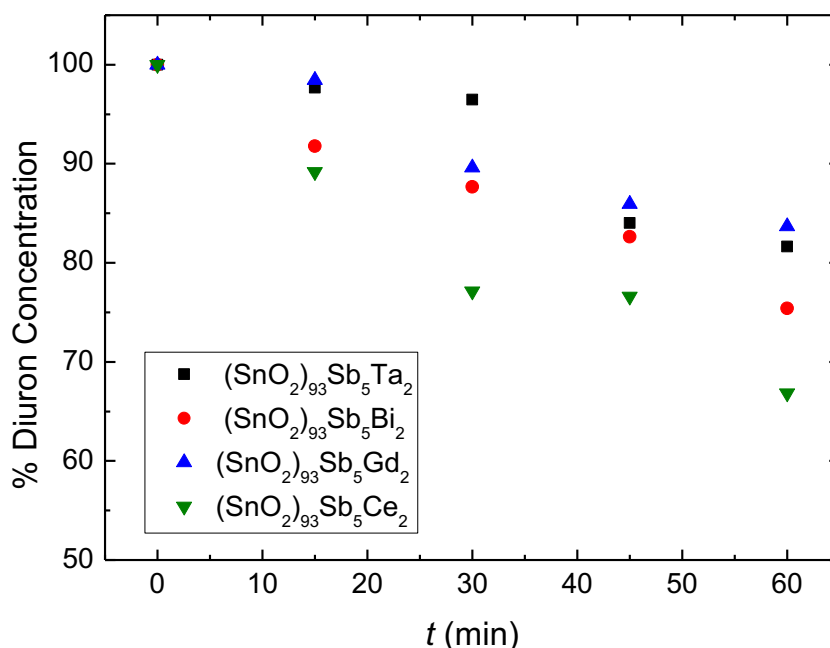
Figure 8. Rates of 10 ppm Diuron removal in 0.33 M Na_2SO_4 applying a 1 h electrolysis treatment using a current density of 10 mA cm^{-2} for electrodes calcined at 550°C.

Although the best degradation outcomes were obtained for $(SnO_2)_{93}Sb_5Ce_2$, considering its considerably shorter service lifetime (50-fold shorter than $(SnO_2)_{93}Sb_5Bi_2$), the second best outcome for Diuron degradation obtained with $(SnO_2)_{93}Sb_5Bi_2$ was chosen for further electrolysis with various electrolytes to determine the positive influence of the metabolites generated **(Figure 9)**.
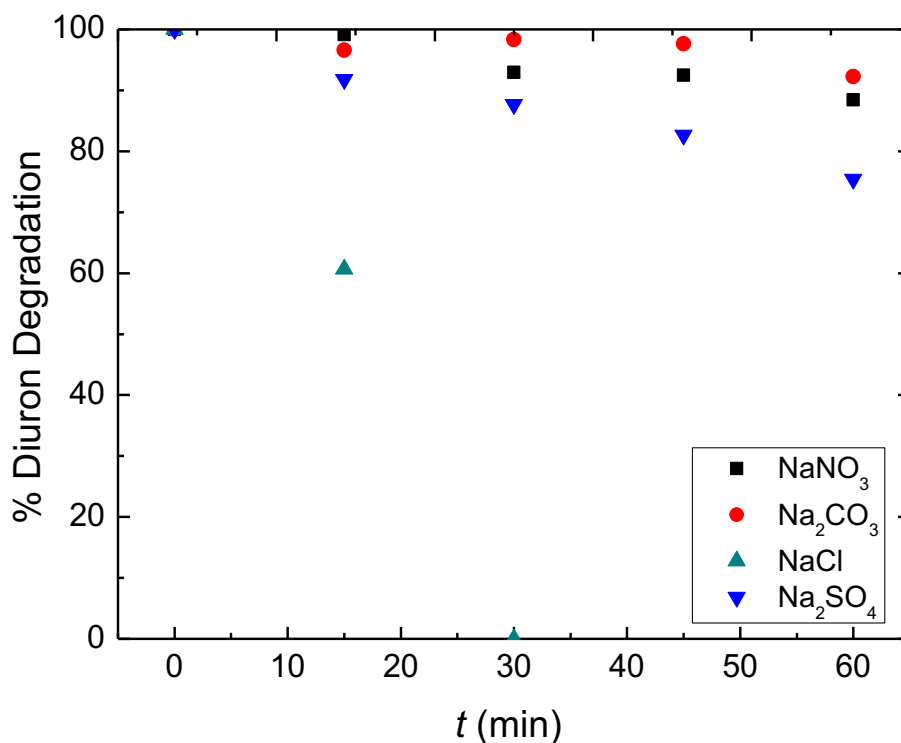
Figure 9. Rates of 10 ppm Diuron removal in various electrolytes (NaNO$_3$, NaCO$_3$, NaCl, Na$_2$SO$_4$) applying a 1 h electrolysis treatment using a current density of 10 mA cm^{-2} with the anode (SnO$_2$)$_{93}$Sb$_5$Bi$_2$ calcined at 550°C.

As would be expected, the presence of chloride ions favored the rapid removal of Diuron from the solution, leading to a 0% concentration after around 27 min. The remaining electrolytes presented slight improvements when compared with each other. Although NaCl presented high rates of Diuron removal, reaching total removal around the first half hour of treatment, the electrode stability was also compromised by the use of this electrolyte and, therefore, will not be recommended.

Previous studies by Djebbar *et al.* (2008) showed that the Diuron molecule is more rapidly degraded when considering interactions with hydroxyl radicals, as is the case of the present study. Similar findings were obtained by Oturan *et al.* (2008) when analyzing Diuron removal for comparison of biological and electrochemical treatments. The specific molecule of Diuron was not satisfactorily degraded biologically due to its genotoxic behavior, reinforcing the advantages of degrading the molecule by electrochemical means.

Moreover, to further understand this considerable increase in electrocatalytic activity associated with (SnO$_2$)$_{93}$Sb$_5$Bi$_2$ electrodes, SEM images with amplifications of 2000× and 5000× were obtained **(Figure 10)**. In fact, such amplifications clearly showed the formation

of structures known as nanoflowers. Reports on Bi doping producing such nanoflowers are commonly seen in the literature (Petrović et al., 2015; Song et al., 2010) and are associated with very stable structures that are electrochemically active. Therefore, the formation of these structures as agglomerates of nanorods tend to reduce mechanical stress in the material coating, improving the service lifetime, as was seen in **Figure 3**. The uniqueness of these formations were clarified when analyzing SEM images with an amplification of 2000× for all remaining electrodes, noting that in no other case were these compact structures formed **(Figures S3, S4)**.
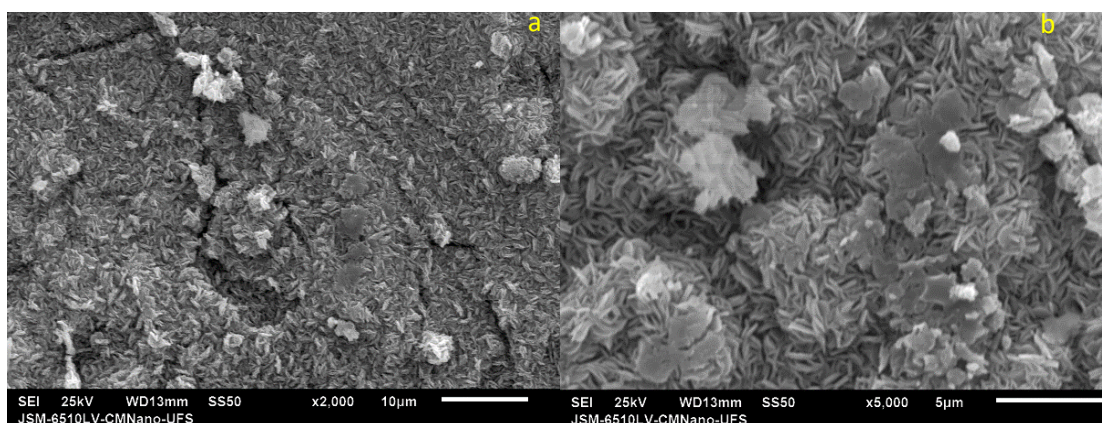
Figure 10. SEM images of $(SnO_2)_{93}Sb_5Bi_2$ obtained by thermal decomposition with a calcination temperature of 550℃ and a magnification of (a) 2000× and (b) 5000×.

However, while carrying out the electrolysis analysis, the stability of most electrodes was an important variable to consider. Although most electrodes indicated accelerated service lifetimes varying from 1 to 30 h, while submitted to a constant application of current density, they were easily contaminated and led to deactivation by poisoning and adsorption. To illustrate this finding, **Figure 11** shows the voltammetric behavior seen for $(SnO_2)_{93}Sb_5Ce_2$ and $(SnO_2)_{93}Sb_5Bi_2$, in Na_2SO_4 electrolyte before and after being submitted to 1 h of electrolysis of Diuron.

Note that for the electrode with Ce doping the electrochemical active area presented a very pronounced reduction of 40% (from 22.81 to 9.17 mC cm^{-2}), which would compromise the application of this material as an electrocatalyst for Diuron electrochemical degradation. The poisoning effect combined with physical detachment is the main cause for the decrease in service lifetime when working with mixed oxide metal electrodes (Jara et al., 2011; Shao, Yan et al., 2014). Recent studies analyzing these effects have shown that poisoning can be reversed for electrochemical activity recoveries (Shao, et al., 2014). However, the pronounced reduction in electrochemical active area seen in **Figure 11a** is commonly associated with detachment

phenomena and cannot be reverted. On the other hand, **Figure 11b**, which shows the $(SnO_2)_{93}Sb_5Bi_2$ cyclic voltammograms before and after electrolysis, show a less pronounced reduction of the electrochemically active area of 19.5% (from 61.45 to 49.43 mC cm^{-2}) with a dislocation of the reduction peak from 0.70 to 0.45 V. Therefore, to apply this material continuously, a surface activation procedure is needed, seeking the detachment of the organic compound that was adsorbed on the surface of the material.
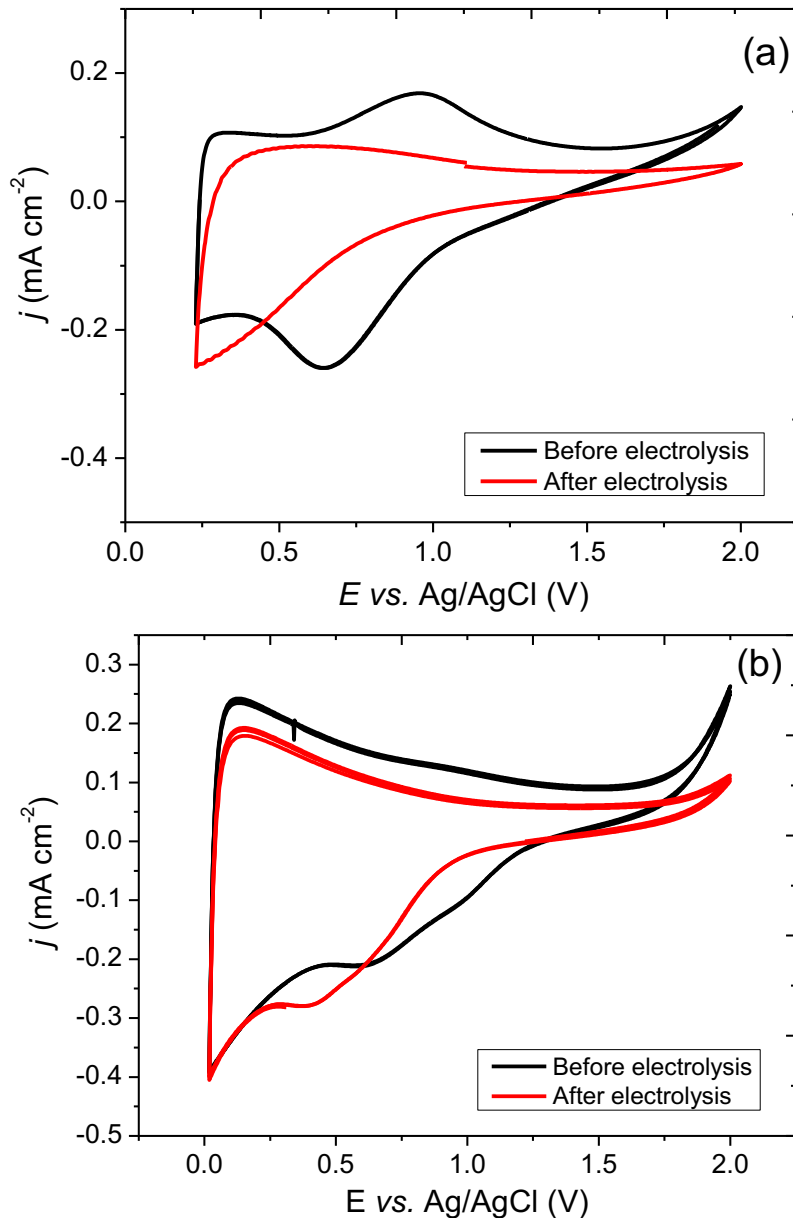
Figure 11. Voltammetric plots obtained in Na_2SO_4 (0.33 M) at 20 mV s^{-1} for (a) $(SnO_2)_{93}Sb_5Ce_2$ and (b) $(SnO_2)_{93}Sb_5Bi_2$ calcined at 550°C before (black line) and after (red line) electrolysis reactions with a current density of 10 mA cm^{-2}, Diuron 10 ppm in 0.33 M of Na_2SO_4.

5.4 Conclusions

The present research focused on the development of a rapid and easy thermal decomposition method for the synthesis of MMOs with enhanced features using an ionic liquid for the preparation of the metal oxide solution. From cyclic voltammetry analysis, it was possible to note that electrochemically active electrodes were obtained for all metals and calcination temperatures proposed. Furthermore, while analyzing service lifetime and electrolysis efficiency, it was noted that the electrodes with mild calcination temperatures in general presented a better outcome, presenting longer service lifetimes and higher degradation efficiencies. Moreover, from SEM images, all electrodes presented highly compact superficial areas with some formation of "*mud-cracked*" structures, highlighting the formation of nanoflowers for $(SnO_2)_{93}Sb_5Bi_2$, which strongly contributed to its improved service lifetime and electrocatalytic activity. From EIS analysis, the charge transfer resistance of the materials was analyzed and it was possible to note that the $(SnO_2)_{93}Sb_5Ce_2$ electrode presented a smaller arc, typically associated with improved charge transfer, which was reflected by the higher degradation rates of up to 32% Diuron removal. However, physical stability tests carried out by means of service lifetimes and analysis of cyclic voltammetry profiles before and after electrolysis reactions showed that $(SnO_2)_{93}Sb_5Bi_2$ was more stable than $(SnO_2)_{93}Sb_5Ce_2$, which it being more suitable for industrial applications. Finally, considering data found in the literature, a removal rate of up to 25% of Diuron while applying 10 mA cm^{-2} represented a good degradation rate for such a persistent compound. Thus, the present study shows that synergistic effects between Sn, Sb, and Bi promoted an electrochemically active material with high physical stability, highlighting the importance of thorough physical and electrochemical studies in to develop a industrially suitable MMO.

References

Ardizzone, S., Bianchi, C. L., Cappelletti, G., Ionita, M., Minguzzi, A., Rondinini, S., & Vertova, A. (2006). Composite ternary SnO_2-IrO_2-Ta_2O_5 oxide electrocatalysts. *J. Electroanal.*

Chem., **589**, 160–166.

Arenas, L. F., Ponce de León, C., & Walsh, F. C. (2016). Electrochemical redox processes involving soluble cerium species. *Electrochim. Acta*, **205**, 226–247.

Berenguer, R., Sieben, J. M., Quijada, C., & Morallón, E. (2014). Pt- and Ru-Doped SnO_2–Sb Anodes with High Stability in Alkaline Medium. *App. Mater. Interf.*, **6**, 22778–22789.

Brillas, E. & Martínez-Huitle, C. A. (2015). Decontamination of wastewaters containing synthetic organic dyes by electrochemical methods. An updated review. *App. Cat. B: Environ.*, **166–167**, 105–145.

Carlesi Jara, C., Salazar-Banda, G. R., Arratia, R. S., Campino, J. S., & Aguilera, M. I., (2011). Improving the stability of Sb doped Sn oxides electrode thermally synthesized by using an acid ionic liquid as solvent. *Chem. Eng. J.*, **171**, 1253–1262.

Chaiyont, R., Badoe, C., Ponce de León, C., Nava, J. L., Recio, F. J., Sirés, I., & Walsh, F. C. (2013). Decolorization of methyl orange dye at IrO_2-SnO_2-Sb_2O_5 coated titanium anodes. *Chem. Eng. Tech.*, **36**, 123–129.

Cui, Y. H., Feng, Y. J., & Liu, Z. Q. (2009). Influence of rare earths doping on the structure and electro-catalytic performance of Ti/Sb–SnO_2 electrodes. *Electrochim. Acta*, **54**, 4903–4909.

Da Silva, L. M., De Faria, L. A., & Boodts, J. F. C. (2001). Determination of the morphology factor of oxide layers. *Electrochim. Acta*, **47**, 395–403.

Del Río, A. I., Fernández, J., Molina, J., Bonastre, J., & Cases, F. (2010). On the behaviour of doped SnO_2 anodes stabilized with platinum in the electrochemical degradation of reactive dyes. *Electrochim. Acta*, **55**, 7282–7289.

Ding, H.-Y., Feng, Y. J., & Lu, J. W. (2010). Study on the service life and deactivation mechanism of Ti/SnO_2-Sb electrode by physical and electrochemical methods. *Russ. J. Electrochem.* **46,** 72–76.

Djebbar, K. E., Zertal, A., Debbache, N., & Sehili, T. (2008). Comparison of Diuron

degradation by direct UV photolysis and advanced oxidation processes. *J. Environm. Manag.*, **88**, 1505–1512.

Dong, W., Xie, X., Jia, J., Du, H., Zhong, L., Liang, Z., & Han, P. (2014). Theoretical calculation and experimental study on the conductivity and stability of Bi-doped SnO$_2$ electrode. *Electrochim. Acta*, **132**, 307–314.

Duan, T., Chen, Y., Wen, Q., & Duan, Y. (2015). Different mechanisms and electrocatalytic activities of Ce ion or CeO$_2$ modified Ti/Sb–SnO$_2$ electrodes fabricated by one-step pulse electro-codeposition. *RSC Adv.*, **5**, 19601–19612.

Duan, T., Wen, Q., Chen, Y., Zhou, Y., & Duan, Y. (2014). Enhancing electrocatalytic performance of Sb-doped SnO$_2$ electrode by compositing nitrogen-doped graphene nanosheets. *J. Haz. Mater.*, **280**, 304–314.

Fathollahi, F., Javanbakht, M., Norouzi, P., & Reza, M. (2011). Comparison of morphology, stability and electrocatalytic. *Russ. J. Electrochem.* **47**, 1281–1286.

Feng, Y., Cui, Y., Logan, B., & Liu, Z. (2008). Performance of Gd-doped Ti-based Sb-SnO$_2$ anodes for electrochemical destruction of phenol. *Chemosphere*, **70**, 1629–1636.

Feng, Y. J. & Li, X. Y. (2003). Electro-catalytic oxidation of phenol on several metal-oxide electrodes in aqueous solution. *Wat. Res.*, **37**, 2399–2407.

Gonçalves, I. C., Santos, W. T. P., Franco, D. V, & Da Silva, L. M. (2014). Fabrication and characterization of oxide fine-mesh electrodes composed of Sb-SnO$_2$ and study of oxygen evolution from the electrolysis of electrolyte-free water in a solid polymer electrolyte filter-press cell : Possibilities for the combustion of organic pollutants. *Electrochim. Acta*, **121**, 1–14.

Gordon, C. M. (2001). New developments in catalysis using ionic liquids. *App. Cat. A: Gen.*, **222,** 101–117.

Li, X., Shao, D., Xu, H., Lv, W., & Yan, W. (2016). Fabrication of a stable Ti/TiO$_x$H$_y$/Sb–SnO$_2$ anode for aniline degradation in different electrolytes. *Chem. Eng. J.*, *285*, 1–10.

Lin, H., Niu, J., Ding, S., & Zhang, L. (2012). Electrochemical degradation of perfluorooctanoic acid (PFOA) by Ti/SnO$_2$–Sb, Ti/SnO$_2$–Sb/PbO$_2$ and Ti/SnO$_2$–Sb/MnO$_2$ anodes. *Wat. Res.*, **46**, 2281–2289.

Liu, Y., Liu, H., Ma, J., & Li, J. (2012). Preparation and electrochemical properties of Ce–Ru–SnO$_2$ ternary oxide anode and electrochemical oxidation of nitrophenols. *J. Haz. Mat.*, **213–214**, 222–229.

Luo, Y., Guo, W., Ngo, H. H., Nghiem, L. D., Hai, F. I., Zhang, J., & Wang, X. C. (2014). A review on the occurrence of micropollutants in the aquatic environment and their fate and removal during wastewater treatment. *Sci. Tot. Environ.*, **473–474**, 619–641.

Malpass, G. R. P., Neves, R. S., & Motheo, A. J. (2006). A comparative study of commercial and laboratory-made Ti/Ru$_{0.3}$Ti$_{0.7}$O$_2$ DSA electrodes: "In situ" and "ex situ" surface characterisation and organic oxidation activity. *Electrochim. Acta*, **52**, 936–944.

Martins, T. S., Hewer, T. L. R., & Freire, R. S. (2007). Cério: Propriedades catalíticas, aplicações tecnológicas e ambientais. *Quim. Nova*, **30**, 2001–2006.

Ni, Q., Kirk, D. W., & Thorpe, S. J. (2015). Characterization of the mixed oxide layer structure of the Ti/SnO$_2$-Sb$_2$O$_5$ anode by photoelectron spectroscopy and impedance spectroscopy. *J. Electrochem. Soc.*, **162**, H40–H46.

Oturan, N., Trajkovska, S., Oturan, M. A., Couderchet, M., & Aaron, J. J. (2008). Study of the toxicity of diuron and its metabolites formed in aqueous medium during application of the electrochemical advanced oxidation process "electro-Fenton." *Chemosphere*, **73**, 1550–1556.

Petrović, M. M., Mitrović, J. Z., Antonijević, M. D., Matović, B., Bojić, D. V., & Bojić, A. L. (2015). Synthesis and characterization of new Ti–Bi$_2$O$_3$ anode and its use for reactive dye degradation. *Mat. Chem. Phys.*, **158**, 31–37.

Pipi, A. R. F., Neto, S. A., & De Andrade, A. R. (2013). Electrochemical degradation of diuron in chloride medium using DSA based anodes. *J. Braz.Chem. Soc.*, **24**, 1259–1266.

Piro, N. A., Robinson, J. R., Walsh, P. J., & Schelter, E. J. (2014). The electrochemical behavior of cerium(III/IV) complexes: Thermodynamics, kinetics and applications in synthesis. *Coord. Chem. Rev.*, **260**, 21–36.

Pupo, M. M. S., Costa, L. S., Figueiredo, A. C., Silva, R. S., Cunha, F. G. C., Eguiluz, K. I. B., & Salazar-Banda, G. R. (2013). Photoelectrocatalytic degradation of indanthrene blue dye using Ti/Ru-based electrodes prepared by a modified Pechini method. *J. Braz. Chem. Soc.*, **24**, 459–472.

Rao, A. N. S. & Venkatarangaiah, V. T. (2014). Metal oxide-coated anodes in wastewater treatment. *Environ. Sci. Pol. Res.*, **21**, 3197–3217.

Rodrigues, E. C. P., & Olivi, P. (2003). Preparation and characterization of Sb-doped SnO_2 films with controlled stoichiometry from polymeric precursors. *J. Phys. Chem. Sol*, **64**, 1105–1112.

Rufino, É. C. G. & Silva, L. M. (2011). Influência das condições de resfriamento sobre as propriedades superficiais e eletroquímicas de anodos dimensionalmente estáveis. *Quim. Nova*, **34,** 200–205.

Sales Solano, A. M., Costa de Araújo, C. K., Vieira de Melo, J., Peralta-Hernandez, J. M., Ribeiro da Silva, D., & Martínez-Huitle, C. A. (2013). Decontamination of real textile industrial effluent by strong oxidant species electrogenerated on diamond electrode: Viability and disadvantages of this electrochemical technology. *App. Cat. B: Environ.*, **130–131**, 112–120.

Santos, T. É. S., Silva, R. S., Eguiluz, K. I. B., & Salazar-Banda, G. R. (2015). Development of $Ti/(RuO_2)_{0.8}(MO_2)_{0.2}$ (M=Ce, Sn or Ir) anodes for atrazine electro-oxidation. Influence of the synthesis method. *Mat. Lett.*, **146**, 4–8.

Särkkä, H., Bhatnagar, A., & Sillanpää, M. (2015). Recent developments of electro-oxidation in water treatment – A Review. *J. Electroanal. Chem.*, **754**, 46–56.

Shao, D., Li, X., Xu, H., & Yan, W. (2014). An improved stable Ti/Sb–SnO_2 electrode with

high performance in electrochemical oxidation. *RSC Adv.*, **4**, 21230–21237.

Shao, D., Yan, W., Li, X., Yang, H., & Xu, H. (2014). A highly stable Ti/TiH$_x$/Sb−SnO$_2$ anode: preparation, characterization and application. *Ind. Eng. Chem. Res.*, **53**, 3898–3907.

Shestakova, M., Bonete, P., Gómez, R., Sillanpää, M., & Tang, W. Z. (2014). Novel Ti/Ta$_2$O$_5$-SnO$_2$ electrodes for water electrolysis and electrocatalytic oxidation of organics. *Electrochim. Acta*, **120**, 302–307.

Shmychkova, O., Luk'yanenko, T., Velichenko, A., Meda, L., & Amadelli, R. (2013). Bi-doped PbO$_2$ anodes: Electrodeposition and physico-chemical properties. *Electrochim. Acta*, **111**, 332–338.

Song, J.-M., Mao, C.-J., Niu, H.-L., Shen, Y.-H., & Zhang, S.-Y. (2010). Hierarchical structured bismuth oxychlorides: self-assembly from nanoplates to nanoflowers via a solvothermal route and their photocatalytic properties. *Cryst Eng Comm*, **12**, 3875.

Song, S., Fan, J., He, Z., Zhan, L., Liu, Z., Chen, J., & Xu, X. (2010). Electrochemical degradation of azo dye C.I. Reactive Red 195 by anodic oxidation on Ti/SnO$_2$-Sb/PbO$_2$ electrodes. *Electrochim. Acta*, **55**, 3606–3613.

Sun, Z., Zhang, H., Wei, X., Ma, X., & Hu, X. (2015). Preparation and electrochemical properties of SnO$_2$-Sb-Ni-Ce oxide anode for phenol oxidation. *J. Solid State Electr.*, **19**, 2445–2456.

Wang, Y., Hu, B., Hu, C., & Zhou, X. (2015). Fabrication of a novel Ti/SnO$_2$–Sb–CeO$_2$@TiO$_2$–SnO$_2$ electrode and photoelectrocatalytic application in wastewater treatment. *Mat. Sci. in Semicond. Proc.*, **40**, 744–751.

Wasserscheid, P., & Keim, W. (2000). Ionic liquids - new solutions for transition metal catalysis. *Angew Chem Int*, **39**, 3772–3789.

Woldemedhin, M. T., Raabe, D., & Hassel, A. W. (2012). Characterization of thin anodic oxides of Ti-Nb alloys by electrochemical impedance spectroscopy. *Electrochim. Acta*, *82*,

324–332.

Wu, W., Huang, Z.-H., & Lim, T.-T. (2014). Recent development of mixed metal oxide anodes for electrochemical oxidation of organic pollutants in water. *App. Cat. A: General*, **480**, 58–78.

Xiaohong, W., Wei, Q., & Weidong, H. (2007). Thin bismuth oxide films prepared through the sol-gel method as photocatalyst. *J. Mol. Cat. A: Chem.*, **261**, 167–171.

Xu, L. & Song, X. (2015). A novel Ti/antimony-doped tin oxide nanoparticles electrode prepared by screen printing method and its application in electrochemical degradation of C.I. Acid Red 73. *Electrochim, Acta*, **185**, 6–16.

Zhang, L., Xu, L., He, J., & Zhang, J. (2014). Preparation of Ti/SnO$_2$-Sb electrodes modified by carbon nanotube for anodic oxidation of dye wastewater and combination with nanofiltration. *Electrochim. Acta*, **117**, 192–201.

Zhang, Q., Liu, Y., Zeng, D., Lin, J., & Liu, W. (2011). The effect of Ce doped in Ti/SnO$_2$-Sb$_2$O$_3$/SnO$_2$-Sb$_2$O$_3$-CeO$_2$ electrode and its electro-catalytic performance in caprolactam wastewater. *Wat. Sci. Techn.*, **64**, 10–15.

Zhang, Y. M., Yang, S., & Evans, J. R. G. (2008). Revisiting Hume-Rothery's Rules with artificial neural networks. *Acta Mater.*, **56**, 1094–1105.

Zhu, M. W., Wang, Z. J., Chen, Y. N., Kobayashi, T., & Maeda, R. (2013). Effect of heating rate on microstructure and electrical properties of sol–gel derived lead zirconate titanate films crystallized by rapid thermal annealing. *Thin Solid Films*, *540*, 73–78.

Supplementary material

Synthesis and characterization of ternary metallic oxide electrodes containing $(SnO_2)_{93}Sb_5M_2$ (M = Ce, Ta, Bi, Gd) using an ionic liquid as precursor solvent

Marilia Moura de Salles Pupo[a,b], Leticia Mirella da Silva[a], Géssica de Oliveira Santiago Santos[a,b], Katlin Ivon Barrios Eguiluz[a,b], Giancarlo Richard Salazar-Banda[a,b*]

[1] Laboratório de Eletroquímica e Nanotecnologia – LEN, Instituto de Tecnologia e Pesquisa, Aracaju, SE, Brazil

[2] Programa de Pós-graduação em Engenharia de Processos, Universidade Tiradentes Aracaju, SE, Brazil

Corresponding author: gianrsb@gmail.com
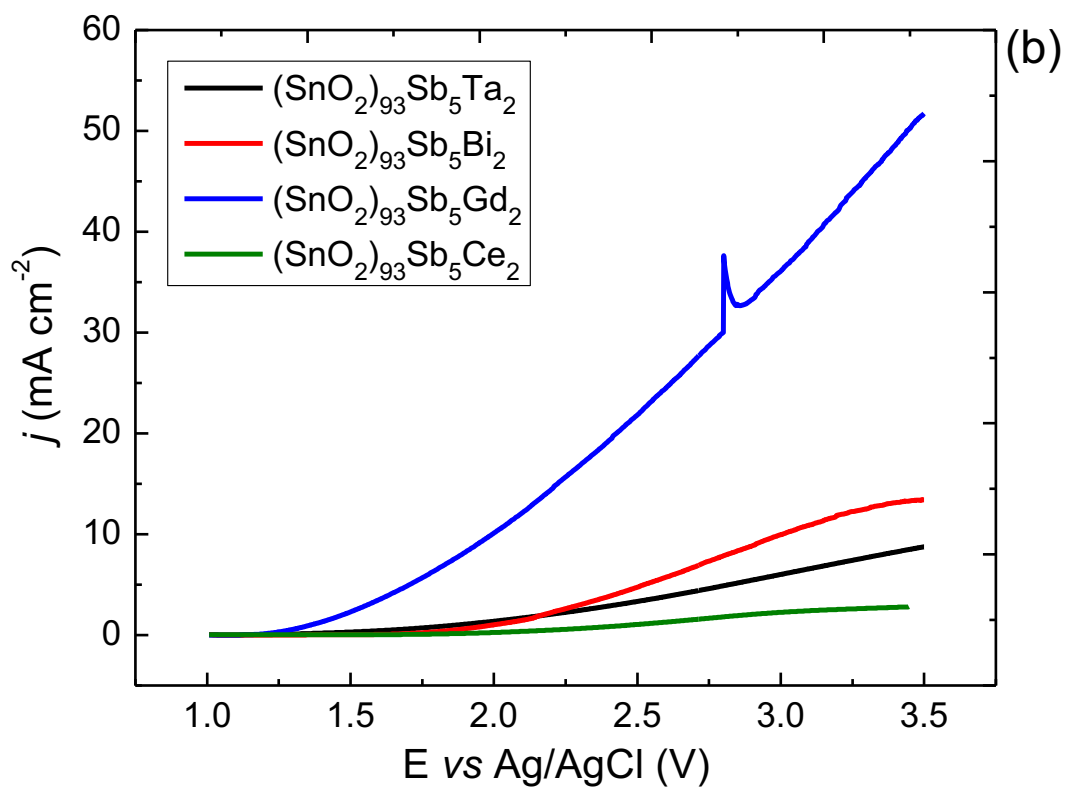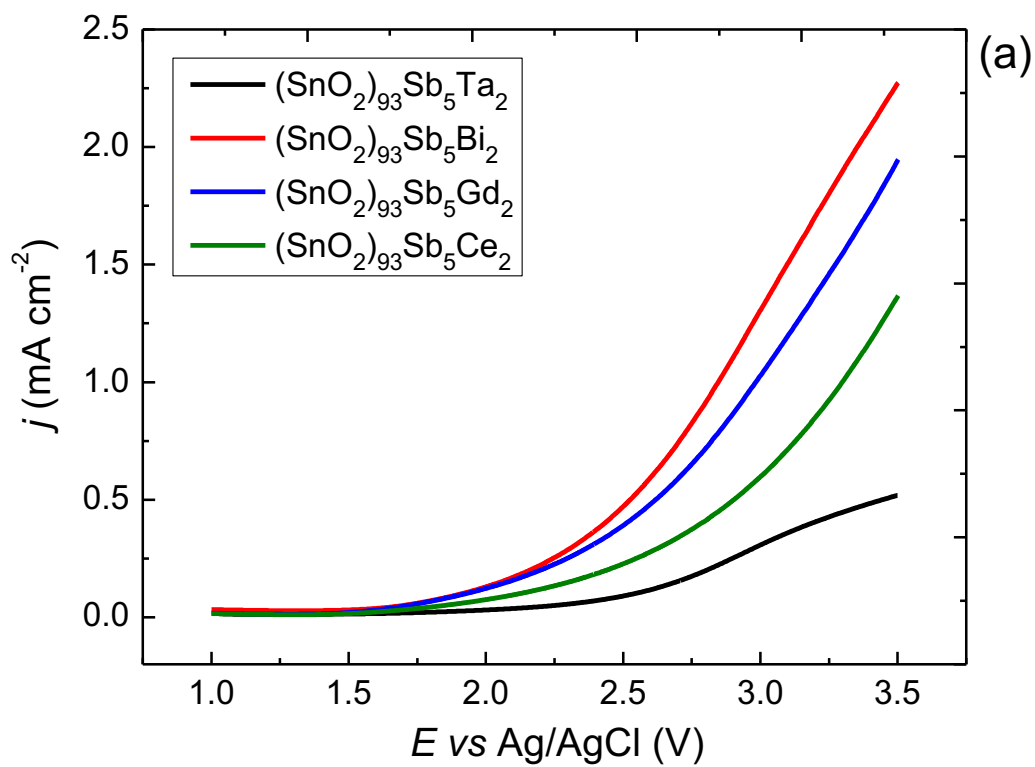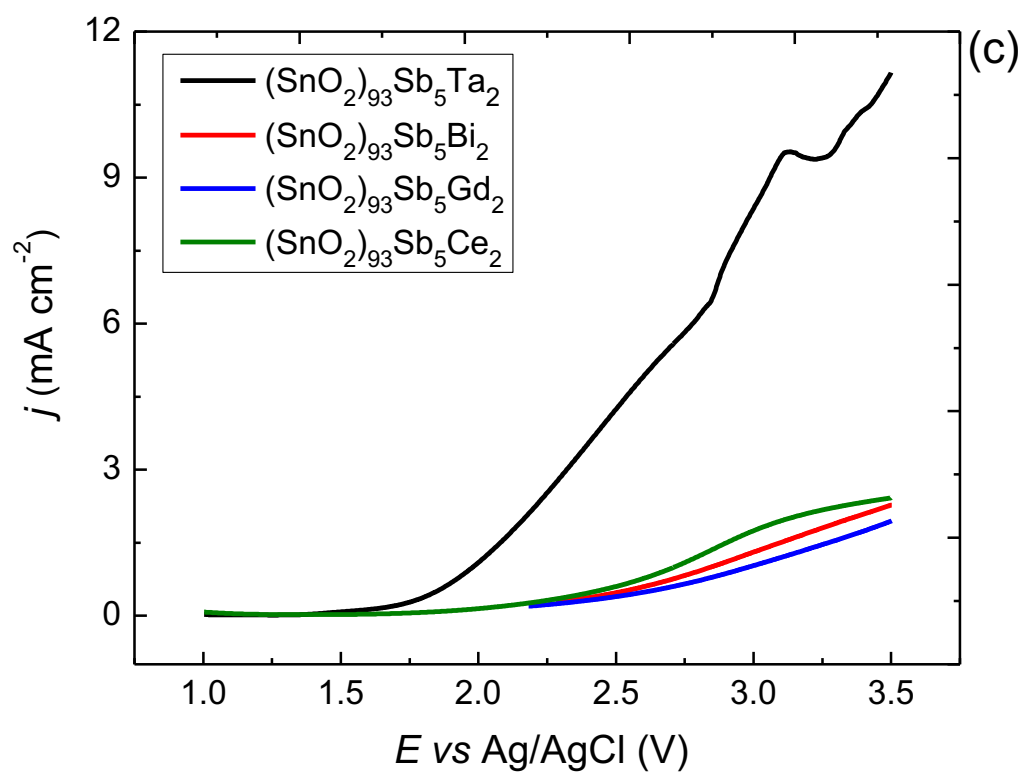
Fig. S1. Linear Voltammetry curves taken between 1.0–3.5 V at 10 mV s⁻¹ for $(SnO_2)_{93}Sb_5M_{2(M=Ta, Bi, Gd\,or\,Ce)}$, electrodes synthetized with calcination temperatures of 500 °C (a) 550 °C (b) and 600 °C (c) in 0.33 M Na_2SO_4.
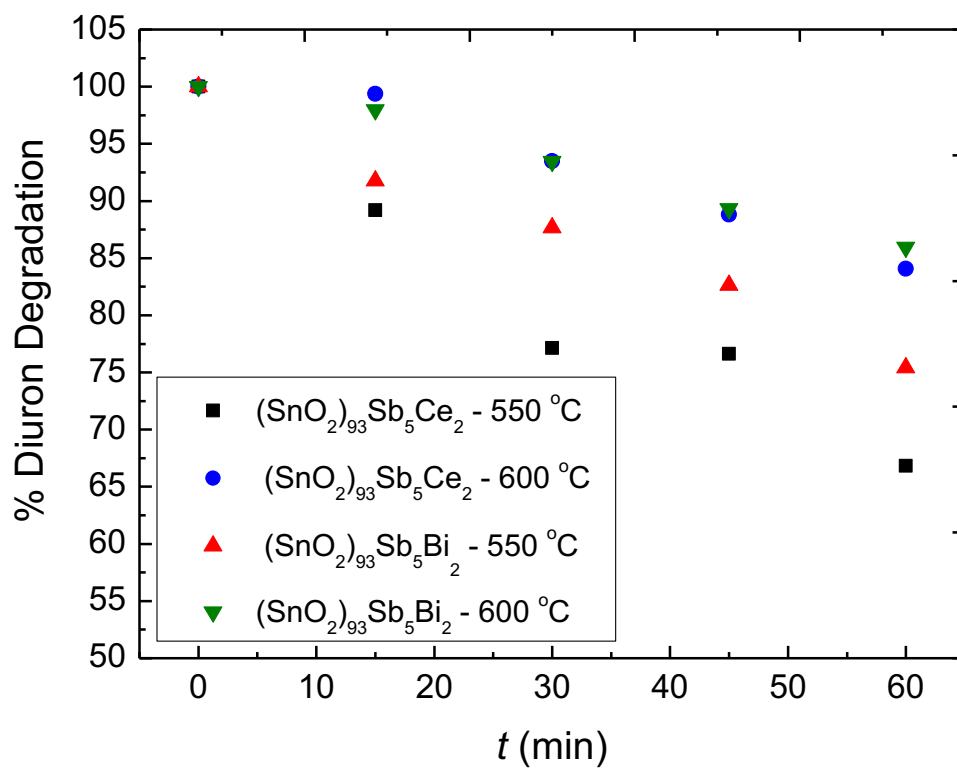
Fig. S2. Rates of 10 ppm Diuron removal in Na₂SO₄ 0.33 M applying an electrolysis treatment of 1 h, using current density of 10 mA cm⁻² for electrodes calcined at 550 and 600 °C.
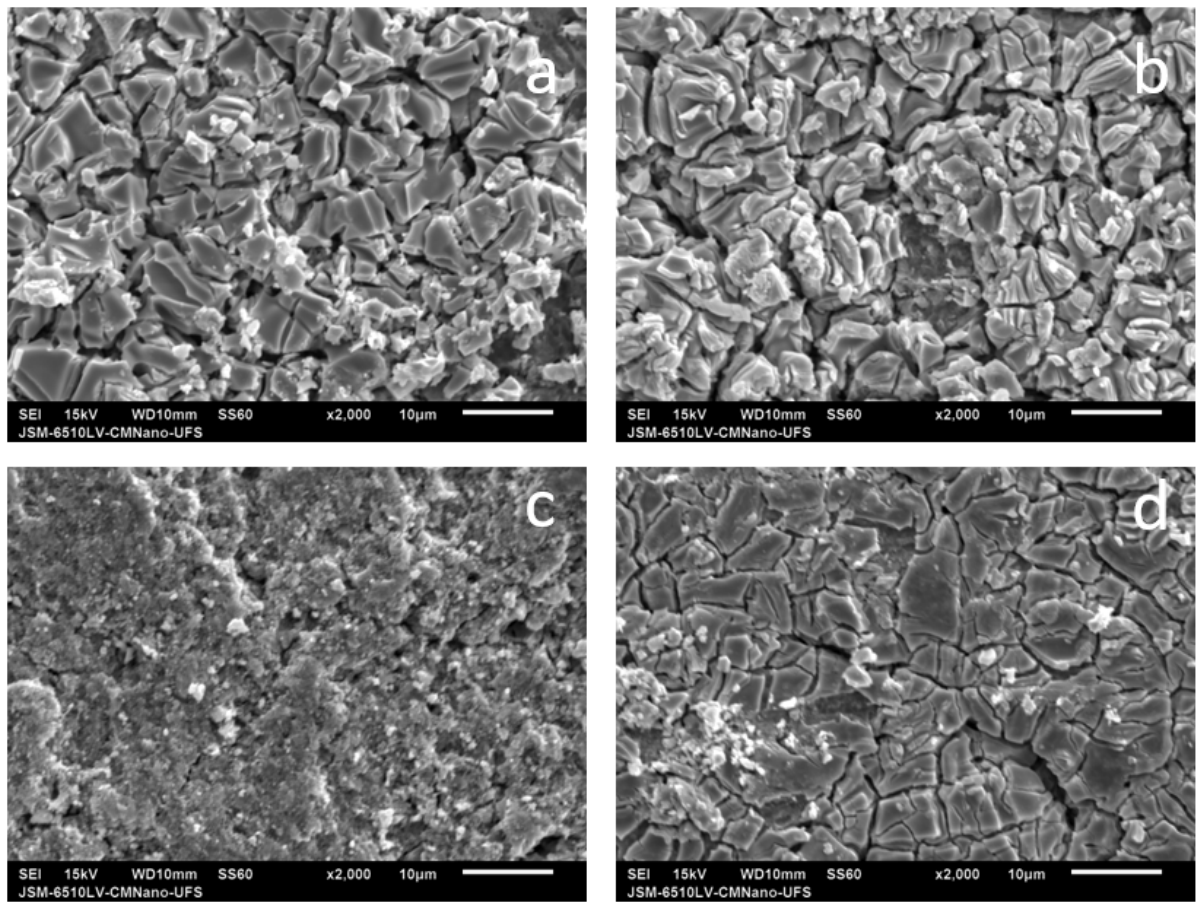
Fig. S3. SEM images of the (a) $(SnO_2)_{93}Sb_5Ta_2$ (b) $(SnO_2)_{93}Sb_5Bi_2$ (c) $(SnO_2)_{93}Sb_5Gd_2$ (d) $(SnO_2)_{93}Sb_5Ce_2$, obtained by thermal decomposition with calcination temperature of 500 °C. Magnification: 2000×.
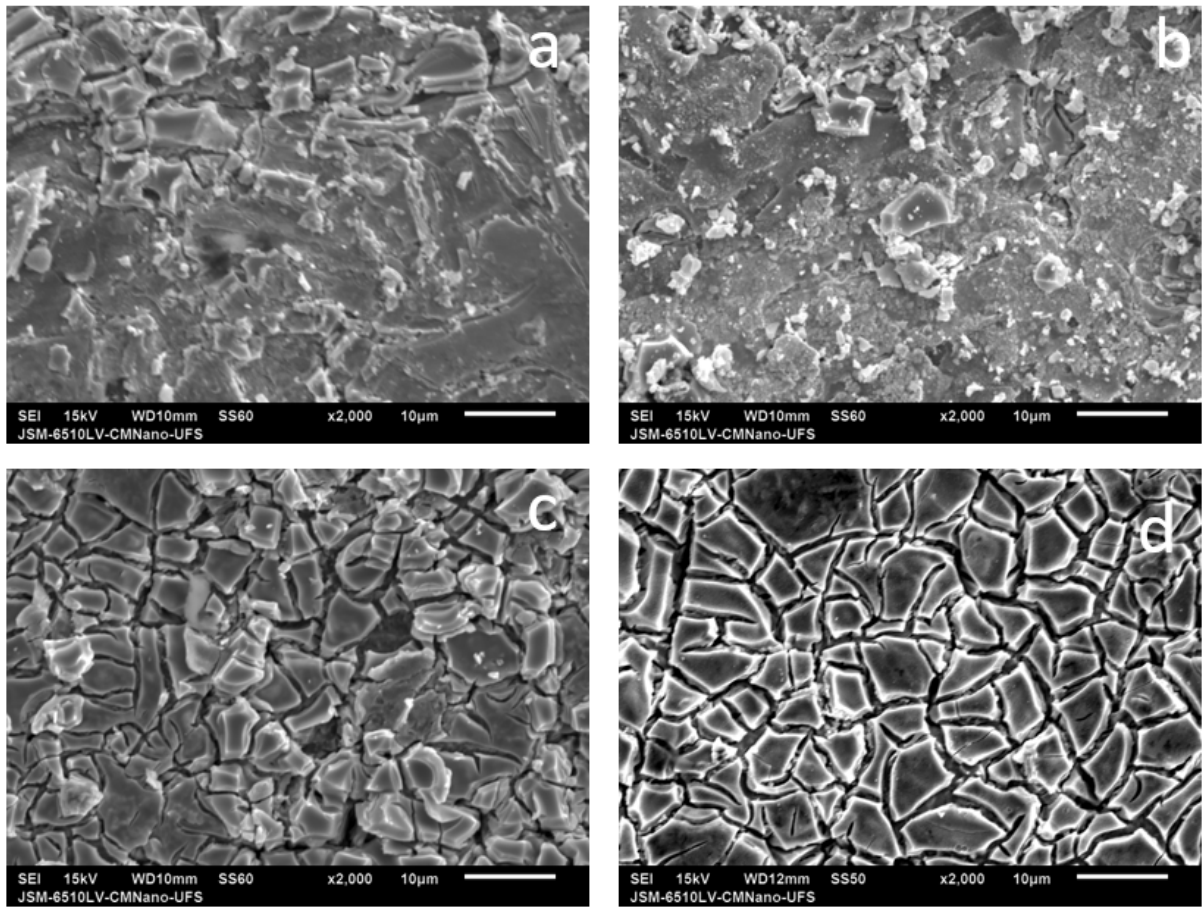
Fig. S4. SEM images of the (a) $(SnO_2)_{93}Sb_5Ta_2$, (b) $(SnO_2)_{93}Sb_5Bi_2$, (c) $(SnO_2)_{93}Sb_5Gd_2$, (d) $(SnO_2)_{93}Sb_5Ce_2$, obtained by thermal decomposition with calcination temperature of 600 °C. Magnification: 2000×.

Capítulo 6

6. SYNTHESIS OF TERNARY MIXED METAL OXIDES MESH ELECTRODES FOR ELECTROCHEMICAL TREATMENT OF X-RAY CONTAMINANTS IN A FLOW THROUGH CELL

Marilia Moura de Salles Pupo[1,2,3], José Miguel Albahaca[2], Katlin Ivon Barrios Eguiluz[1,3], Giancarlo Richard Salazar-Banda[1,3], Jelena Radjenovic[2,4*]

[1] *Process Engineering Post-Graduation Program, Universidade Tiradentes, Av. Murilo Dantas, s/n, Aracaju – SE, Brazil*

[2] *Catalan Institute of Water Research, Emili Grahit 101, Girona, Spain*

[3] *Instituto de Tecnologia e Pesquisa, Av. Murilo Dantas, s/n, Aracaju – SE, Brazil*

[4] *Catalan Institution for Research and Advanced Studies (ICREA), Passeig Lluís Companys 23, 08010 Barcelona, Spain*

*Corresponding author: Jelena Radjenovic (jradjenovic@icra.cat)

ABSTRACT

This work presents a 3D flow-through electrochemical reactor operating with a boron doped diamond (BDD) or a Ti/SnO$_2$SbBi electrode as anode focusing on the oxidation of X-ray contaminants (contrast agents). Ti/SnO$_2$SbBi mesh anodes were synthetized by thermal decomposition using ionic liquid methyl imidazolium, as precursor solvent. A new proposed configuration of Ti/NTs-SnO$_2$SbBi presenting an interlayer of Ti nanotubes (NTs) was also synthetized. The electrodes obtained were analyzed electrochemically through cyclic voltammetry, linear sweep voltammetry, and accelerated service lifetime tests. The anodes were also analyzed physically by X-ray diffraction, scanning electron microscopy and energy dispersive X-ray spectroscopy. Electrochemical oxidation was carried out applying 50, 100 or 150 A m^{-2} to the anode in a 1 L batch flow-through reactor configuration. Samples were collected at 0, 20, 40, 60, 90, 120, 150 and 180 min and analyzed by liquid chromatography – mass spectrometry, and by total organic iodide tests. The electrode presenting an interlayer of Ti nanotubes performed slightly better than the anode without the interlayer of nanotubes. Increases in nearly 4-folds in accelerated service lifetime was obtained with the insertion of the Ti nanotube, also presenting an increase in electrochemically active area and a dislocation of the oxygen evolution reaction potential of 0.2 V to higher potentials. All electrodes studied presented a good electrocatalytic activity removing contaminants and organic iodide in rates of up to 80%. Therefore, the methodology proposed for a new Ti/Nts-SnO$_2$SbBi was able to synthetize a high electrocatalytic material, with performance comparable with a commercial BDD reaching final contaminants concentrations of lower than 20% in all cases and with an accelerated service lifetime 4-fold longer than the material synthetized by traditional thermal decomposition without the proposed interlayer.

6.1 Introduction

X-ray contrast agents used to increase the contrast of structures or fluids within the body in medical imaging have been approached as an environmental hazard for many years. The most common among them are the iodinated contrast media (ICM) species which are known for being highly persistent and several approaches proposing innovative treatment methods to reach their mineralization are found in literature [1, 2]. For any random X-ray analysis, ICM can be injected in the body in up to 200 g per person being excreted almost unchanged [3].

From all iodized species, diatrizoate (DTR) is known as one of the most persistent compounds. Previous studies carried out by Wu et al. [4], applied MF_2O_4 to carbon nanotubes, for use in electro-peroxone treatment finding a slight improvement of 13% when doping the carbon nanotubes, but still reaching only up to 70% of DTR removal. Moreover, other compounds such as iopromide (IPM) has also been brought to focus and attempts to electrochemically degrade these compounds have shown that one compartment cells, and operational conditions of 20 mA in 0.25 g L^{-1} sodium chloride solution was enough to effectively treat IPM in various initial concentrations.

Furthermore, iohexol (IOX) as an additional x-ray contrast agent presents most of the chemical features as the previous two compounds also being highly persistent in the environment. however, electrochemical degradation systems were previously proposed by electrolysis reaching a 85% removal of the compound after 210 minutes [5].

In this sense, electrochemical oxidation has been pointed out lately as one of the most cost and time effective methods for treatment of several wastewaters contaminated with highly persistent compounds [5, 6]. Fundamentally, electrochemical oxidation is based on the formation of highly oxidative species that interact with the contaminant by cleaving its bonds breaking down the compound to more easily degradable products slowly leading to total mineralization into CO_2 and H_2O [7].

Moreover, one of the most relevant variables studied in order to optimize the electrochemical process is the anode composition used. Anodes can typically be divided into active and non-active anodes. Active anodes present reactive oxides on their surface and promote physisorption of the contaminants on the surface of the anode interacting directly on the cleavage of the compound. Inactive anodes, on the other hand, promote the intensive formation of hydroxyl (•OH) radicals, a strong oxidant. The hydroxyl migrates from the surface

of the anode into the bulk of the solution and promotes intense oxidation reactions without allowing any interaction on the surface of the anode to occur [8].

The most common material applied as inactive electrode is the boron-doped diamond (BDD) which has been intensively investigated and presents both high oxidative capacity and long service lifetime [9–11]. However, the commercial BDD is rated at a very high cost, and operational problems due to surface detachment have been previously reported in literature [12]. Therefore, in order to overcome the technical limitations presented, scientific community has been eagerly working on developing anode materials that present similar features to BDD but are of lower cost, easy synthesis while still presenting similar catalytic behavior [13, 14].

Thus, the development of mixed metal oxides (MMO) have been a growing field in material science seeking to potentially match or even surpass the qualities of commercial BDD. One of the most common metal oxides composition studied is SnO_2-Sb [15–18], which presents similar features to BDD and mostly behaves as an inactive electrode. However, due to surface coating cracking and problems in fixation, this material has been reported repeatedly as having problems in service lifetime and has not been applied commercially due to these operational limitations [19].

As a result, studies on different approaches to increase the service lifetime of these materials have been growing throughout the years [20–22]. Research on different synthesis routes [21, 23], physical structure [24], use of interlayers [25, 26] and even doping [17, 27] have proposed several paths in order to improve the materials service lifetime. In this sense, the present work develops a new rapid, low cost synthesis route that applies ionic liquid (e.g. 1-methylimidazole hydrogen sulfate) as precursor solvent for a thermal decomposition synthesis method. This method has been previously reported in literature [23, 28, 29] and is capable of reducing in up to 5-folds the synthesis time by reducing the amount of coating steps required when compared to the traditional sol-gel [30] or Pechini methods [31].

Additionally, considering the improvements reported in literature with doping of metal oxides to the traditional SnO_2-Sb structure [32, 33], the present work also proposes the doping of Bi to the material. Finally, as considerable improvement has been found with the insertion of interlayers to the anode structure [20, 24, 25, 34], TiO_2 nanotubes were grown on the supporting substrate prior to metal oxide coating. Hence, the present work seeks to obtain an improved SnO_2-Sb-Bi anode by applying three modifications to the traditional synthesis

route: (i) use of ionic liquid as metal salt precursor solvent; (ii) formation of TiO_2 nanotube interlayer and (iii) study on a geometrically different structure in the form of meshes.

The materials obtained were analyzed electrochemically by cyclic voltammetry (CV), linear sweep voltammetry (LSV), and accelerated service lifetime tests. The material was also analyzed physically by X-ray diffraction (XRD), scanning electron microscopy (SEM) and energy dispersive X-ray spectroscopy (EDS). To analyze the electrocatalytic features of the anodes obtained electrochemical oxidation was carried out studying the degradation of three X-ray agents (iopromide, iohexol and diatrizoate) in sodium sulfate medium, using a flow-through electrochemical reactor. Oxidation rates and mineralization values were estimated by liquid chromatography – mass spectrometry (LC-MS) and total organic iodide analysis (AOI). Finally, comparative analysis within the materials obtained showed considerable improvement in accelerate service lifetime for the anode with a TiO_2 nanotube interlayer, while both synthetized materials were capable of reaching catalytic activity similar to commercial BDD.

6.2 Materials and methods

6.2.1 Synthesis of mixed metal oxide anode

Mixed metal oxide anodes were synthetized using thermal decomposition method adopted from Silva et al. [23] using 1-Methylimidazole hydrogen sulfate to dissolve the metallic salts of Tin (II) Chloride ($SnCl_2$, ≥99.99%, Sigma Aldrich), Antimony (III) Chloride ($SbCl_3$, ≥99.95%, Sigma Aldrich) and Bismuth (III) Chloride ($BiCl_3$, ≥98, Sigma Aldrich).

The Ti mesh substrate (ASTM B265 Gr. 1) used was provided by De Nora® with 10×10 cm, and submitted to pre-treatment in order to remove the oxide layer naturally formed and any additional contamination found. For that, the substrate was immersed in HCl (20%) (Sigma Aldrich, 37%) in a Becker and submitted to heating at 110 °C for 1 hour, followed by rinsing with ultrapure water (by a Milli–Q system). The material was then immersed in $C_2H_2O_4$ (10%) (Scharlau, 99%), heated to 140 °C for 1 hour, finally being cleaned with ultrapure water.

Precursor solution was prepared by adding the metal salts considering the ratio of 93:5:2 for Sn:Sb:Bi in 1 M concentration to 10 mL of 1-Methylimidazole hydrogen sulfate. This solution was heated for 30 min up to 160 °C and sonicated for 1 hour in ultrasound bath. The precursor solution was then applied on the Ti mesh support through brush painting method and submitted to conventional oven with heating rate of 10 °C min^{-1}, up to 550 °C and kept there for 10 min followed by natural cooling of the system. This process was repeated until the

total mass of 1.2 mg cm^{-2} of precursor solution was deposited over the substrate, where a final calcination process was applied with the same heating rate and keeping the material at 550 °C for 1 hour.

For the Ti/NTs-SnO$_2$SbBi electrodes obtained, methodology was adapted from Rao et al. [34] using 0.05 M KF (Sigma Aldrich, ≥99), 0.075 M HF (Sigma Aldrich 48%) and 0.05 M H$_2$SO$_4$ (Sigma Aldrich, 95%) dissolved in ultrapure water. The titanium mesh substrate already pre-treated was immersed in this solution and connected to a power source Keysight E3649A applying 20 V for 1 hour using the titanium mesh substrate as anode and a stainless-steel mesh as cathode. The substrate was then submitted to ultrasonication for 30 min in a solution of 20% ethanol in water. A second anodization process applying 20 V for an additional 1 hour was carried out. The titanium mesh with the nanotubes formed was then submitted to thermal treatment at 550 °C for 1 h applying a heating rate of 10 °C min. Moreover, tests applying 40 and 60 V in the consecutive anodization process described were also carried out in order to determine the influence of anodization potential on the dimensions of the nanotubes obtained.

The titanium mesh substrate was then submitted to the same procedure described previously coating the material with the precursor solution previously prepared and submitting it to thermal treatment under the same conditions. Both titanium meshes presented the same composition of 93:5:2 for Sn:Sb:Bi in 1 M concentration and will hereon after be referred to as Ti/SnO$_2$SbBi and Ti/NTs-SnO$_2$SbBi for the mesh without and with the nanotube interlayer, respectively. All the heating procedures described were carried out in an Oven Carbolite AAF 11/18.

6.2.2 Electrochemical Characterization

A glass one-compartment cell with 100 × 50 × 120 mm dimensions provided by Duran was used for the electrochemical tests carried out. Ti/SnO$_2$SbBi, Ti/NTs-SnO$_2$SbBi or a commercial 1000 ppm BDD$^{®}$/Ni (8 × 8 cm) were submitted to cyclic voltammetry (CV). The counter electrode used was a stainless-steel mesh of 10 × 25 cm dimensions, working electrode was either the Ti/SnO$_2$SbBi, the Ti/NTs-SnO$_2$SbBi or BDD, and reference electrode was an Ag/AgCl electrode. CV was carried out in 0.033 M Na$_2$SO$_4$ (Sigma Aldrich, ≥99) applying 20 mV s^{-1} at scan rate from 0.2 to 2.0 V. For LSV 0.1 M H$_2$SO$_4$ was used as electrolyte, scan rate was 10 mV s^{-1} and potential was varied from 0.2 to 2.5 V.

Advanced service lifetime tests were carried out applying 150 A m^{-2} to Ti/SnO$_2$SbBi or Ti/NTs-SnO$_2$SbBi in 0.033 M Na$_2$SO$_4$ using a stainless-steel mesh as counter electrode and Ag/AgCl as reference electrode.

Production of $^\bullet$OH was evaluated by analyzing CV scan following methodology proposed by Chaplin et al. [35]. CV scans were carried out from 1.5 to 3.0 V with scanning rate of 5 mV s^{-1} for electrodes, varying the terephtalic acid (TA) concentration in 1, 2.5 and 5 mM and using 0.1 M NaClO$_4$ as electrolyte. Chronopotentiometry applying 100 A m^{-2} was carried out for 1 h and samples were collected at 0, 5, 10, 15, 20, 25, 30, 40, 50 and 60 min in order to rule out oxidation of the target compounds by surface reaction on the anodes.

For the present study TA was used, considering the second-order rate constant (k$_{TA \cdot OH}$) as 4×10^9 M^{-1} s^{-1} as found in literature [36]. Thus, the quasi steady-state concentration of $\bullet$OH ([$\bullet$OH]ss) during electrolysis with a particular electrode can be estimated with the pseudo first-order rate constant (k$_{TA}$) for TA concentration decay [37].

$$\frac{d\,[TA]}{dt} = k_{TA,OH}[TA][\bullet\,OH]ss \qquad\qquad EQ.\ 1$$

$$[\bullet\,OH]ss = \frac{k_{TA}}{k_{TA,OH}} \qquad\qquad EQ.\ 2$$

Where *d[TA]* is the variation in TA concentration, *dt* is the delta of time for the reaction, *k$_{TA \cdot OH}$* is the second-order rate constant and *[•OH]ss* the quasi steady-state concentration of •OH.

The TA concentration was monitored by high-performance liquid chromatography (HPLC) using a variable wavelength UV visible detector set at 248 nm and a reverse-phase C18 column (Phenomenex, 4.6 mm × 250 mm, 5 μm). Acetonitrile: water with 0.1% (v/v) formic acid (20:80 (v/v)) were used as mobile phases at a total flow rate of 1.0 mL·min^{-1}. The injection volume was set at 100 μL.

Multi-Potentiostat/Galvanostat Biologic VMP with a booster connected to reach 2A/30V operated by ECLab software was used to carry out all electrochemical analysis.

6.2.3 Physical Characterization

XRD and SEM measurements were carried out to determine the crystalline structure and surface morphology of the material synthetized, respectively. EDS was also carried out to determine surface composition. The measurements were made in a Bruker D8 Advance powder diffractometer, with a Bragg-Brentano geometry, in Theta-2Theta reflection mode. The source

was a Cu sealed ceramic X-ray tube. A secondary monochromator was also used. The diffracted intensity was measured in a NaI(Tl) scintillation detector. SEM analysis were carried out in a Zeiss DSM 960 A with 3.5 nm resolution operating at 20 kV, images were treated using Bruker Esprit 1.9 software. EDS analysis were obtained using a Bruker Nano XFlash Detector 5010 with 129 eV resolution in Mn.

6.2.4 Electrolysis

Sodium diatrizoate hydrate (Sigma Aldrich, ≥99), Iopromide (European Pharmacopeia Reference, , ≥99) and Iohexol (European Pharmacopeia Reference, ≥99) were all dissolved in 20 µM concentration in 15 mM of $NaClO_4$ (Sigma Aldrich, , ≥99) and submitted to electrolysis in a one compartment flow-through electrochemical cell (internal dimensions 80 × 80 × 60 mm) equipped with a stainless steel counter electrode, a leak-free Ag/AgCl reference electrode and either BDD, Ti/SnO_2SbBi or $Ti/NTs-SnO_2SbBi$ as working electrodes and a final volume of 1L.

Electrolysis were carried out for a total of 3 h applying current density of 50, 100 and 150 A m^{-2} and samples were taken at 0, 20, 40, 60, 90, 120, 150 and 180 min. The system was kept in constant flow using a mechanical pump Watson Marlow 530 Bp with no temperature control applied to the system.

6.2.5. LC-MS Analysis

LC-MS tests were used to analyze the samples in order to determine degradation of the target compounds. Chromatographic separations were carried out with a Waters Acquity Ultra-Performance™ liquid chromatography system, coupled to a 5500 QTRAP hybrid triple quadrupole-linear ion trap mass spectrometer (Applied Biosystems, Foster City, CA, USA) with a turbo Ion Spray source. Furthermore, the target analytes were eluted from the column into the chromatograph with the LC-mobile phase, and the separation was achieved with two binary pump systems (Milford, MA, USA), using an Acquity HSS T3 column (50 mm × 2.1 mm i.d., 1.8 µm particle size) for the compounds analyzed under positive electrospray ionization (PI) and both purchased from Waters Corporation Electrospray.

Samples were prepared by quenching 200 µL of sample in 250 µL of methanol and dissolving it in 550 µL of ultrapure water. Samples were analyzed in positive mode using

organic mobile phase of acetonitrile and formic acid (0.1 %) and an aquatic mobile phase of water and formic acid (0.1%).

Samples were collected with a 5 mL syringe from the mixture tank of the electrochemical flow through 3D cell on the times determined and filtered through a 20 μm filter before being added to methanol for quenching.

6.2.6 Total organic iodide

Total absorbable organic iodide (AOI) was analyzed using a Thermo-scientific system which was composed of an Automatic Quick Furnace AQR-2100h and a Gas Absorption Unit GA-210 preceding a final Dionex Integrion HPIC system. 20 mL of sample was concentrated in two consecutive activated carbon cartridges (40 mg activated carbon per glass column (Mitsubishi Chemical Analytech) using a TXA-04 AOI Adsorption Module. The enriched cartridge was then washed with 10 mL of washing solution which consisted of 5% stock solution dissolved in water. The stock solution contained 17g $NaNO_3$, 25 mL HNO_3 (65%) in a 1 L volume dissolved with ultrapure water. The cartridge was then combusted into iodide gas in the automatic quick furnace in the presence of oxygen for 28 min at 900 ℃. The produced gas was absorbed in the gas adsorption unit with 10 mL hydrogen peroxide solution to reduce iodide gas into iodide ions, which were further measured by the HPIC unit. The results of I^- correspond to the total AOI.

6.3 Results

6.3.1 Electrochemical characterization

Cyclic voltammetry was carried out to assess the electrochemical behavior of the electrodes synthetized in comparison with commercial BDD. Thus, Fig. 1 shows the voltammograms obtained with 20 mV s^{-1} of scanning rate, between 0.02 and 2.0 V using 0.03 M Na_2SO_4 as electrolyte medium. Note that the addition of nanotubes interlayer shifted the OER potential to more positive potentials in 0.2 V, from 1.73 V for Ti/SnO_2SbBi to 1.93 V for $Ti/NTs-SnO_2SbBi$.

Similar results were previously found by Cui et al. [38] while adding an interlayer of TiO_2 nanotubes previous to $SnO_2-Sb_2O_5$ coating by thermal decomposition. From LSV experiments carried out in 0.1 M Na_2SO_4 a similar shift of nearly 0.2 V was seen when

comparing Ti/SnO$_2$-Sb$_2$O$_5$ and TiO$_2$-NTs/SnO$_2$-Sb$_2$O$_5$. Furthermore, since OER is a competitive reaction with indirect electrochemical oxidation of contaminants, it is suggested that the higher the OER potential, the less energy is required to electrolyze contaminants found in the medium.

Due to the inactive nature of SnO$_2$ anodes, the surface only provides electroactive sites for the physisorption of the $^\bullet$OH radicals [22], as detailed in the reaction mechanisms:

$$SnO_2[\ \ ] + H_2O_{ads} \rightarrow SnO_2[\ ^\bullet OH]_{ads} + H^+ + e^- \qquad\qquad Eq\ 3$$

$$R + SnO_2[\ ^\bullet OH]_{ads} \rightarrow SnO_2[\ \ ] + RO + H^+ + e^- \qquad\qquad Eq\ 4$$
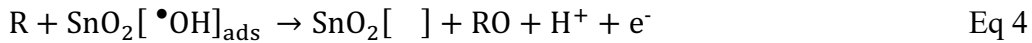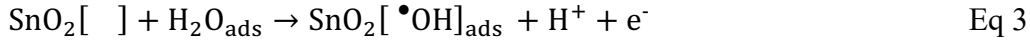
Where SnO$_2$[ ] represents the active sites of the anode, R represents the organic compounds and RO represents the organic compounds oxidation products.

Considering findings reported by Wang *et al.* [39] it is expected that variations in length and width of nanotubes obtained can be tailored by manipulating time and potential applied in the anodization step. For the procedure proposed, 2 steps of one hour each of anodization is carried out, and further investigation was done by repeating tests with various anodization potentials. Fig. S1 shows the result for 20, 40 and 60 V applied in the anodization steps. It is possible to note that for both 20 and 60 V, OER is also around 1.93 V, while the median 40 V presented a value closer to 1.88 V which can be associated to a specific nanotube width that does not favor coating adhesion.

Furthermore, when comparing the OER found in previous reports [22, 39], it is noted that OER potential can vary according to voltage and synthesis time applied when preparing the nanotube interlayer. Considering the synthesis process of applying 20 V in a two-step procedure of 1 h each run, the OER of close to 1.93 V found in the present research is considered an improvement when compared with results found in literature. Wang et al. [39], when preparing TiO$_2$-NTs/SnO$_2$-Sb electrodes, found an OER of 1.88 V when applying 45 V for a period of 3 h for nanotubes synthesis. In that sense, the proposed two-step methodology and Bi doping was able to improve in nearly 0.05 V the OER when applying less than half the potential in a process 1 h faster. These improvements considerably reduce costs both in the synthesis procedure, as well as the electrochemical oxidation treatment.

Furthermore, following methodology proposed by De Mello et al. [28], LSV was carried out in 0.1 M H$_2$SO$_4$ with scanning speed of 10 mV s^{-1} in order to adequately determine the OER potentials. Slight change is noted between the OER in Figure 1 and 2, specially associated with the change in electrolyte medium and also in scanning rate, which allowed a

higher conductivity of the solution and slower scanning speed. Therefore, the OER potentials all shifted to slightly higher potentials but still following the same trend seen in Figure 1.
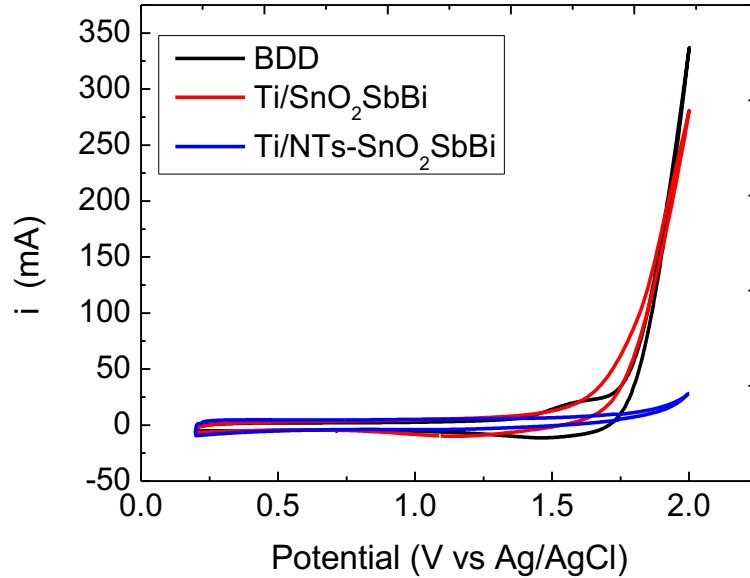
Figure 1: Cyclic voltammetry of the Ti/SnO$_2$SbBi, Ti/NTs-SnO$_2$SbBi and commercial BDD anodes scanned with 20 mV s^{-1} scanning rate, from 0.02 to 2.0 V, in 0.03 M Na$_2$SO$_4$ electrolyte using a stainless-steel counter electrode and Ag/AgCl reference electrode.

Figure 2 shows that OER onset potential for BDD, Ti/SnO$_2$SbBi and Ti/NTs-SnO$_2$SbBi were 2.04, 2.18 and 2.33 V respectively. The increase in OER potential seen when comparing Ti/SnO$_2$SbBi and Ti/NTs-SnO$_2$SbBi can be associated with the increase in surface active area, due to the addition of tridimensional structures deposited on the nanotubes formed. Similar increase was also reported by Xu et al. [40], when adding Cu nanorods on the surface of Ti previous to SnO$_2$-Sb coating.
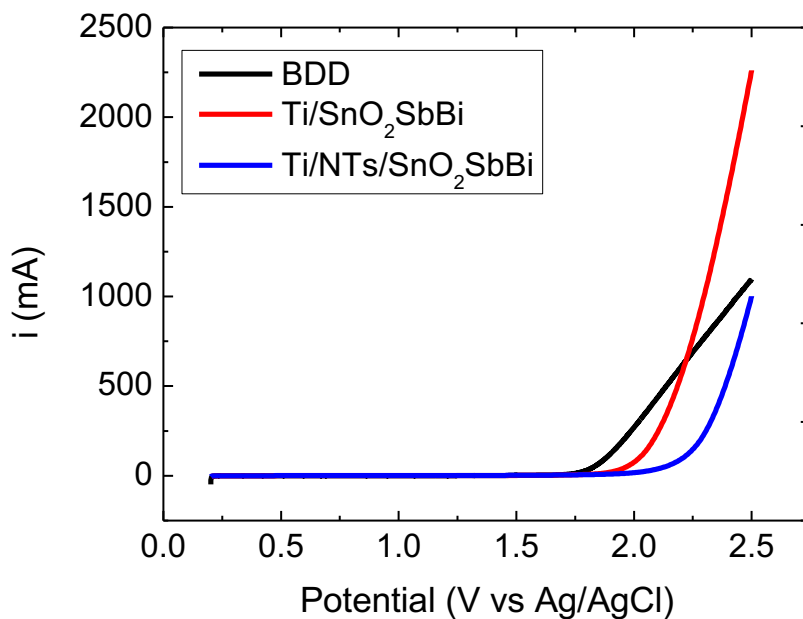
Figure 2: Linear sweep voltammetry of the Ti/SnO$_2$SbBi, Ti/NTs-SnO$_2$SbBi and commercial BDD anodes scanned with 10 mV s^{-1} scanning rate, from 0.02 to 2.5 V, in 0.1 M H$_2$SO$_4$ electrolyte using a stainless-steel counter electrode and Ag/AgCl reference electrode.

Finally, when considering operational viability for industrial use, service lifetime of the materials proposed play an important role in determining viability of the material. From the anodes analyzed BDD was not tested for advanced service lifetime since it is a commercial material. On the other hand, Ti/SnO$_2$SbBi and Ti/NTs-SnO$_2$SbBi electrodes were tested by applying 150 A m^{-2} in 0.03 M Na$_2$SO$_4$ using Ag/AgCl as reference electrode and a stainless-steel mesh as counter electrode. The tests were carried out until anode potential reached 12 V which was considered the operational limit of the potentiostat used. Under the conditions applied, Ti/SnO$_2$SbBi and Ti/NTs-SnO$_2$SbBi presented advanced service lifetimes of 31 and 81 h, respectively (Figure 3). The considerable increase in service lifetime seen for Ti/NTs-SnO$_2$SbBi compared to what has been previously reported specially when adding a TiO$_2$ nanotube interlayer to the surface of the substrate [34, 37, 41, 42].

Also, in order to ensure adequate superficial conformation to optimize the results for accelerated service lifetime, tests were carried out considering altering anodization potential for nanotubes synthesis from 20, to 40 and 60 V. Results presented in Fig S2 show that 20V formed the most favorable superficial structure to increase service lifetime of the electrode. Similar results are presented by Shao *et al.* [42] showing that specially in cases of sequential

electrochemical treatment a lower potential is preferred due to the formation of smaller width nanotubes that tend to be more physically stable and compact more uniformly.

The increase in surface area and further mechanical stability obtained by adding an interlayer previous to final metal oxide coating has been extensively reported in recent studies and has proven to be effective. Mostly this is because the interlayer acts as a protective agent avoiding the formation of deep cracks due to the expansion and contraction of Ti substrate and the metal oxide coating, which occur at different rates [43]. Furthermore, in the present study, by also adding ionic liquid to the precursor solution, and considering its specific properties (boiling point at 450 °C), the final effect is further enhanced when both aspects are applied simultaneously.
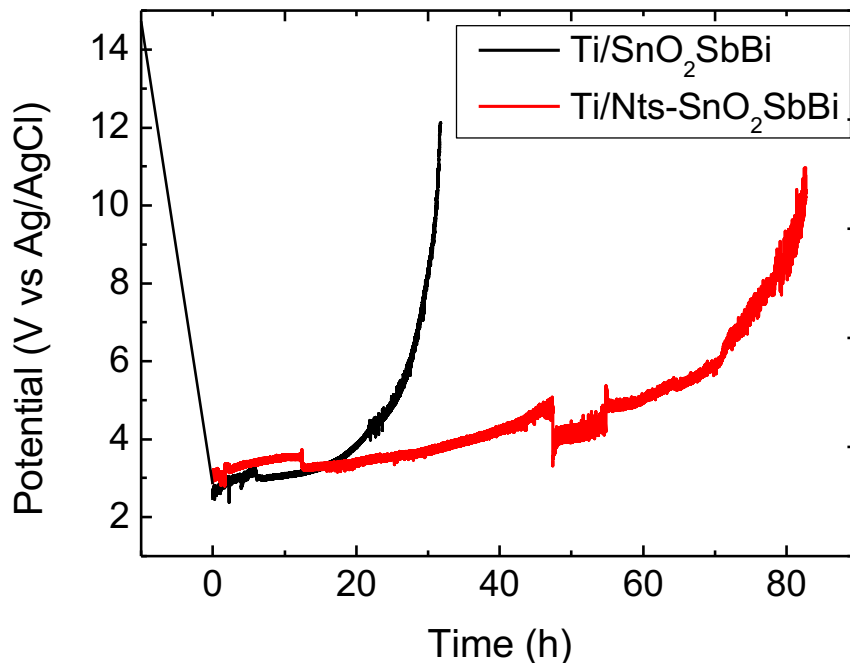
Figure 3: Advanced service lifetime carried out for Ti/SnO$_2$SbBi and Ti/NTs-SnO$_2$SbBi applying 150 A m^{-2} current density in 0.03 M Na$_2$SO$_4$ using Ag/AgCl as reference electrode and a stainless-steel mesh as counter electrode.

6.3.2 Physical Characterization

For further understanding of the physical aspects of the anode's surface, X-rays diffractometry were carried out analyzing both the Ti/SnO$_2$SbBi and also the Ti/NTs-SnO$_2$SbBi

electrode. All peaks were compared to the Joint Committee on Powder Diffraction Standards (JCPDS). Figure 4 shows the XRD patterns obtained for both electrodes highlighting the peaks associated with SnO_2 in red triangles (JCPDS No 88-0287), Ti in blue circles (JCPDS No. 89-3073) and TiO_2 in green squares (JCPDS No. 89-4920).

As previously discussed, the presence of both Sb and Bi were not seen and this is associated with their low concentration (only a total of 8%) when compared with the more predominant Sb. Similar results were also reported by Silva (2018) [44], noting that due to technical limitations of the method, only the more superficial layers are analyzed.
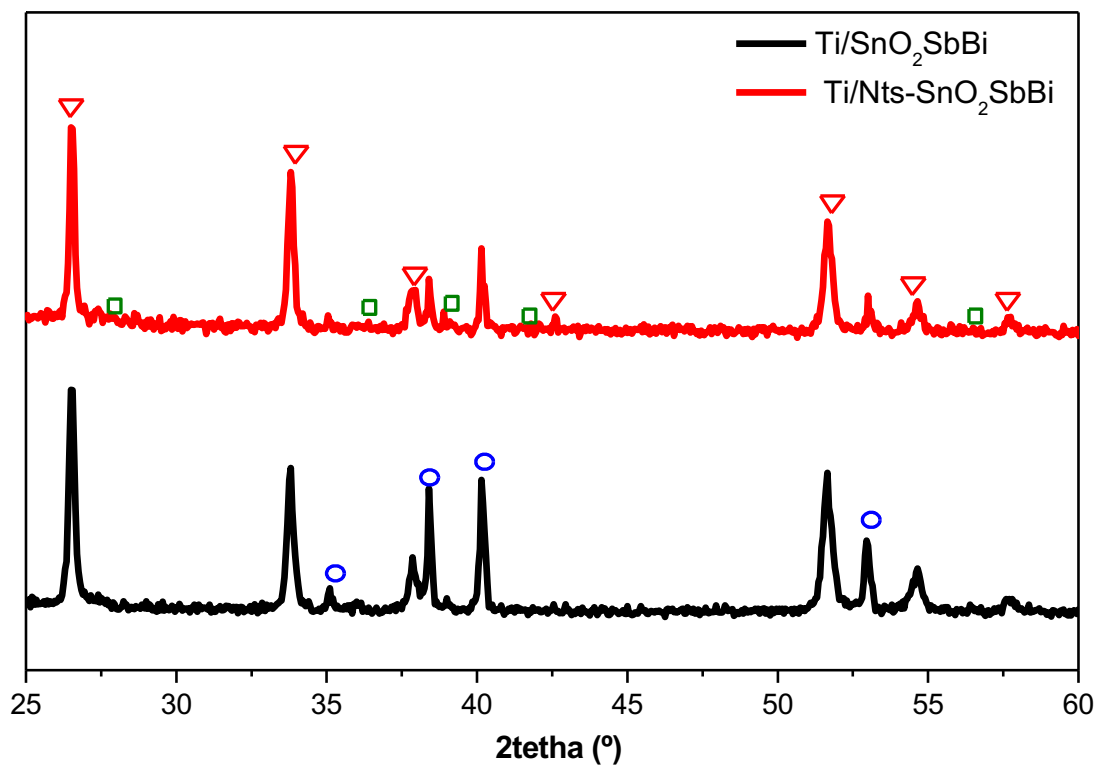
Figure 4: XRD patterns for Ti/SnO₂SbBi and Ti/Nts-SnO₂SbBi with a Bragg-Brentano geometry, in Theta-2Theta reflection mode. The source was a Cu sealed ceramic X-ray tube. Image shows SnO₂ in red triangles, Ti in blue circles and TiO₂ in green squares.

For further investigation SEM analysis were carreid out coupled with EDS generating nominal composition estimates that are shown in Figure 5 (a-e). Figures 5(a) and 5(b) show micrographies with 500× magnification for Ti/NTs-SnO₂SbBi and Ti/ SnO₂SbBi, respectively. As expected, the microscopy for Ti/SnO₂SbBi shows the presence of marked cracks, which are typically associated with the thermal decomposition synthesis method

applied. Several researches [16, 45] report the formation of these cracks considering a positive influence in the overall degradation reaction. The cracks favor the increase in superficial electrochemically active area therefore increasing the active sites that lead to degradation of organic compounds.

However, in an opposite trend, some researchers [28, 46] associate the formation of excessive or deep cracks in thermal decomposition process as a disadvantage. To a degree, the cracks formed in the coatings applied also help expose the Ti substrate, which further oxidizes forming a TiO_2 oxidative layer, both reducing the conductivity of the coating and also increasing the system electrical resistance. Furthermore, these cracks also provide "caves" where bubbles accumulate and slowly lead to deactivation by coating detachment due to the mechanical stress caused in the event of bubble migration [47].

Figure 5(b) on the other hand shows a more uniformly coated layer, where small granular acumulation is seen without the presence of deep craks. In a higher zoom, as shown in Figure 5 (c) and (e), note that the formation with nanotubes on the surface presented very well compacted structure which favor coating physical stability [24].
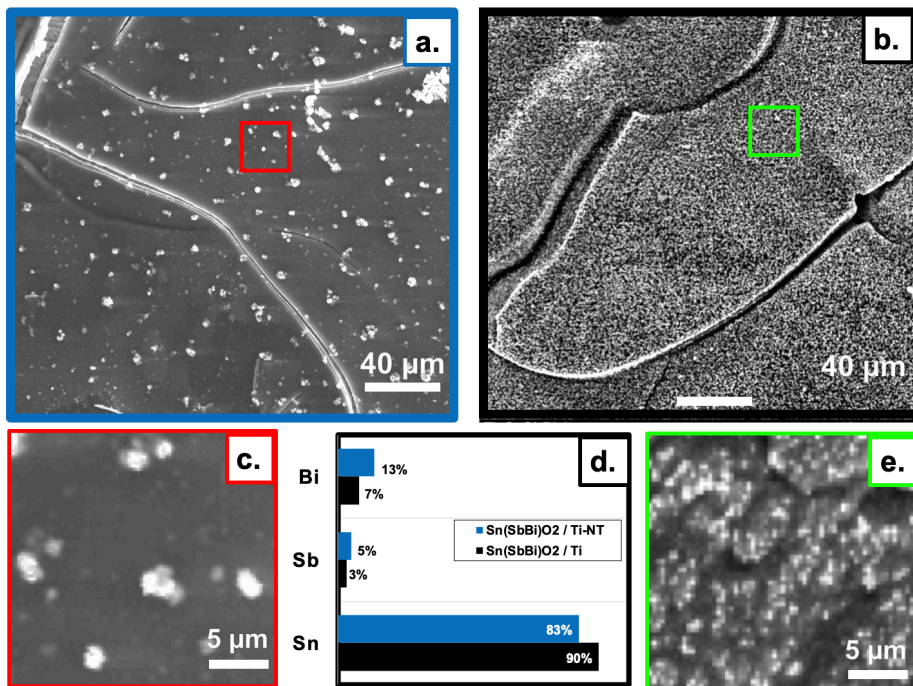
Figure 5: SEM analysis for Ti/SnO₂SbBi and Ti/NTs-SnO₂SbBi carried out with 3.5 nm resolution operating at 20 kV and EDS results obtained using 129 eV resolution in Mn. Where in (a) shows the surface of Ti/NTs-SnO₂SbBi anode; (b) shows the surface of Ti/SnO₂SbBi

anode (both 500× zoom), (c) is a 2000× zoom of the area in red, (d) is the nominal composition for the area selected, (e) is 2000× zoom of the area in red.

LC-MS Analysis

To analyze the electrocatalytic activity of the anodes synthetized, electrochemical oxidation of three X-ray agents (namely iopromide, iohexol and diatrizoate) were carried out varying the current density in 50, 100 and 150 A m^{-2}.

The samples collected were taken to analysis in a LC-MS system and the results obtained are seen in Figure 6. All electrodes, under all current densities presented comparable concentration decay for all the compounds treated. Individually, IPM was degraded to under 20% concentration within the 180 min of analysis for all the anodes proposed. The reaction kinetics is clearly faster for BDD reaching values below 20% within 120 min for all the current densities applied.

Concerning current densities, the degradation slope for IPM when using BDD clearly show the same response for all the current densities applied. This effect is commonly reported in electrochemical degradation systems where the limiting current density is surpassed [8, 48, 49]. On the other hand, for both Ti/SnO$_2$SbBi and Ti/NTs-SnO$_2$SbBi a clear improvement is noted when the current density applied is increased, suggesting that these anodes require higher current densities in order to surpass their overpotential [50].

Similar effects are noted for both IOX and DTR where in all the degradations proposed the compound's concentration decreases in a similar ratio independent of current density applied for BDD electrodes, while a clear evidence of current density applied is seen for the two MMO proposed. However, the compound degradation significantly decreased only in cases where current density was 50 A m^{-2}. Similar effects were found by Guzman-Duque et al. [48], while studying BDD, MMO and platinum as anode materials, finding that in cases where the reaction was carried out under current control regime ($j_{app} < j_{lim,0}$) the degradation reaction is highly compromised at lower current densities.

Therefore, for the Ti/NTs-SnSbBi anode, all reactions carried out with 50 A m^{-2} are closer to a current control regime, where a smaller formation of reactive oxygen species (ROS) is expected.
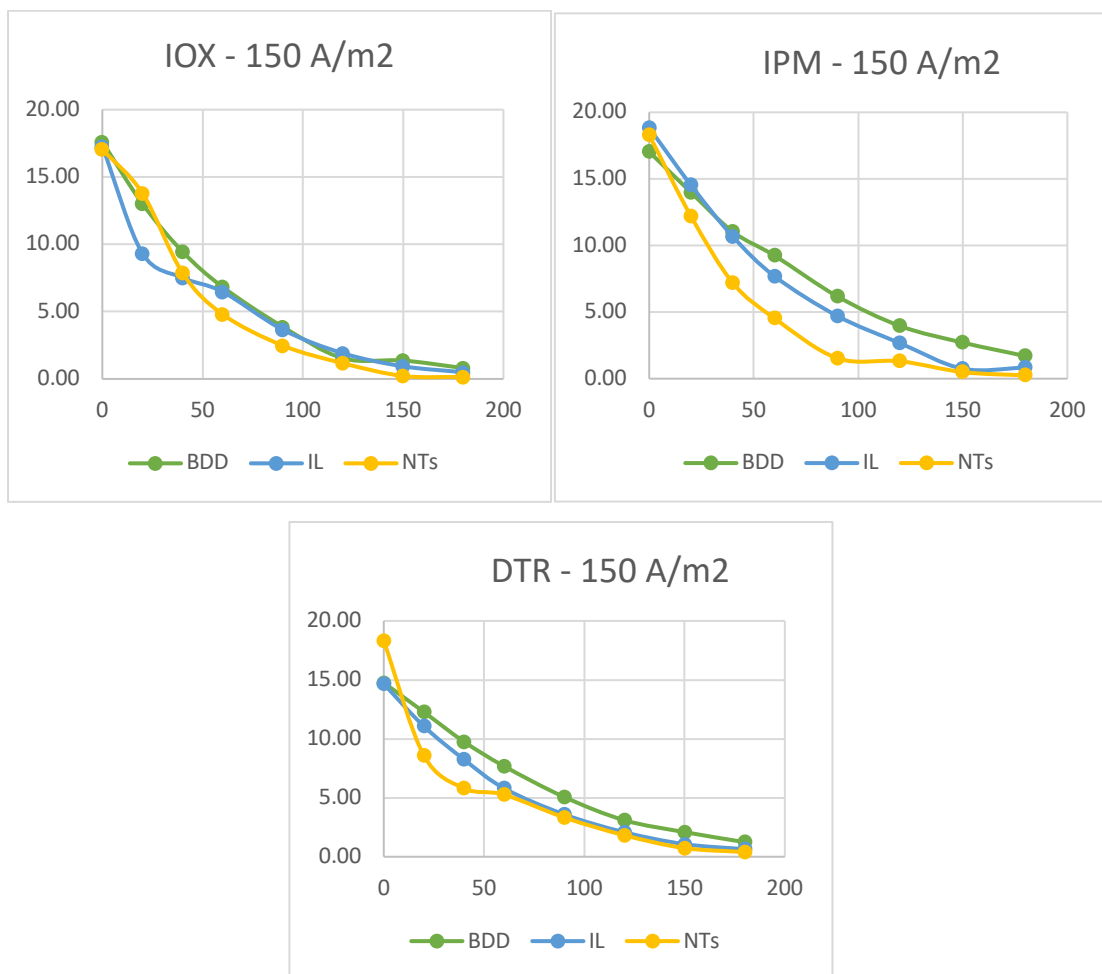
Figure 6: LC-MS x-ray compound degradation results found for IPM, IOX and DTR electro-oxidation at various current densities (150 A m^{-2}) testing all working electrodes proposed (BDD, Ti/SnO$_2$SbBi and Ti/NTs-SnO$_2$SbBi). Current densities results for 50 and 100 A m^{-2} are not shown.

AOI

Finally, iodide concentration was determined to allow the estimation of the final products produced. Although, the presence of iodide has not been positively associated with a number of environmental risks, it has been proven to present some estrogen activity [51]. Moreover, due to their recalcitrant chemical nature and extensive application, a proper treatment route for these compounds is essential to ensure the safety of its use. Thus, samples were collected throughout the electrochemical oxidation and analyzed in order to determine the persistency of iodide products.

Figure 8 presents the concentration of iodide (%) found for samples collected from the experiments carried out with all three different electrodes and all the current densities applied. Contrary to Figure 7, the iodide level was estimated for the stock solution altogether. Therefore, the values seen for iodide concentration in Figure 7 represent a sum of all the organic iodide still present in the solution irrespective of its original compound.

Once more, the trends noted in electrochemical oxidation results were seen. For the BDD electrode, a removal between 80 and 60% were seen in all cases, presenting a steady decline for iodide concentration throughout the analysis. For the 100 A m^{-2} current density and BDD electrode a stabilization of iodide concentration is noted, which can be associated with the formation of more stable final products in that specific current density. As the electrochemical oxidation in filter-press reactors present a delicate balance between electrochemically active surface area and the residence time distribution, the degradation value can be associated with formation and stagnation of bubbles in the surface of the electrode or the formation of some highly persistent intermediary [52].

Moreover, for both Ti/SnO$_2$SbBi and Ti/NTs-SnO$_2$SbBi the similar trend to the EO results was also repeated, where when current density is 50 A m^{-2} a considerable decay in organic iodide removed is noted, shifting from 80 to 50% removal for both electrodes when compared to 150 A m^{-2}. On the other hand, when 100 and 150 A m^{-2} are applied, the final organic iodide concentration value is very similar, around 20%. These results reinforce that the limiting current density for this system is found in between 50 and 100 A m^2. Studies like these play an important role in energy efficiency during electrochemical reaction systems. By determining the optimal current density applied to the system, one avoids the use of excess current density, which represents a direct decrease in final energy costs for the system.
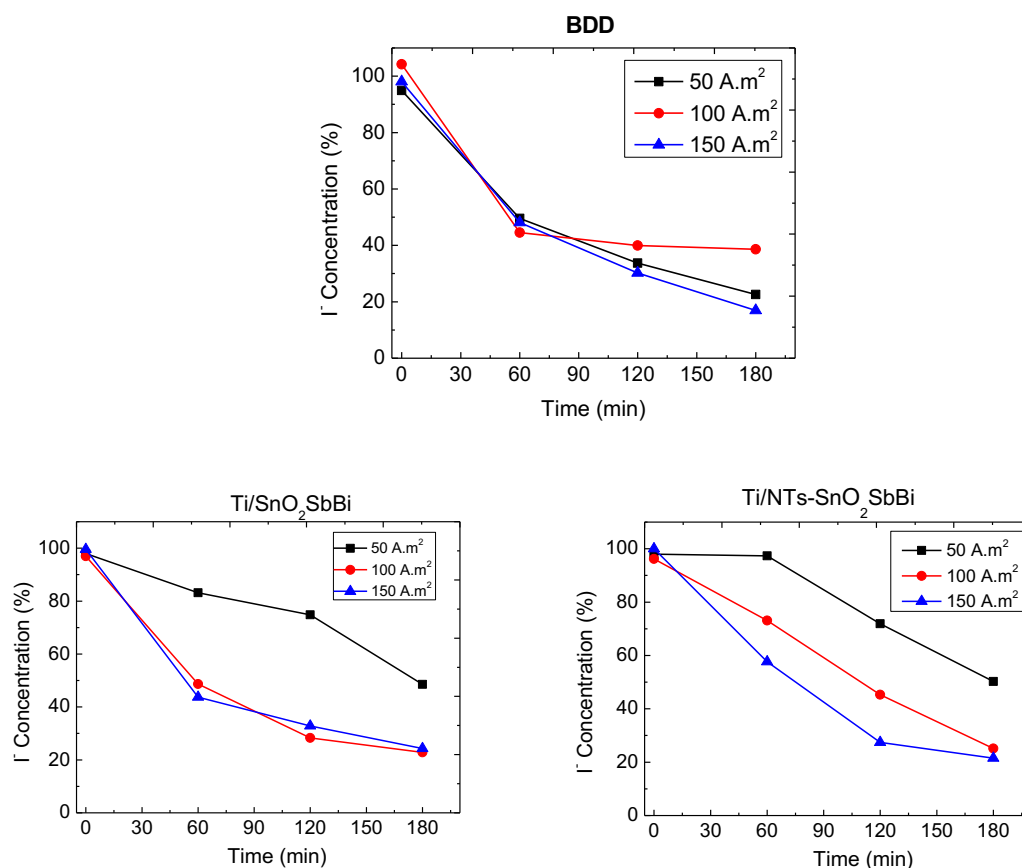
Figure 7: Iodide removal after electrolysis in flow-through cell under current densities of 50, 100 and 150 A m^{-2}, using either BDD, Ti/SnO$_2$SbBi or Ti/Nts-SnO$_2$SbBi as anode, stainless steel as counter electrode and Ag/AgCl as reference electrode. The initial concentration of contaminants was 20 μM of diatrizoate, iopromide and iohexol each, dissolved in 15mM of NaClO$_4$ used as electrolyte.

Hydroxyl Generation

Considering that electro-oxidation can occur by means of direct or indirect oxidation, the present study focused on the later since the electrodes analyzed are all considered inactive electrodes supporting their electrocatalytic activity on their ability to promote hydroxyl radicals [8]. Therefore, the estimation of the capacity that an anode has to promote hydroxyl formation in given solution is extremely important. This estimation can be carried out using probe molecules that are resistant to direct oxidation reactions but highly active to degradation with $^\bullet$OH.

In order to rule out participation of direct electrochemical degradation on TA degradation, CV experiments were conducted with various concentrations of this compound.

As can be seen in Figure 8 for all the anodes tested, no increase in current was observed in the selected potential range when the CV was performed in presence of TA for any tested concentration. The absence of a current response for TA indicates this compound did not undergo direct electron transfer reactions on any electrode [36]. Therefore, TA degradation can be ascribed to reaction with •OH.
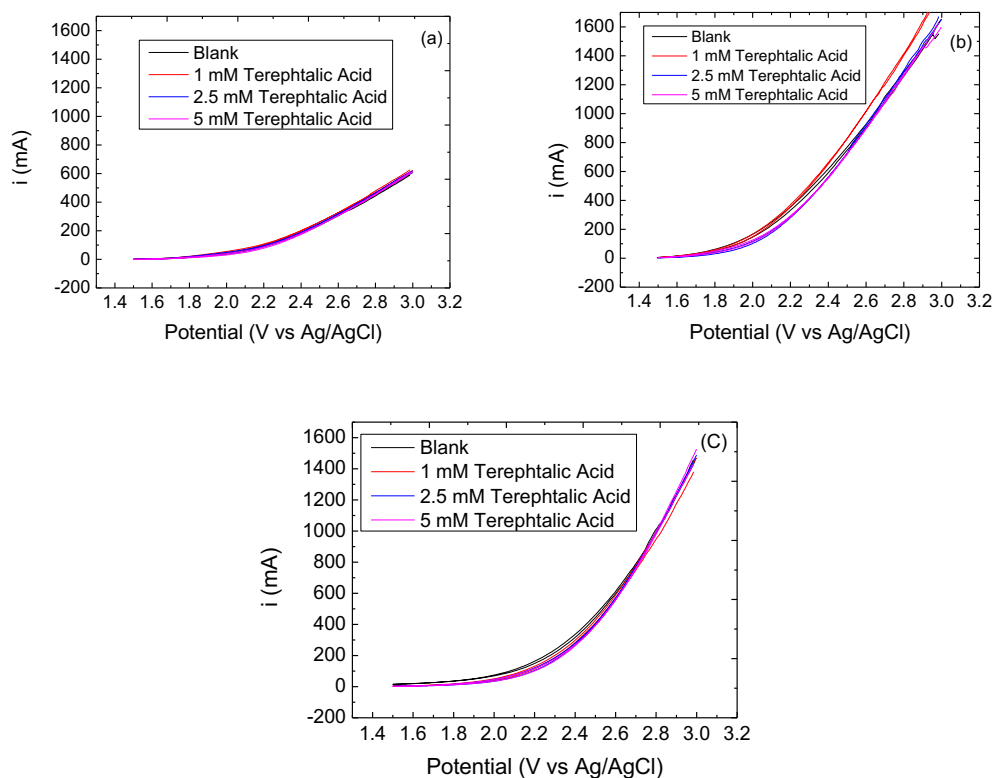
Figure 8: Cyclic voltammograms for (a) BDD, (b) Ti/SnO$_2$SbBi and (c) Ti/NTs-SnO$_2$SbBi anodes carried out from 1.5 to 3.0 V with scanning rate of 5 mV s^{-1} for electrodes varying Terephtalic Acid concentration in 1, 2.5 and 5 mM and using 0.1 M NaClO$_4$ as electrolyte. A filter-press flow-through electrochemical reactor equipped with Ag/AgCl as reference electrode and Stainless-steel mesh as counter electrode was used.

From the TA concentration values obtained by HPLC, the Pseudo-first-order rate constants were calculated from the TA concentration decay profiles during electrolysis obtaining values of [•OH]ss for the three electrodes.

Table 1 shows that Ti/SnO$_2$SbBi presented the highest activity for •OH production, which is in agreement with the main findings for both electrochemical oxidation for X-ray agents (Figure 7), and the degradation of terephtalic acid (Figure 8). In both cases it is possible

to distinguish a faster degradation of the organic compounds by the Ti/SnO$_2$SbBi when compared with the Ti/NTs-SnO$_2$SbBi.

Table 1. Pseudo-first-order rate constants (ks) and quasi steady-state concentration of •OH ([•OH]ss) of different electrodes

Electrode	ks (s^{-1})	[•OH]ss (M)
BDD	3.0×10^{-5}	7.5×10^{-15}
Ti/NTs-SnO$_2$SbBi	5.9×10^{-5}	1.5×10^{-14}
Ti/SnO$_2$SbBi	3.2×10^{-4}	8.0×10^{-14}

It can be seen that Ti/SnO$_2$SbBi showed the highest activity for •OH production, followed by BDD and Ti/NTs-SnO$_2$SbBi. Thus, the Ti/SnO$_2$SbBi material displayed higher capability for TA oxidation, in accordance to our electrochemical data. Furthermore, the reaction rate found for Ti/NTs-SnO$_2$SbBi also suggests that some secondary reaction is occurring leading to favoring in the degradation rates as they were almost 2-folds higher for Ti/NTs-SnO$_2$SbBi than for Ti/SnO$_2$SbBi and BDD. Although no surface reaction is present in all electrodes, as shown in Figure 8, coating the SnO$_2$SbBi onto a previously prepared nanotube structure surface showed significant variations in layer distribution as noted by nominal composition obtained in EDS. When in presence of nanotubes structure, the nominal concentration of Bi was significantly higher, which could explain the differences noted.

Bi doping is considerably interesting in electrochemical oxidation since its presence in nanotubes structures has been previously reported to increase conductivity and improve physical stability of the material [53]. Furthermore, since the presence of perchlorate induces OH radical-mediate surface reactions on the substrate [32], it is possible to presume that to some degree an increase in electrocatalytic activity was seen when a higher ratio of Bi was present in the surface favoring certain degradation routes for TA.

6.4 Conclusion

The present research aimed to develop a new mixed metal oxide material prepared by thermal decomposition applying an ionic liquid during the preparation of the precursor solutions. Experimental data showed that a highly stable and electrocatalytic material was

obtained. The coating of Ti meshes with SnO_2SbBi produced a highly conductive material with electrochemical outcomes similar to commercial BDD. The onset of OER for the Ti/NTs-SnO_2SbBi was more positive than the one presented by the BDD mesh, which presents a commercial advantage of increased operation potential for organic compound degradation. Moreover, both MMO anodes synthetized are very conductive materials.

Physical characterization showed that the material presented a higher concentration of Sn than estimated overall. Also, the addition of the nanotube structure to the material improved the coating uniformity, which was noted by the smaller presence of TiO_2 on the Ti/NTs-SnO_2SbBi anode and also increased the surface distribution of Bi, which proved to have electrocatalytic activity.

Finally, all electrodes presented high electrocatalytic activity, removing the concentration of X-ray agents in at least 50% for all cases. However, a trend was clearly seen in both analysis where the BDD overcame all the estimated degradations presenting similar outcome no matter what current density was applied. On the other hand, for both Ti/SnO_2SbBi and Ti/NTs-SnO_2SbBi anodes, degradation results showed a similar decrease when 100 or 150 A m^{-2} were applied, but a considerable decrease in degradation when only 50 A m^{-2} was applied. These results suggest that at some point below 100 A m^{-2} the system efficiency is controlled by mass-transfer, being necessary a higher current applied to overcome the natural resistance seen in these scenarios.

Acknowledgements

References

1. Lütke Eversloh C, Henning N, Schulz M, Ternes TA (2014) Electrochemical treatment of iopromide under conditions of reverse osmosis concentrates - Elucidation of the degradation pathway. Water Res 48:237–246. https://doi.org/10.1016/j.watres.2013.09.035

2. Del Moro G, Pastore C, Di Iaconi C, Mascolo G (2015) Iodinated contrast media electro-

degradation: Process performance and degradation pathways. Sci Total Environ 506–507:631–643. https://doi.org/10.1016/j.scitotenv.2014.10.115

3. Sacher F, Raue B, Brauch HJ (2005) Analysis of iodinated X-ray contrast agents in water samples by ion chromatography and inductively-coupled plasma mass spectrometry. J Chromatogr A 1085:117–123. https://doi.org/10.1016/j.chroma.2005.01.031

4. Wu D, Lu G, Zhang R, et al (2017) Effective degradation of diatrizoate by electro-peroxone process using ferrite/carbon nanotubes based gas diffusion cathode. Electrochim Acta 236:297–306. https://doi.org/10.1016/j.electacta.2017.03.196

5. Farhat A, Keller J, Tait S, Radjenovic J (2015) Removal of Persistent Organic Contaminants by Electrochemically Activated Sulfate. Environ Sci Technol 49:14326–14333. https://doi.org/10.1021/acs.est.5b02705

6. Vilar DS, Carvalho GO, Pupo MMS, et al (2018) Vinasse degradation using Pleurotus sajor-caju in a combined biological – Electrochemical oxidation treatment. Sep Purif Technol 192:287–296. https://doi.org/10.1016/j.seppur.2017.10.017

7. Garcia-Segura S, Ocon JD, Chong MN (2017) Electrochemical Oxidation Remediation of Real Wastewater Effluents − A review. Process Saf Environ Prot 113:48–67. https://doi.org/10.1016/j.psep.2017.09.014

8. Sopaj F, Rodrigo MA, Oturan N, et al (2015) Influence of the anode materials on the electrochemical oxidation efficiency. Application to oxidative degradation of the pharmaceutical amoxicillin. Chem Eng J 262:286–294. https://doi.org/10.1016/j.cej.2014.09.100

9. Bu L, Zhu S, Zhou S (2018) Degradation of atrazine by electrochemically activated persulfate using BDD anode: Role of radicals and influencing factors. Chemosphere 195:236–244. https://doi.org/10.1016/j.chemosphere.2017.12.088

10. Coledam DAC, Pupo MMDS, Silva BF, et al (2016) Electrochemical mineralization of cephalexin using a conductive diamond anode: A mechanistic and toxicity investigation. Chemosphere in press: https://doi.org/10.1016/j.jrp.2008.02.007

11. García-Espinoza JD, Mijaylova-Nacheva P, Avilés-Flores M (2018) Electrochemical carbamazepine degradation: Effect of the generated active chlorine, transformation pathways and toxicity. Chemosphere 192:142–151. https://doi.org/10.1016/j.chemosphere.2017.10.147

12. Aquino JM, Rodrigo M a., Rocha-Filho RC, et al (2012) Influence of the supporting electrolyte on the electrolyses of dyes with conductive-diamond anodes. Chem Eng J 184:221–227. https://doi.org/10.1016/j.cej.2012.01.044

13. Kim C, Kim S, Choi J, et al (2014) Blue TiO2nanotube array as an oxidant generating novel anode material fabricated by simple cathodic polarization. Electrochim Acta 141:113–119. https://doi.org/10.1016/j.electacta.2014.07.062

14. Ganiyu SO, Oturan N, Raffy SS, et al (2016) Sub-stoichiometric titanium oxide (Ti4O7) as a suitable ceramic anode for electrooxidation of organic pollutants: A case study of kinetics, mineralization and toxicity assessment of amoxicillin. Water Res 106:171–182. https://doi.org/10.1016/j.watres.2016.09.056

15. Lim D, Kim Y, Nam D, et al (2018) Influence of the Sb content in Ti/SnO2-Sb electrodes on the electrocatalytic behaviour for the degradation of organic matter. J Clean Prod. https://doi.org/10.1016/j.jclepro.2018.06.301

16. Li L, Huang Z, Fan X, et al (2017) Preparation and Characterization of a Pd modified Ti/SnO2-Sb anode and its electrochemical degradation of Ni-EDTA. Electrochim Acta 231:354–362. https://doi.org/10.1016/j.electacta.2017.02.072

17. Choi J, Qu Y, Hoffmann MR (2012) SnO2, IrO2, Ta2O5, Bi2O3 and TiO2 nanoparticles anodes: electrochemical oxidation coupled with the cathodic reduction of water to yield molecular H 2. J Nanoparticles Res 14:983–995. https://doi.org/10.1007/s11051-012-0983-5

18. Berenguer R, Sieben JM, Quijada C, Morallón E (2016) Electrocatalytic degradation of phenol on Pt- and Ru-doped Ti/SnO2-Sb anodes in an alkaline medium. Appl Catal B Environ 199:394–404. https://doi.org/10.1016/j.apcatb.2016.06.038

19. Ding H-Y, Feng Y-J, Lu J-W (2010) Study on the service life and deactivation mechanism of Ti/SnO2-Sb electrode by physical and electrochemical methods. Russ J Electrochem 46:72–76. https://doi.org/10.1134/S1023193510010088

20. Zhang L, Xu L, He J, Zhang J (2014) Preparation of Ti/SnO2-Sb electrodes modified by carbon nanotube for anodic oxidation of dye wastewater and combination with nanofiltration. Electrochim Acta 117:192–201. https://doi.org/10.1016/j.electacta.2013.11.117

21. Ding HY, Feng YJ, Liu JF (2007) Preparation and properties of Ti/SnO2-Sb2O5

electrodes by electrodeposition. Mater Lett 61:4920–4923. https://doi.org/10.1016/j.matlet.2007.03.073

22. Chen Y, Hong L, Xue H, et al (2010) Preparation and characterization of TiO_2-NTs/SnO_2-Sb electrodes by electrodeposition. J Electroanal Chem 648:119–127. https://doi.org/10.1016/j.jelechem.2010.08.004

23. da Silva LM, de Oliveira Santiago Santos G, de Salles Pupo MM, et al (2018) Influence of heating rate on the physical and electrochemical properties of mixed metal oxides anodes synthesized by thermal decomposition method applying an ionic liquid. J Electroanal Chem 813:127–133. https://doi.org/10.1016/j.jelechem.2018.02.026

24. Wu W, Huang ZH, Hu ZT, et al (2017) High performance duplex-structured SnO_2-Sb-CNT composite anode for bisphenol A removal. Sep Purif Technol 179:25–35. https://doi.org/10.1016/j.seppur.2017.01.032

25. Li X, Shao D, Xu H, et al (2016) Fabrication of a stable Ti/TiOxHy/Sb−SnO_2 anode for aniline degradation in different electrolytes. Chem Eng J 285:1–10. https://doi.org/10.1016/j.cej.2015.09.089

26. Shao C, Yu J, Li X, et al (2017) Influence of the Pt nanoscale interlayer on stability and electrical property of Ti/Pt/Sb-SnO_2 electrode: A synergetic experimental and computational study. J Electroanal Chem 804:140–147. https://doi.org/10.1016/j.jelechem.2017.09.057

27. Liu Y, Liu H, Ma J, Li J (2012) Preparation and electrochemical properties of Ce–Ru–SnO2 ternary oxide anode and electrochemical oxidation of nitrophenols. J Hazard Mater 213–214:222–229. https://doi.org/10.1016/j.jhazmat.2012.01.090

28. de Mello R, Santos LHE, Pupo MMS, et al (2017) Alachlor removal performance of Ti/Ru0.3Ti0.7O2 anodes prepared from ionic liquid solution. J Solid State Electrochem. https://doi.org/10.1007/s10008-017-3700-6

29. Carlesi Jara C, Salazar-Banda GR, Arratia RS, et al (2011) Improving the stability of Sb doped Sn oxides electrode thermally synthesized by using an acid ionic liquid as solvent. Chem Eng J 171:1253–1262. https://doi.org/10.1016/j.cej.2011.05.039

30. Salazar-Banda GR, Eguiluz KIB, Pupo MMS, et al (2012) The influence of different co-catalysts in Pt-based ternary and quaternary electro-catalysts on the electro-oxidation of methanol and ethanol in acid media. J Electroanal Chem 668:13–25.

https://doi.org/10.1016/j.jelechem.2012.01.006

31. Aguilar ZG, Coreño O, Salazar M, et al (2018) Ti|Ir–Sn–Sb oxide anode: Service life and role of the acid sites content during water oxidation to hydroxyl radicals. J Electroanal Chem 820:82–88. https://doi.org/10.1016/j.jelechem.2018.04.053

32. Ahn YY, Yang SY, Choi C, et al (2016) Electrocatalytic activities of Sb-SnO$_2$ and Bi-TiO$_2$ anodes for water treatment: Effects of electrocatalyst composition and electrolyte. Catal Today 1–8. https://doi.org/10.1016/j.cattod.2016.03.011

33. Zhuo Q, Deng S, Yang B, et al (2011) Efficient electrochemical oxidation of perfluorooctanoate using a Ti/SnO2-Sb-Bi anode. Environ Sci Technol 45:2973–2979. https://doi.org/10.1021/es1024542

34. Subba Rao AN, Venkatarangaiah VT (2018) Preparation, characterization, and application of Ti/TiO$_2$-NTs/Sb-SnO$_2$ electrode in photo-electrochemical treatment of industrial effluents under mild conditions. Environ Sci Pollut Res. https://doi.org/10.1007/s11356-017-1179-4

35. Jing Y, Chaplin BP (2017) Mechanistic Study of the Validity of Using Hydroxyl Radical Probes to Characterize Electrochemical Advanced Oxidation Processes. Environ Sci Technol 51:2355–2365. https://doi.org/10.1021/acs.est.6b05513

36. Charbouillot T, Brigante M, Mailhot G, et al (2011) Journal of Photochemistry and Photobiology A : Chemistry Performance and selectivity of the terephthalic acid probe for • OH as a function of temperature , pH and composition of atmospherically relevant aqueous media. "Journal Photochem Photobiol A Chem 222:70–76. https://doi.org/10.1016/j.jphotochem.2011.05.003

37. Yang Y, Hoffmann MR (2016) Synthesis and Stabilization of Blue-Black TiO$_2$ Nanotube Arrays for Electrochemical Oxidant Generation and Wastewater Treatment. Environ Sci Technol 50:11888–11894. https://doi.org/10.1021/acs.est.6b03540

38. Cui X, Zhao G, Lei Y, et al (2009) Novel vertically aligned TiO$_2$ nanotubes embedded with Sb-doped SnO2 electrode with high oxygen evolution potential and long service time. Mater Chem Phys 113:314–321. https://doi.org/10.1016/j.matchemphys.2008.07.087

39. Wang Q, Jin T, Hu Z, et al (2013) TiO$_2$-NTs/SnO$_2$-Sb anode for efficient electrocatalytic degradation of organic pollutants: Effect of TiO$_2$-NTs architecture AADRT. Sep Purif

Technol 102:180–186. https://doi.org/10.1016/j.seppur.2012.10.006

40. Xu L, Li M, Xu W (2015) Preparation and characterization of Ti/SnO2-Sb electrode with copper nanorods for AR 73 removal. Electrochim Acta 166:64–72. https://doi.org/10.1016/j.electacta.2015.02.233

41. Abbasi M, Backtrom J, Cornell A (2018) Fabrication of Spin-Coated Ti/TiHx/Ni-Sb-SnO$_2$ Electrode : Stability and Electrocatalytic Activity. J Electrochem Soc 165:568–574. https://doi.org/10.1149/2.1171809jes

42. Shao D, Yan W, Li X, et al (2014) A Highly Stable Ti / TiH x / Sb − SnO$_2$ Anode : Preparation , Characterization and Application. Ind Eng Chem Res 53:3898–3907

43. Santos TÉS, Silva RS, Eguiluz KIB, Salazar-Banda GR (2015) Development of Ti/(RuO2)0.8(MO2)0.2 (M=Ce, Sn or Ir) anodes for atrazine electro-oxidation. Influence of the synthesis method. Mater Lett 146:4–8. https://doi.org/10.1016/j.matlet.2015.01.145

44. Mirella Da Silva L, De Oliveira G, Santos S, et al (2018) Influence of heating rate on the physical and electrochemical properties of mixed metal oxides anodes synthesized by thermal decomposition method applying an ionic liquid. J Electroanal Chem 813:127–133. https://doi.org/10.1016/j.jelechem.2018.02.026

45. Faria ER, Ribeiro FM, Franco D V., da Silva LM (2017) Fabrication and characterisation of a mixed oxide-covered mesh electrode composed of NiCo$_2$O$_4$ and its capability of generating hydroxyl radicals during the oxygen evolution reaction in electrolyte-free water. J Solid State Electrochem 1–14. https://doi.org/10.1007/s10008-017-3815-9

46. Montilla F, Morallón E, De Battisti A, Vázquez JL (2004) Preparation and Characterization of Antimony-Doped Tin Dioxide Electrodes. Part 1. Electrochemical Characterization. J Phys Chem B 108:5036–5043. https://doi.org/10.1021/jp037480b

47. Martínez-Huitle CA, Rodrigo MA, Scialdone O (2018) Electrochemical water and wastewater treatment

48. Guzman-Duque FL, Palma-Goyes RE, Gonzalez I, Torres-Palma RA (2014) Relationship between anode material, supporting electrolyte and current density during electrochemical degradation of organic compounds in water. J Hazard Mater 278:221–226. https://doi.org/10.1016/j.jhazmat.2014.05.076

49. Martínez-Huitle CA, Dos Santos EV, De Araújo DM, Panizza M (2012) Applicability

of diamond electrode/anode to the electrochemical treatment of a real textile effluent. J Electroanal Chem 674:103–107. https://doi.org/10.1016/j.jelechem.2012.02.005

50. Coledam DAC, Pupo MMS, Silva BF, et al (2017) Electrochemical mineralization of cephalexin using a conductive diamond anode: A mechanistic and toxicity investigation. Chemosphere 168:638–647. https://doi.org/10.1016/j.chemosphere.2016.11.013

51. Chan TW, Graham NJD, Chu W (2010) Degradation of iopromide by combined UV irradiation and peroxydisulfate. J Hazard Mater 181:508–513. https://doi.org/10.1016/j.jhazmat.2010.05.043

52. Martínez-Huitle CA, Rodrigo MA, Sirés I, Scialdone O (2015) Single and Coupled Electrochemical Processes and Reactors for the Abatement of Organic Water Pollutants: A Critical Review. Chem. Rev. 115

53. Dong W, Xie X, Jia J, et al (2014) Theoretical calculation and experimental study on the conductivity and stability of Bi-doped SnO2 electrode. Electrochim Acta 132:307–314. https://doi.org/10.1016/j.electacta.2014.03.160

Supplementary Information

Synthesis of Ternary mixed metal oxides mesh electrodes for electrochemical treatment of X-ray contaminants in a flow through cell

Marilia Moura de Salles Pupo[1], José Miguel Albahaca[2], Katlin Ivon Barrios Eguiluz[1,3], Giancarlo Richard Salazar-Banda[1,3], Jelena Radjenovic[2,4*]

[1] *Process Engineering Post-Graduation Program, Universidade Tiradentes, Av. Murilo Dantas, s/n, Aracaju – SE, Brazil*

[2] *Catalan Institute of Water Research, Emili Grahit 101, Girona, Spain*

[3] *Instituto de Tecnologia e Pesquisa, Av. Murilo Dantas, s/n, Aracaju – SE, Brazil*

[4] *Catalan Institution for Research and Advanced Studies (ICREA), Passeig Lluís Companys 23, 08010 Barcelona, Spain*

*Corresponding author: Jelena Radjenovic (jradjenovic@icra.cat)

Fig. S1: Cyclic voltammograms of Ti/NTs-SnO$_2$ obtained by applying 20, 40 or 60 V during anodization step according to methodology proposed. Scan rate of 20 mV s^{-1}, in 0.03 M Na$_2$SO$_4$ using stainless steel mesh as counter electrode and Ag/AgCl as reference electrode.
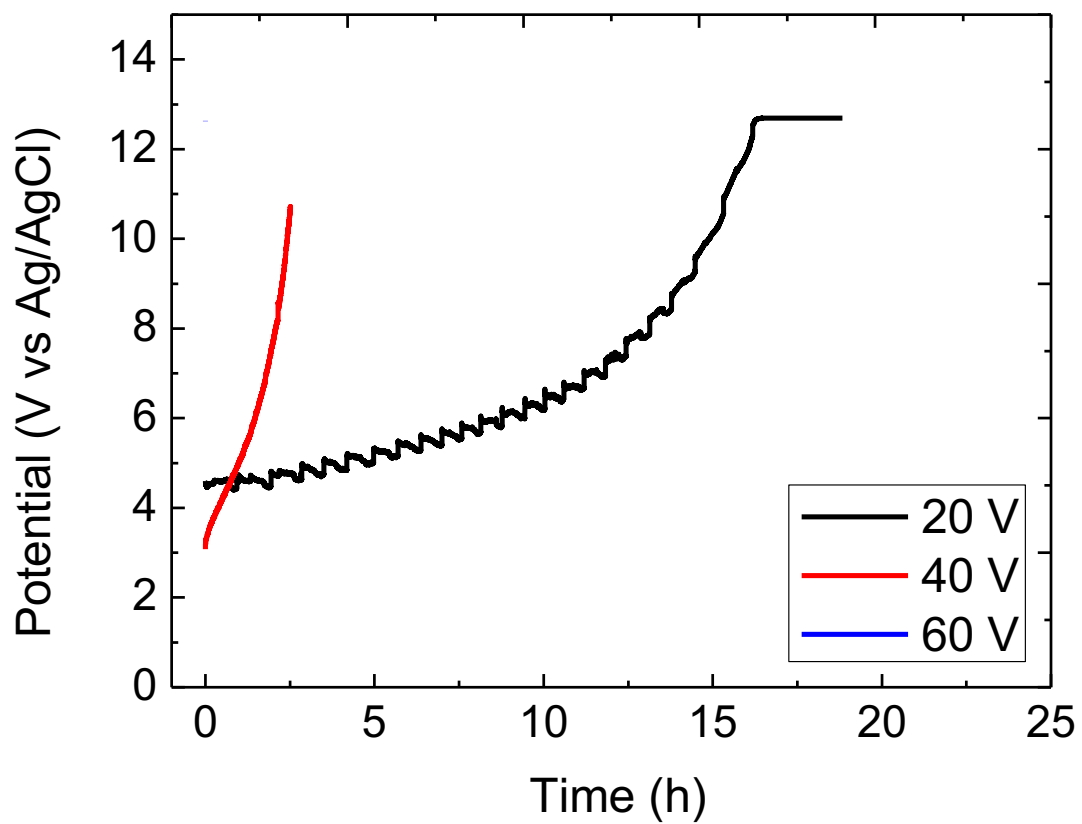
Fig S2: Accelerated service lifetime of Ti/NTs-SnO$_2$ obtained by applying 20, 40 or 60 V during anodization step according to methodology proposed in 0.03 M Na$_2$SO$_4$ using stainless steel mesh as counter electrode and Ag/AgCl as reference electrode.

7. CONCLUSÕES

O presente trabalho teve como como objetivo geral o desenvolvimento de ânodos de mistura de óxidos metálicos com alta atividade eletrocatalítica e propriedades físicas e eletroquímicas melhoradas para degradação de compostos orgânicos variados.

Por meio de estudos de degradação eletroquímica em reator do tipo filtro prensa equipado com DDB oi possível determinar que para a degradação da Cefalexina, pH ácidos a neutros apresentam melhor taxa de remoção do composto alvo, densidade de correntes muito elevadas não são favoráveis ao sistema e o eletrólito de sulfato de sódio favorece a degradação de compostos orgânicos nestes sistemas. Com isso, foi possível remover completamente a Cefalexina da solução inicial dentro de tempos de reação de até 180 minutos, identificando ainda sua rota de degradação por meio de levantamento em HPLC e análise da toxicidade do efluente para *E. coli*.

Para o desenvolvimento de ânodos de mistura de óxidos metálicos de $Ti/Sn_{93}O_2Sb_5M_2$(M=Ce, Gd, Ta e Bi) rotas de decomposição térmica utilizando metil imidazolium no preparo da solução precursora levaram a materiais com alta capacidade eletrocatalítica, removendo até 32% da molécula alvo de Diuron dentro de um tempo de reação de 1 hora em uma célula eletroquímica com volume de 100 mL, aplicando-se densidade de corrente de 10 mA cm^2 em meio de Na_2SO_4 0.33M. Para este estudo, temperaturas de calcinação de 550 °C e composição de $Ti/Sn_{93}O_2Sb_5Bi_2$ apresentou melhores taxas de remoção além de um significante aumento no tempo de vida do eletrodo quando comparado aos demais indicando efeito sinérgico entre os óxidos metálicos utilizados.

Finalmente, para melhora no tempo de vida do eletrodo de $Ti/Sn_{93}O_2Sb_5Bi_2$, intercamadas de nanotubos de TiO_2 foram geradas no substrato de titânio formando eletrodos de $Ti/NTs-Sn_{93}O_2Sb_5Bi_2$. Esta modificação levou a um aumento do tempo de vida de cerca de 31 para 85 horas ao passo que manteve uma atividade eletrocatalítica considerável com desempenho comparável ao eletrodo comercial de DDB quando tratando soluções de agentes de contraste de raios x (iopromide, iohexol e diatrizoate). Todos os eletrodos foram capazes de levar a completa remoção dos contaminantes dentro de um período de reação de 180 minutos

em solução de Na_2SO_4 aplicando 50, 100 e 150 A m² em reatores do tipo filtro-prensa de fluxo perpendicular 3D comportando volumes de solução de até 1 L.

Assim, o presente trabalho foi capaz de analisar os principais fatores de influência na eficiência de remoção de compostos orgânicos variados por meio de degradação eletroquímica em células eletroquímicas e reatores de bancada. Com este estudo, foi possível entender os mecanismos de interação física e eletroquímica que levam ao melhoramento das propriedades eletrocatalíticas de eletrodos de misturas de óxidos metálicas, tais como temperatura de calcinação, compostos utilizados para dopagem e inserção de intercamadas de nanotubos. Finalmente, por meio de estudos em reatores do tipo filtro prensa de fluxo perpendicular 3D foi possível obter um material com alta capacidade eletrocatalítica e atividade eletroquímica comparável ao eletrodo comercial de DDB.

REFERENCIAS BIBLIOGRAFICAS

Adams, B., Tian, M., & Chen, A. (2009). Design and electrochemical study of SnO_2-based mixed oxide electrodes. *Electrochimica Acta*, *54*(5), 1491–1498. http://doi.org/10.1016/j.electacta.2008.09.034

Ahn, Y. Y., Yang, S. Y., Choi, C., Choi, W., Kim, S., & Park, H. (2016). Electrocatalytic activities of Sb-SnO_2 and Bi-TiO_2 anodes for water treatment: Effects of electrocatalyst composition and electrolyte. *Catalysis Today*, 1–8. http://doi.org/10.1016/j.cattod.2016.03.011

Anglada, Á.´, Urtiaga, A., & Ortiz, I. (2009). Contributions of electrochemical oxidation to waste-water treatment: Fundamentals and review of applications. *Journal of Chemical Technology and Biotechnology*, *84*(12), 1747–1755. http://doi.org/10.1002/jctb.2214

Anirudhan, T. S., Deepa, J. R., & Nair, A. S. (2016). Fabrication of chemically modified graphene oxide/nano hydroxyapatite composite for adsorption and subsequent photocatalytic degradation of aureomycine hydrochloride. *Journal of Industrial and Engineering Chemistry*. http://doi.org/10.1016/j.jiec.2016.12.014

Aquino, J. M., Rocha-Filho, R. C., Bocchi, N., & Biaggio, S. R. (2014). Microwave-assisted crystallization into anatase of amorphous TiO_2 nanotubes electrochemically grown on a Ti substrate. *Materials Letters*, *126*, 52–54. http://doi.org/10.1016/j.matlet.2014.04.005

Ardizzone, S., Bianchi, C. L., Cappelletti, G., Ionita, M., Minguzzi, a., Rondinini, S., & Vertova, (2006). Composite ternary SnO_2-IrO_2-Ta_2O_5 oxide electrocatalysts. *Journal of Electroanalytical Chemistry*, *589*(1), 160–166. http://doi.org/10.1016/j.jelechem.2006.02.004

Aymerich, I., Acuna, V., Barcelo, D., Garcia, M. J., Petrovic, M., Poch, M., Corominas, L. (2016). Attenuation of pharmaceuticals and their transformation products in a wastewater treatment plant and its receiving river ecosystem. *Water Research*, *100*, 126–136. http://doi.org/10.1016/j.watres.2016.04.022

Berenguer, R., Sieben, J. M., Quijada, C., & Morallón, E. (2014). Pt- and Ru-Doped SnO_2−Sb Anodes with High Stability in Alkaline Medium Rau l. *Applied Materials & Interfaces*, *6*, 22778–22789.

Bogdanowicz, R., Fabiaska, A., Golunski, L., Sobaszek, M., Gnyba, M., Ryl, J., Siedlecka, E. M. (2013). Influence of the boron doping level on the electrochemical oxidation of the azo dyes at

Si/BDD thin film electrodes. *Diamond and Related Materials*, *39*. http://doi.org/10.1016/j.diamond.2013.08.004

Bouras, O., Bollinger, J. C., Baudu, M., & Khalaf, H. (2007). Adsorption of diuron and its degradation products from aqueous solution by surfactant-modified pillared clays. *Applied Clay Science*, *37*(3–4), 240–250. http://doi.org/10.1016/j.clay.2007.01.009

Brillas, E., & Martínez-Huitle, C. A. (2015). Decontamination of wastewaters containing synthetic organic dyes by electrochemical methods. An updated review. *Applied Catalysis B: Environmental*. http://doi.org/10.1016/j.apcatb.2014.11.016

Brillas, E., Thiam, A., & Garcia-Segura, S. (2016). Incineration of acidic aqueous solutions of dopamine by electrochemical advanced oxidation processes with Pt and BDD anodes. *Journal of Electroanalytical Chemistry*, *775*, 189–197. http://doi.org/10.1016/j.jelechem.2016.04.054

Brungs, Haddadi-Asl, V., & Skyllas-Kazacos, M. (1996). Preparation and evaluation of electrocatalytic oxide coatings on conductive carbon-polymer composite substrates for use as dimensionally stable anodes. *Journal of Applied Electrochemistry*, *26*(11), 1117–1123. http://doi.org/10.1007/BF00243736

Carlesi, C., Salazar-Banda, G. R., Schrebler, R., Silva, J., Irrazábal, M., Carlesi Jara, C., Aguilera, M. I. (2011). Improving the stability of Sb doped Sn oxides electrode thermally synthesized by using an acid ionic liquid as solvent. *Chemical Engineering Journal*, *171*(3), 1253–1262. http://doi.org/10.1016/j.cej.2011.05.039

Cesarino, I., Moraes, F. C., Ferreira, T. C. R., Lanza, M. R. V, & Machado, S. S. (2012). Real-time electrochemical determination of phenolic compounds after benzene oxidation. *Journal of Electroanalytical Chemistry*, *672*, 34–39. http://doi.org/10.1016/j.jelechem.2012.03.006

Chaiyont, R., Badoe, C., Ponce de León, C., Nava, J. L., Recio, F. J., Sirés, I.,Walsh, F. C. (2013). Decolorization of Methyl Orange Dye at IrO_2-SnO_2-Sb_2O_5 Coated Titanium Anodes. *Chemical Engineering & Technology*, *36*(1), 123–129. http://doi.org/10.1002/ceat.201200231

Chen, S., Chen, P., Wu, M., Pan, D., & Wang, Y. (2010). Graphene supported Sn-Sb@carbon core-shell particles as a superior anode for lithium ion batteries. *Electrochemistry Communications*, *12*(10), 1302–1306. http://doi.org/10.1016/j.elecom.2010.07.005

Chen, X., Gao, F., & Chen, G. (2005). Comparison of Ti/BDD and Ti/SnO_2–Sb_2O_5 electrodes for pollutant oxidation. *Journal of Applied Electrochemistry*, *35*, 185–191. http://doi.org/10.1007/s10800-004-6068-0

Chen, X., Ru, Q., Wang, Z., Hou, X., & Hu, S. (2016). Ternary Sn-Sb-Co alloy particles embedded in reduced graphene oxide as lithium ion battery anodes. *Materials Letters*, 10–13. http://doi.org/10.1016/j.matlet.2016.12.058

Chen, Y., Hong, L., Xue, H., Han, W., Wang, L., Sun, X., & Li, J. (2010). Preparation and characterization of TiO_2-NTs/SnO_2-Sb electrodes by electrodeposition. *Journal of Electroanalytical Chemistry*, *648*(2), 119–127. http://doi.org/10.1016/j.jelechem.2010.08.004

Cheng, M., Zeng, G., Huang, D., Lai, C., Xu, P., Zhang, C., & Liu, Y. (2016). Hydroxyl radicals based advanced oxidation processes (AOPs) for remediation of soils contaminated with organic compounds: A review. *Chemical Engineering Journal*. http://doi.org/10.1016/j.cej.2015.09.001

Correa-Lozano, B., Comninellis, C., & Battisti, A. D. E. (1997). Service life of Ti/SnO_2±Sb_2O_5 anodes. *Journal of Applied Electrochemistry*, *27*(October 1996), 970–974

Cui, Y. H., Feng, Y. J., & Liu, Z. Q. (2009). Influence of rare earths doping on the structure and electro-catalytic performance of Ti/Sb–SnO_2 electrodes. *Electrochimica Acta*, *54*(21), 4903–4909. http://doi.org/10.1016/j.electacta.2009.04.041

Silva, A. J. C., dos Santos, E. V., de Oliveira Morais, C. C., Martínez-Huitle, C. A., & Castro, S. S. L. (2013). Electrochemical treatment of fresh, brine and saline produced water generated by petrochemical industry using Ti/IrO_2-Ta_2O_5 and BDD in flow reactor. *Chemical Engineering Journal*, *233*, 47–55. http://doi.org/10.1016/j.cej.2013.08.023

Dbira, S., Bensalah, N., & Bedoui, A. (2016). Mechanism and kinetics of electrochemical degradation of uric acid using conductive-diamond anodes. *Environmental Technology*, *37*(23), 2993–3001. http://doi.org/10.1080/09593330.2016.1173115

Del Río, a. I., Fernández, J., Molina, J., Bonastre, J., & Cases, F. (2010). On the behaviour of doped SnO2 anodes stabilized with platinum in the electrochemical degradation of reactive dyes. *Electrochimica Acta*, *55*(24), 7282–7289. http://doi.org/10.1016/j.electacta.2010.07.008

Domínguez, J. R., González, T., Palo, P., & Sánchez-Martín, J. (2010). Electrochemical advanced oxidation of carbamazepine on boron-doped diamond anodes. Influence of operating variables. *Industrial and Engineering Chemistry Research*, *49*(18), 8353–8359. http://doi.org/10.1021/ie101023u

Dong, H., Su, H., Chen, Z., Yu, H., & Yu, H. (2016). Fabrication of Electrochemically Reduced Graphene Oxide Modified Gas Diffusion Electrode for In-situ Electrochemical Advanced

Oxidation Process under Mild Conditions. *Electrochimica Acta*. http://doi.org/10.1016/j.electacta.2016.11.131

Dong, W., Xie, X., Jia, J., Du, H., Zhong, L., Liang, Z., & Han, P. (2014). Theoretical calculation and experimental study on the conductivity and stability of Bi-doped SnO_2 electrode. *Electrochimica Acta*, *132*, 307–314. http://doi.org/10.1016/j.electacta.2014.03.160

Dorion, E., Severo, E., Olea, P., Nodari, C., & De Guimaraes, J. F. (2012). Hospital Environmental and Residues Management: Brazilian Experiences. *Journal of Environmental Assessment Policy and Management*, *14*(3), 1–18. http://doi.org/10.1142/S1464333212500184

Duan, T., Wen, Q., Chen, Y., Zhou, Y., & Duan, Y. (2014). Enhancing electrocatalytic performance of Sb-doped SnO_2 electrode by compositing nitrogen-doped graphene nanosheets. *Journal of Hazardous Materials*, *280* (SEPTEMBER), 304–314. http://doi.org/10.1016/j.jhazmat.2014.08.018

Dussault, E. B., Balakrishna, V. B., Servko, E., Solomon, K. R., & Sibley, P. K. (2008). Toxicity of Human Pharmaceuticals and Personal Care Products To Benthic Invertebrates. *Environmental Toxicology and Chemistry*, *27*(2), 425–432. http://doi.org/10.1897/07-354R.1

Eguiluz, K. I. B., Malpass, G. R. P., Pupo, M. M. S., Salazar-Banda, G. R., & Avaca, L. a. (2010). Synthesis, characterization, and electrocatalytic activity toward methanol oxidation of carbon-supported Ptx-$(RuO_2$-M)$_{1-x}$ composite ternary catalysts (M = CeO_2, MoO_3, or PbOx). *Energy and Fuels*, *24*(7), 4012–4024. http://doi.org/10.1021/ef100424m

Emmanuel, A., Zuxin, M., Joshua, W., & Lefebvre, O. (2016). Physico-chemical properties of pristine graphene and its performance as electrode material for electro-Fenton treatment of wastewater. *Electrochimica Acta*. http://doi.org/10.1016/j.electacta.2016.08.002

Ensano, B. M. B., Borea, L., Naddeo, V., Belgiorno, V., de Luna, M. D. G., & Ballesteros, F. C. (2017). Removal of pharmaceuticals from wastewater by intermittent electrocoagulation. *Water (Switzerland)*, *9*(2), 1–15. http://doi.org/10.3390/w9020085

Estrada, A. L., Li, Y.-Y., & Wang, A. (2012). Biodegradability enhancement of wastewater containing cefalexin by means of the electro-Fenton oxidation process. *Journal of Hazardous Materials*, *227–228*, 41–48. http://doi.org/10.1016/j.jhazmat.2012.04.079

Evdokimov, S. V. (2000). Corrosion Behavior of Dimensionally Stable Anodes in Chlorine Electrolyses. *Russian Journal of Electrochemistry*, *36*(3), 259–264.

Fan, J., Zhao, G., Zhao, H., Chai, S., & Cao, T. (2013). Fabrication and application of mesoporous Sb-doped SnO_2 electrode with high specific surface in electrochemical degradation of ketoprofen. *Electrochimica Acta*, *94*, 21–29. http://doi.org/10.1016/j.electacta.2013.01.129

Fathollahi, F., Javanbakht, M., Norouzi, P., & Reza, M. (2011). Comparison of Morphology , Stability and Electrocatalytic. *Russian Journal of Electrochemistry*, *47*(11), 1281–1286. http://doi.org/10.1134/S1023193511110061

Feng, L., van Hullebusch, E. D., Rodrigo, M. A., Esposito, G., & Oturan, M. A. (2013). Removal of residual anti-inflammatory and analgesic pharmaceuticals from aqueous systems by electrochemical advanced oxidation processes. A review. *Chemical Engineering Journal*, *228*(May), 944–964. http://doi.org/10.1016/j.cej.2013.05.061

Feng, Y., Cui, Y.-H., Liu, J., & Logan, B. E. (2010). Factors affecting the electro-catalytic characteristics of Eu doped SnO_2/Sb electrode. *Journal of Hazardous Materials*, *178*(1–3), 29–34. http://doi.org/10.1016/j.jhazmat.2009.12.101

Feng, Y., Cui, Y., Logan, B., & Liu, Z. (2008). Performance of Gd-doped Ti-based Sb-SnO_2 anodes for electrochemical destruction of phenol. *Chemosphere*, *70*(9), 1629–1636. http://doi.org/10.1016/j.chemosphere.2007.07.083

Feng, Y. J., & Li, X. Y. (2003). Electro-catalytic oxidation of phenol on several metal-oxide electrodes in aqueous solution. *Water Research*, *37*(10), 2399–2407. http://doi.org/10.1016/S0043-1354(03)00026-5

Ferrari, B., Paxéus, N., Giudice, R. Lo, Pollio, A., & Garric, J. (2003). Ecotoxicological impact of pharmaceuticals found in treated wastewaters: Study of carbamazepine, clofibric acid, and diclofenac. *Ecotoxicology and Environmental Safety*, *55*(3), 359–370. http://doi.org/10.1016/S0147-6513(02)00082-9

Ganzenko, O., Huguenot, D., Hullebusch, E. D. Van, Esposito, G., & Oturan, M. A. (2014). Electrochemical advanced oxidation and biological processes for wastewater treatment: a review of the combined approaches. *Environmental Science Pollution Research*, *21*, 8493–8524. http://doi.org/10.1007/s11356-014-2770-6

Giannakis, S., Gamarra Vives, F. A., Grandjean, D., Magnet, A., De Alencastro, L. F., & Pulgarin, C. (2015). Effect of advanced oxidation processes on the micropollutants and the effluent organic matter contained in municipal wastewater previously treated by three different secondary methods. *Water Research*, *84*. http://doi.org/10.1016/j.watres.2015.07.030

Gordon, C. M. (2001). New developments in catalysis using ionic liquids. *Applied Catalysis A: General*, *222*(1–2), 101–117. http://doi.org/10.1016/S0926-860X(01)00834-1

Goswami, S., Banerjee, P., Datta, S., Mukhopadhayay, A., & Das, P. (2017). Graphene oxide nanoplatelets synthesized with carbonized agro-waste biomass as green precursor and its application for the treatment of dye rich wastewater. *Process Safety and Environmental Protection*, *106*, 163–172. http://doi.org/10.1016/j.psep.2017.01.003

Groenen-Serrano, K., Weiss-Hortala, E., Savall, & Spiteri, P. (2013). Role of Hydroxyl Radicals During the Competitive Electrooxidation of Organic Compounds on a Boron-Doped Diamond Anode. *Electrocatalysis*, *4*(4), 346–352. http://doi.org/10.1007/s12678-013-0150-5

Gulkowska, A., Leung, H. W., So, M. K., Taniyasu, S., Yamashita, N., Yeung, L. W. Y., … Lam, P. K. S. (2008). Removal of antibiotics from wastewater by sewage treatment facilities in Hong Kong and Shenzhen, China. *Water Research*, *42*, 395–403. http://doi.org/10.1016/j.watres.2007.07.031

Guzman-Duque, F. L., Palma-Goyes, R. E., Gonzalez, I., & Torres-Palma, R. A. (2014). Relationship between anode material, supporting electrolyte and current density during electrochemical degradation of organic compounds in water. *Journal of Hazardous Materials*, *278*, 221–226. http://doi.org/10.1016/j.jhazmat.2014.05.076

Haidar, M., Dirany, A., Sirés, I., Oturan, N., & Oturan, M. A. (2013). Electrochemical degradation of the antibiotic sulfachloropyridazine by hydroxyl radicals generated at a BDD anode. *Chemosphere*, *91*(9). http://doi.org/10.1016/j.chemosphere.2013.02.058

Han, W., Zhong, C., Liang, L., Sun, Y., Guan, Y., Wang, L. Li, J. (2014). Electrochemical degradation of triazole fungicides in aqueous solution using TiO_2-NTs/SnO_2-Sb/PbO2 anode: Experimental and DFT studies. *Electrochimica Acta*, *130*, 179–186. http://doi.org/10.1016/j.electacta.2014.02.119

Heberer, T. (2002). Occurrence, fate, and removal of pharmaceutical residues in the aquatic environment: a review of recent research data. *Toxicology Letters*, *131*, 5–17. http://doi.org/10.1016/S0378-4274(02)00041-3

Hirose, J., Kondo, F., Nakano, T., Kobayashi, T., Hiro, N., Ando, Y., Sano, K. (2005). Inactivation of antineoplastics in clinical wastewater by electrolysis. *Chemosphere*, *60*(8), 1018–1024. http://doi.org/10.1016/j.chemosphere.2005.01.024

Hong, W., Bai, H., Xu, Y., Yao, Z., Gu, Z., & Shi, G. (2010). Preparation of gold nanoparticle/graphene composites with controlled weight contents and their application in biosensors. *Journal of Physical Chemistry C*, *114*(4), 1822–1826. http://doi.org/10.1021/jp9101724

Hor, Y. S., & Cava, R. J. (2009). Thermoelectric properties of Sn-doped Bi-Sb. *Journal of Alloys and Compounds*, *479*, 368–371. http://doi.org/10.1016/j.jallcom.2008.12.071

Hurwitz, G., Pornwongthong, P., Mahendra, S., & Hoek, E. M. V. (2014). Degradation of phenol by synergistic chlorine-enhanced photo-assisted electrochemical oxidation. *Chemical Engineering Journal*, *240*, 235–243. http://doi.org/10.1016/j.cej.2013.11.087

Hussain, S. N., De las Heras, N., Asghar, H. M. a, Brown, N. W., & Roberts, E. P. L. (2014). Disinfection of water by adsorption combined with electrochemical treatment. *Water Research*, *54*, 170–178. http://doi.org/10.1016/j.watres.2014.01.043

Ikehata, K., Jodeiri Naghashkar, N., & Gamal El-Din, M. (2006). Degradation of Aqueous Pharmaceuticals by Ozonation and Advanced Oxidation Processes: A Review. *Ozone: Science & Engineering*, *28*(6), 353–414. http://doi.org/10.1080/01919510600985937

Kannan, R., Rhan, A., & Seok, J. (2016). 3D graphene-mixed metal oxide supported carbon palladium quantum dot nanoarchitectures - A facile bifunctional electrocatalyst for direct ethylene glycol fuel cells and oxygen evolution reactions. *International Journal of Hydrogen Energy*, *41*(40), 1–11. http://doi.org/10.1016/j.ijhydene.2016.07.179

Kapałka, A., Lanova, B., Baltruschat, H., Fóti, G., & Comninellis, C. (2008). Electrochemically induced mineralization of organics by molecular oxygen on boron-doped diamond electrode. *Electrochemistry Communications*, *10*(9), 1215–1218. http://doi.org/10.1016/j.elecom.2008.06.005

Katsumata, H., Sada, M., Nakaoka, Y., Kaneco, S., Suzuki, T., & Ohta, K. (2009). Photocatalytic degradation of diuron in aqueous solution by platinized TiO_2. *Journal of Hazardous Materials*, *171*(1–3), 1081–1087. http://doi.org/10.1016/j.jhazmat.2009.06.110

Kim, S. D., Cho, J., Kim, I. S., Vanderford, B. J., & Snyder, S. A. (2007). Occurrence and removal of pharmaceuticals and endocrine disruptors in South Korean surface, drinking, and waste waters. *Water Research*, *41*(5), 1013–1021. http://doi.org/10.1016/j.watres.2006.06.034

Komtchou, S., Dirany, A., Drogui, P., & Bermond, A. (2015). Removal of carbamazepine from spiked municipal wastewater using electro-Fenton process. *Environmental Science and Pollution Research*, *22*(15), 11513–11525. http://doi.org/10.1007/s11356-015-4345-6

Kümmerer, K. (2001). Drugs in the environment: emission of drugs, diagnostic aids and disinfectants into wastewater by hospitals in relation to other sources – a review. *Chemosphere*, *45*(6–7), 957–969. http://doi.org/10.1016/S0045-6535(01)00144-8

Kümmerer, K. (2009). Antibiotics in the aquatic environment - A review - Part I. *Chemosphere*, *75*(4), 417–434. http://doi.org/10.1016/j.chemosphere.2008.11.086

López-Suárez, F. E., Carvalho-Filho, C. T., Bueno-López, A., Arboleda, J., Echavarra, A., Eguiluz, K. I. B., & Salazar-Banda, G. R. (2015). Platinum-tin/carbon catalysts for ethanol oxidation: Influence of Sn content on the electroactivity and structural characteristics. *International Journal of Hydrogen Energy*, *40*(37), 12674–12686. http://doi.org/10.1016/j.ijhydene.2015.07.135

Labiadh, L., Barbucci, A., Carpanese, M. P., Gadri, A., Ammar, S., & Panizza, M. (2016). Comparative depollution of Methyl Orange aqueous solutions by electrochemical incineration using $TiRuSnO_2$, BDD and PbO_2 as high oxidation power anodes. *Journal of Electroanalytical Chemistry*, *766*. http://doi.org/10.1016/j.jelechem.2016.01.036

Li, S. W., & Lin, A. Y. C. (2015). Increased acute toxicity to fish caused by pharmaceuticals in hospital effluents in a pharmaceutical mixture and after solar irradiation. *Chemosphere*, *139*, 190–196. http://doi.org/10.1016/j.chemosphere.2015.06.010

Liu, Y., Liu, H., Ma, J., & Li, J. (2012). Preparation and electrochemical properties of $Ce–Ru–SnO_2$ ternary oxide anode and electrochemical oxidation of nitrophenols. *Journal of Hazardous Materials*, *213–214*, 222–229. http://doi.org/10.1016/j.jhazmat.2012.01.090

Locatelli, M. A. F., Sodré, F. F., & Jardim, W. F. (2011). Determination of antibiotics in Brazilian surface waters using liquid chromatography-electrospray tandem mass spectrometry. *Archives of Environmental Contamination and Toxicology*, *60* (3), 385–393. http://doi.org/10.1007/s00244-010-9550-1

Lu, X., Zhen, G., Liu, Y., Hojo, T., Ledezma, A., & Li, Y. (2014). Bioresource Technology Long-term effect of the antibiotic cefalexin on methane production during waste activated sludge anaerobic digestion. *Bioresource Technology*, *169*, 644–651. http://doi.org/10.1016/j.biortech.2014.07.056

Malarvizhi, A., Kavitha, C., Saravanan, M., & Ramesh, M. (2012). Carbamazepine (CBZ) induced enzymatic stress in gill, liver and muscle of a common carp, Cyprinus carpio. *Journal of King Saud University - Science*, *24*(2), 179–186. http://doi.org/10.1016/j.jksus.2011.01.001

Martínez-Huitle, C. A., Rodrigo, M. A., Sirés, I., & Scialdone, O. (2015). Single and Coupled Electrochemical Processes and Reactors for the Abatement of Organic Water Pollutants: A Critical Review. *Chemical Reviews*. http://doi.org/10.1021/acs.chemrev.5b00361

Martins, T. S., Hewer, T. L. R., & Freire, R. S. (2007). Cério: Propriedades catalíticas, aplicações tecnológicas e ambientais. *Quimica Nova*, *30*(8), 2001–2006. http://doi.org/10.1590/S0100-40422007000800035

Matamoros, V., Rodríguez, Y., & Albaigés, J. (2016). A comparative assessment of intensive and extensive wastewater treatment technologies for removing emerging contaminants in small communities. *Water Research*, *88*. http://doi.org/10.1016/j.watres.2015.10.058

Michael, I., Rizzo, L., McArdell, C. S., Manaia, C. M., Merlin, C., Schwartz, T. Fatta-Kassinos, D. (2013). Urban wastewater treatment plants as hotspots for the release of antibiotics in the environment: A review. *Water Research*, *47*(3), 957–995. http://doi.org/10.1016/j.watres.2012.11.027

Mohapatra, D. P., Brar, S. K., Tyagi, R. D., Picard, P., & Surampalli, R. Y. (2014). Analysis and advanced oxidation treatment of a persistent pharmaceutical compound in wastewater and wastewater sludge-carbamazepine. *Science of the Total Environment*. http://doi.org/10.1016/j.scitotenv.2013.09.034

Moreira, F. C., Garcia-Segura, S., Boaventura, R. A. R., Brillas, E., & Vilar, V. J. P. (2014). Degradation of the antibiotic trimethoprim by electrochemical advanced oxidation processes using a carbon-PTFE air-diffusion cathode and a boron-doped diamond or platinum anode. *Applied Catalysis B: Environmental*, *160–161*(1). http://doi.org/10.1016/j.apcatb.2014.05.052

Moura, D. C., Araújo, C. K. C., Zanta, C. L. P. S., Salazar, R., & Martínez-Huitle, C. A. (2014). Active chlorine species electrogenerated on Ti/RuTiO$_2$ surface: Electrochemical behavior, concentration determination and their application. *Journal of Electroanalytical Chemistry*, *731*. http://doi.org/10.1016/j.jelechem.2014.08.008

Moura, D. C. De, Quiroz, M. A., Silva, D. R. Da, Salazar, R., & Martínez-Huitle, C. A. (2016). Electrochemical degradation of Acid Blue 113 dye using TiO$_2$-nanotubes decorated with PbO$_2$ as anode. *Environmental Nanotechnology, Monitoring and Management*, *5*, 13–20. http://doi.org/10.1016/j.enmm.2015.11.001

Nethaji, S., & Sivasamy, A. (2017). Graphene oxide coated with porous iron oxide ribbons for 2, 4-Dichlorophenoxyacetic acid (2,4-D) removal. *Ecotoxicology and Environmental Safety*, *138*(December 2016), 292–297. http://doi.org/10.1016/j.ecoenv.2017.01.001

Oliveira, V. L., Morais, C., Servat, K., Napporn, T. W., Tremiliosi-Filho, G., & Kokoh, K. B. (2014). Studies of the reaction products resulted from glycerol electrooxidation on Ni-based materials in alkaline medium. *Electrochimica Acta*, *117*, 255–262. http://doi.org/10.1016/j.electacta.2013.11.127

Orias, F., & Perrodin, Y. (2013). Characterisation of the ecotoxicity of hospital effluents: A review. *Science of the Total Environment*, *454–455*, 250–276. http://doi.org/10.1016/j.scitotenv.2013.02.064

Oturan, M. A., & Aaron, J.-J. (2014). Advanced Oxidation Processes in Water/Wastewater Treatment: Principles and Applications. A Review. *Critical Reviews in Environmental Science and Technology*, *44*. http://doi.org/10.1080/10643389.2013.829765

Oturan, N., Trajkovska, S., Oturan, M. A., Couderchet, M., & Aaron, J. J. (2008). Study of the toxicity of diuron and its metabolites formed in aqueous medium during application of the electrochemical advanced oxidation process "electro-Fenton." *Chemosphere*, *73*(9), 1550–1556. http://doi.org/10.1016/j.chemosphere.2008.07.082

Palma-Goyes, R. E., Silva-Agredo, J., González, I., & Torres-Palma, R. a. (2014). Comparative degradation of indigo carmine by electrochemical oxidation and advanced oxidation processes. *Electrochimica Acta*, *140*, 427–433. http://doi.org/10.1016/j.electacta.2014.06.096

Panakoulias, T., Kalatzis, P., Kalderis, D., & Katsaounis, (2010). Electrochemical degradation of Reactive Red 120 using DSA and BDD anodes. *Journal of Applied Electrochemistry*, *40*(10), 1759–1765. http://doi.org/10.1007/s10800-010-0138-2

Panizza, M., Brillas, E., & Comninellis, C. (2008). Application of Boron-Doped Diamond Electrodes for Wastewater Treatment. *J. Environ. Eng. Manage.*, *18*(3), 139–153. Retrieved from http://ser.cienve.org.tw/download/18-3/jeeam18-3_139-153.pdf

Patra, S., Roy, E., Tiwari, A., Madhuri, R., & Sharma, P. K. (2015a). 2-Dimensional graphene as a route for emergence of additional dimension nanomaterials. *Biosensors and Bioelectronics*. http://doi.org/10.1016/j.bios.2016.02.067

Patra, S., Roy, E., Tiwari, A., Madhuri, R., & Sharma, P. K. (2015b). 2-Dimensional graphene as a route for emergence of additional dimension nanomaterials. *Biosensors and Bioelectronics*. http://doi.org/10.1016/j.bios.2016.02.067

Pereira, J. H. O. S., Vilar, V. J. P., Borges, M. T., González, O., Esplugas, S., & Boaventura, R. a R. (2011). Photocatalytic degradation of oxytetracycline using TiO_2 under natural and simulated solar radiation. *Solar Energy*, *85*(11), 2732–2740. http://doi.org/10.1016/j.solener.2011.08.012

Pinheiro, R. A., De Lima, C. M. E., Cardoso, L. D. R., Trava-Airoldi, V. J., & Corat, E. J. (2016). Methods to grow porous diamond film doped with boron and nitrogen by deposition on carbon nanotubes. *Diamond and Related Materials*, *65*, 198–203. http://doi.org/10.1016/j.diamond.2016.03.022

Pipi, A. R. F., Neto, S. A., & De Andrade, A. R. (2013). Electrochemical degradation of diuron in chloride medium using DSA based anodes. *Journal of the Brazilian Chemical Society*, *24*(8), 1259–1266. http://doi.org/10.5935/0103-5053.20130159

Polcaro, A. M., Mascia, M., Palmas, S., & Vacca, A. (2004). Electrochemical degradation of diuron and dichloroaniline at BDD electrode. *Electrochimica Acta*, *49*(4), 649–656. http://doi.org/10.1016/j.electacta.2003.09.021

Pruneanu, S., Pogacean, F., Biris, A. R., Coros, M., Watanabe, F., Dervishi, E., & Biris, A. S. (2013). Electro-catalytic properties of graphene composites containing gold or silver nanoparticles. *Electrochimica Acta*, *89*, 246–252. http://doi.org/10.1016/j.electacta.2012.10.163

Puckowski, A., Mioduszewska, K., Łukaszewicz, P., Borecka, M., Caban, M., Maszkowska, J., & Stepnowski, P. (2016). Bioaccumulation and analytics of pharmaceutical residues in the environment: A review. *Journal of Pharmaceutical and Biomedical Analysis*. http://doi.org/10.1016/j.jpba.2016.02.049

Pupo, M. M. S., López-Suárez, F. E., Bueno-López, A., Meneses, C. T., Eguiluz, K. I. B., & Salazar-Banda, G. R. (2014). Sn@Pt and Rh@Pt core–shell nanoparticles synthesis for glycerol oxidation. *Journal of Applied Electrochemistry*, *45*(2), 139–150. http://doi.org/10.1007/s10800-014-0757-0

Radjenović, J., Petrović, M., Barceló, D., & Petrović, M. (2007). Advanced mass spectrometric methods applied to the study of fate and removal of pharmaceuticals in wastewater treatment. *TrAC - Trends in Analytical Chemistry*, *26*(11), 1132–1144. http://doi.org/10.1016/j.trac.2007.10.002

Radjenovic, J., & Sedlak, D. L. (2015). Challenges and Opportunities for Electrochemical Processes as Next-Generation Technologies for the Treatment of Contaminated Water. *Environmental Science and Technology*. http://doi.org/10.1021/acs.est.5b02414

Ranade, V. V., & Bhandari, V. M. (2014). Industrial Wastewater Treatment, Recycling, and Reuse: An Overview. In *Industrial Wastewater Treatment, Recycling and Reuse*. http://doi.org/10.1016/B978-0-08-099968-5.00001-5

Rao, A. N. S., & Venkatarangaiah, V. T. (2014). Metal oxide-coated anodes in wastewater treatment. *Environmental Science Pollution Research*, *21*, 3197–3217. http://doi.org/10.1007/s11356-013-2313-6

Ribeiro, A. R., Nunes, O. C., Pereira, M. F. R., & Silva, A. M. T. (2015). An overview on the advanced oxidation processes applied for the treatment of water pollutants defined in the recently launched Directive 2013/39/EU. *Environment International*. http://doi.org/10.1016/j.envint.2014.10.027

Rivera-Utrilla, J., Sánchez-Polo, M., Ferro-García, M. Á., Prados-Joya, G., & Ocampo-Pérez, R. (2013). Pharmaceuticals as emerging contaminants and their removal from water. A review. *Chemosphere*. http://doi.org/10.1016/j.chemosphere.2013.07.059

Ruhí, A., Acuna, V., Barceló, D., Huerta, B., Mor, J. R., Rodríguez-Mozaz, S., & Sabater, S. (2015). Bioaccumulation and trophic magnification of pharmaceuticals and endocrine disruptors in a Mediterranean river food web. *Science of the Total Environment*, *540*(August), 250–259. http://doi.org/10.1016/j.scitotenv.2015.06.009

Salazar-Banda, G. R., Eguiluz, K. I. B., Pupo, M. M. S., Suffredini, H. B., Calegaro, M. L., & Avaca, L.(2012). The influence of different co-catalysts in Pt-based ternary and quaternary electro-catalysts on the electro-oxidation of methanol and ethanol in acid media. *Journal of Electroanalytical Chemistry*, *668*, 13–25. http://doi.org/10.1016/j.jelechem.2012.01.006

Sales Solano, A. M., Costa de Araújo, C. K., Vieira de Melo, J., Peralta-Hernandez, J. M., Ribeiro da Silva, D., & Martínez-Huitle, C. A. (2013). Decontamination of real textile industrial effluent by strong oxidant species electrogenerated on diamond electrode: Viability and disadvantages of this electrochemical technology. *Applied Catalysis B: Environmental*, *130–131*, 112–120. http://doi.org/10.1016/j.apcatb.2012.10.023

Santos, T. É. S., Silva, R. S., Eguiluz, K. I. B., & Salazar-Banda, G. R. (2015). Development of Ti/$(RuO_2)_{0.8}(MO_2)_{0.2}$ (M=Ce, Sn or Ir) anodes for atrazine electro-oxidation. Influence of the synthesis method. *Materials Letters*, *146*, 4–8. http://doi.org/10.1016/j.matlet.2015.01.145

Särkkä, H., Bhatnagar, A., & Sillanpää, M. (2015). Recent developments of electro-oxidation in water treatment –A Review. *Journal of Electroanalytical Chemistry*, *754*, 46–56. http://doi.org/10.1016/j.jelechem.2015.06.016

Sebastine, I. M., & Wakeman, R. J. (2003). Consumption and Environmental Hazards of Pharmaceutical Substances in the UK. *Process Safety and Environmental Protection*, *81*(4), 229–235. http://doi.org/10.1205/095758203322299743

Shan, S. J., Zhao, Y., Tang, H., & Cui, F. Y. (2017). A Mini-review of Carbonaceous Nanomaterials for Removal of Contaminants from Wastewater. *Earth and Environmental Science*, *68*, 1–7.

Shao, D., Li, X., Xu, H., & Yan, W. (2014). An improved stable Ti/Sb–SnO$_2$ electrode with high performance in electrochemical oxidation. *Royal Society of Chemistry*, *4*, 21230–21237. http://doi.org/10.1039/c4ra01990c

Shao, D., Yan, W., Cao, L., Li, X., & Xu, H. (2014). High-performance Ti/Sb-SnO$_2$/Pb$_3$O$_4$ electrodes for chlorine evolution: Preparation and characteristics. *Journal of Hazardous Materials*, *267*, 238–244. http://doi.org/10.1016/j.jhazmat.2013.12.064

Shao, D., Yan, W., Li, X., Yang, H., & Xu, H. (2014). A Highly Stable Ti / TiH x / Sb − SnO 2 Anode: Preparation , Characterization and Application. *Industrial & Engineering Chemistry Research*, *53*, 3898–3907.

Shestakova, M., Bonete, P., Gómez, R., Sillanpää, M., & Tang, W. Z. (2014). Electrochimica Acta Novel Ti/Ta$_2$O$_5$-SnO$_2$ electrodes for water electrolysis and electrocatalytic oxidation of organics. *Electrochimica Acta*, *120*, 302–307. http://doi.org/10.1016/j.electacta.2013.12.113

Shmychkova, O., Luk'yanenko, T., Velichenko, Meda, L., & Amadelli, R. (2013). Bi-doped PbO$_2$ anodes: Electrodeposition and physico-chemical properties. *Electrochimica Acta*, *111*, 332–338. http://doi.org/10.1016/j.electacta.2013.08.082

Sirés, I., Brillas, E., Oturan, M. A., Rodrigo, M. A., & Panizza, M. (2014). Electrochemical advanced oxidation processes: today and tomorrow. A review. *Environmental Science Pollution Research*, *21*, 8336–8367. http://doi.org/10.1007/s11356-014-2783-1

Souza, F. L., Teodoro, T. Q., Vasconcelos, V. M., Migliorini, F. L., Lima Gomes, P. C. F., Ferreira, N. G. Lanza, M. R. V. (2014). Electrochemical oxidation of imazapyr with BDD electrode in titanium substrate. *Chemosphere*, *117*(1). http://doi.org/10.1016/j.chemosphere.2014.09.051

Sun, Z., Zhang, H., Wei, X., Ma, X., & Hu, X. (2015). Preparation and electrochemical properties of SnO_2-Sb-Ni-Ce oxide anode for phenol oxidation. *Journal of Solid State Electrochemistry*, *19*(8), 2445–2456. http://doi.org/10.1007/s10008-015-2892-x

Tixier, C., Bogaerts, P., Sancelme, M., Bonnemoy, F., Twagilimana, L., Cuer, A., Veschambre, H. (2000). Fungal biodegradation of a phenylurea herbicide, diuron: Structure and toxicity of metabolites. *Pest Management Science*, *56*(5), 455–462. http://doi.org/10.1002/(SICI)1526-4998(200005)56:5

Tran, N., Drogui, P., & Brar, S. K. (2015). Sonoelectrochemical oxidation of carbamazepine in waters: Optimization using response surface methodology. *Journal of Chemical Technology and Biotechnology*, *90*(5), 921–929. http://doi.org/10.1002/jctb.4399

Tran, N., Drogui, P., Brar, S. K., & De Coninck, A. (2017). Synergistic effects of ultrasounds in the sonoelectrochemical oxidation of pharmaceutical carbamazepine pollutant. *Ultrasonics Sonochemistry*, *34*, 380–388. http://doi.org/10.1016/j.ultsonch.2016.06.014

Trasatti, S. (2000). Electrocatalysis: understanding the success of DSA®. *Electrochimica Acta*, *45*(15–16), 2377–2385. http://doi.org/10.1016/S0013-4686(00)00338-8

van den Brandhof, E. J., & Montforts, M. (2010). Fish embryo toxicity of carbamazepine, diclofenac and metoprolol. *Ecotoxicology and Environmental Safety*, *73*(8), 1862–1866. http://doi.org/10.1016/j.ecoenv.2010.08.031

Vasudevan, S., & Oturan, M. A. (2014). Electrochemistry: As cause and cure in water pollution-an overview. *Environmental Chemistry Letters*. http://doi.org/10.1007/s10311-013-0434-2

Wang, W., Liu, Y., Zhang, H., Qian, Y., & Guo, Z. (2017). Re-investigation on reduced graphene oxide/Ag_2CO_3 composite photocatalyst: An insight into the double-edged sword role of RGO. *Applied Surface Science*, *396*, 102–109. http://doi.org/10.1016/j.apsusc.2016.11.030

Wang, X. H., & Lin, A. Y. C. (2014). Is the phototransformation of pharmaceuticals a natural purification process that decreases ecological and human health risks? *Environmental Pollution*, *186*, 203–215. http://doi.org/10.1016/j.envpol.2013.12.007

Wang, Y., Hu, B., Hu, C., & Zhou, X. (2015). Fabrication of a novel Ti/SnO_2–Sb–CeO_2@TiO_2–SnO_2 electrode and photoelectrocatalytic application in wastewater treatment. *Materials Science in Semiconductor Processing*, *40*, 744–751. http://doi.org/10.1016/j.mssp.2015.06.020

Wang, Y., Liu, S., Li, R., Huang, Y., & Chen, C. (2016). Electro-catalytic degradation of sulfisoxazole by using graphene anode. *Journal of Environmental Sciences (China)*, *43*, 54–60. http://doi.org/10.1016/j.jes.2015.08.014

Wasserscheid, P., & Keim, W. (2000). Ionic Liquids - New Solutions for Transition Metal Catalysis. *Angew Chem Int*, *39*, 3772–3789.

Wei, J., Zhu, X., Lü, F., & Ni, J. (2011). Comparative study of oxidation ability between boron-doped diamond (BDD) and lead oxide (PbO_2) electrodes, *18*(5), 589–593. http://doi.org/10.1007/s12613-011-0482-1

Wu, W., Huang, Z.-H., & Lim, T.-T. (2014). Recent development of mixed metal oxide anodes for electrochemical oxidation of organic pollutants in water. *Applied Catalysis A: General*, *480*, 58–78. http://doi.org/10.1016/j.apcata.2014.04.035

Xiaohong, W., Wei, Q., & Weidong, H. (2007). Thin bismuth oxide films prepared through the sol-gel method as photocatalyst. *Journal of Molecular Catalysis A: Chemical*, *261*(2), 167–171. http://doi.org/10.1016/j.molcata.2006.08.016

Xu, L., Li, M., & Xu, W. (2015). Preparation and characterization of Ti/SnO_2-Sb electrode with copper nanorods for AR 73 removal. *Electrochimica Acta*, *166*, 64–72. http://doi.org/10.1016/j.electacta.2015.02.233

Zhang, C., Du, X., Zhang, Z., & Fu, D. (2016). The peculiar roles of chloride electrolytes in BDD anode cells. *RSC Adv.*, *6*(70), 65638–65643. http://doi.org/10.1039/C6RA10828H

Zhang, J., Chang, V. W. C., Giannis, A., & Wang, J. (2013). Removal of cytostatic drugs from aquatic environment: a review. *The Science of the Total Environment*, *445–446*, 281–98. http://doi.org/10.1016/j.scitotenv.2012.12.061

Zhang, L., Xu, L., He, J., & Zhang, J. (2014). Preparation of Ti/SnO_2-Sb electrodes modified by carbon nanotube for anodic oxidation of dye wastewater and combination with nanofiltration. *Electrochimica Acta*, *117*, 192–201. http://doi.org/10.1016/j.electacta.2013.11.117

Zhang, Y. M., Yang, S., & Evans, J. R. G. (2008). Revisiting Hume-Rothery's Rules with artificial neural networks. *Acta Materialia*, *56*(5), 1094–1105. http://doi.org/10.1016/j.actamat.2007.10.059